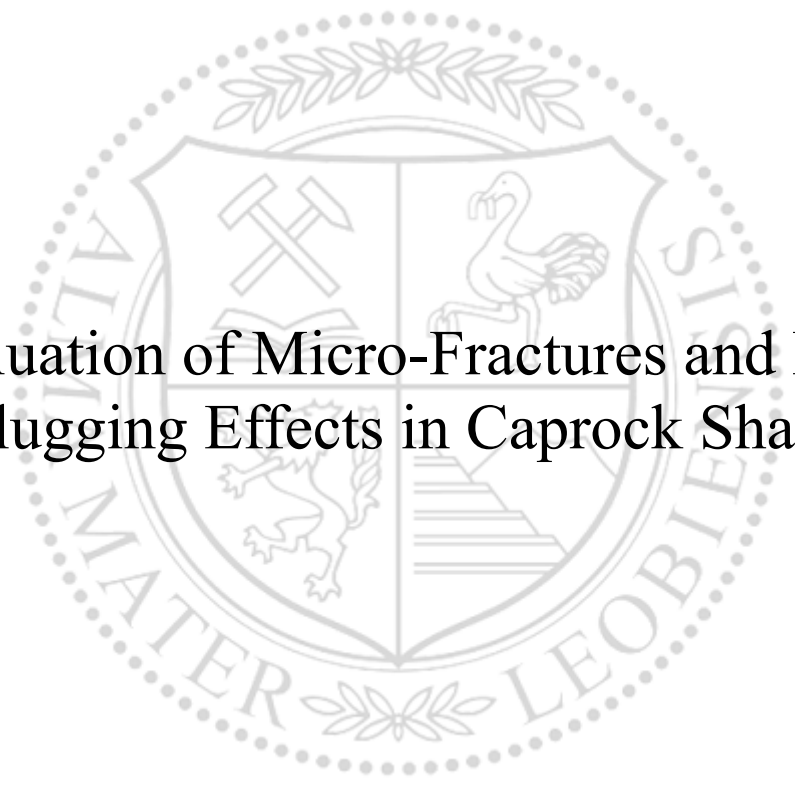




Chair of Drilling and Completion Engineering

Master's Thesis



Evaluation of Micro-Fractures and Pore
Plugging Effects in Caprock Shale

Sharen Monserrat Leon Escobar

May 2019

AFFIDAVIT

I declare on oath that I wrote this thesis independently, did not use other than the specified sources and aids, and did not otherwise use any unauthorized aids.

I declare that I have read, understood, and complied with the guidelines of the senate of the Montanuniversität Leoben for "Good Scientific Practice".

Furthermore, I declare that the electronic and printed version of the submitted thesis are identical, both, formally and with regard to content.

Date 14.05.2019

Signature Author
Sharen Monserrat, Leon Escobar
Matriculation Number: 01535729

This achievement is especially dedicated to my uncle Alberto León López and aunt Lidia Alejandro & to my parents Lilia Escobar Guzmán and José Martin León López† for their full support and unconditional love during this journey.

Le dedico este logro especialmente a mi tío, Alberto León López, a mi tía, Lidia Alejandro & a mis padres, Lilia Escobar Guzmán y José Martin León López† por todo el apoyo y amor incondicional durante esta travesía.

Acknowledgements

Special thanks to my friend and mentor, Alejandro Montiel, for his full support from the beginning of this master thesis. This work would not have been possible without you.

To my advisors, Prof. Kris Ravi, Prof. Gerhard Thonhauser and Dr. Thomas Finkbeiner, for their valuable feedback, remarks and engagement through this learning process. Many thanks for being immediately responsive and helpful to my doubts and thousands of questions and e-mails.

I would also like to express my gratitude to Dipl.-Ing. Marc-Philipp Liebenberger and Dipl.-Ing. Asad Elmgerbi, for their advice and assistance in key subjects and experimental work included in this analysis. Especially when the experiments got a little bit messy and muddy.

Thanks to the specialists of the company and Montanuniversität staff, who helped me whether, collecting and sending information or handling the samples and providing means to accomplish all the tasks: Pamela López, Eden Araujo, Isaac Orozco, Jorge López, Naim Pita, Profs. Ott and Hofstätter, David Misch, Michael Koopmans and Marie-Luise Harmsen.

To my dearest friends who proofread the text and were always cheering me up and encouraging me to keep working: Fabian Fasching, Magdalena Pupp, Maxime Fontaine and Dani Cage.

Finally, I must express my very profound gratitude to the most important people in my life, my family: my parents, Lilia Escobar and José Martín León[†], my brothers, Mauricio León and Martín León, and my aunt and uncle, Lidia Alejandro and Alberto León. Thank you for providing me with unfailing support and continuous encouragement throughout my years of study.

Abstract

Wellbore instability problems are frequently encountered in drilling operations. Large cavings, which are recovered on the shale shakers, are the most prominent indicators and often give an abundance of information. For instance, the evaluation of the micro-fractures and the interaction between the drilling fluid and the shale itself, which are key factors to draw a better conclusion of the possible cause and prescribe solutions to prevent such problems in the future.

By analyzing the samples of cavings obtained from a caprock shale of an oil field in Mexico, this master thesis aims to propose a methodology to better understand the root cause of the wellbore instability problems in this type of formations.

The wellbore instability problem presented in the Mexican onshore wells included in this master thesis is associated with micro-fractured shale, anisotropic failure and weak bedding planes. This is evident by the appearance of three to four centimetres tabular cavings which causes a main problem when controlling the well and handling the cavings on the surface.

This study covers in an integrated manner the real-time monitoring data analysis, geomechanical analysis, micro-CT scanning, shale characterization as well as an experimental set up of the HPHT (High Pressure High Temperature) filter press use for permeability plugging tests.

The proposed setup of the HPHT filter press is designed to analyze the pore plugging effects in shale as well as the interaction between the drilling fluid and the actual rock. This is achieved by developing a replacement of the conventional ceramic disk with the shale samples obtained from the cavings. A methodology to prepare disk for the permeability plugging test from shale cavings was developed and is presented.

The results of the laboratory tests, the geomechanical analysis and the shale characterization give us a better understanding of the behaviour of the shale under borehole conditions, the in-situ stress state of the area and the possible causes of the problem. The methodology applied in this thesis can be beneficial to optimize the selection of the LCM (lost circulation material) by analyzing the micro-fracture width in relation with the pore plugging effects.

Zusammenfassung

Instabilitätsprobleme bei Bohrungen treten häufig bei Bohrvorgängen auf. Große Bruchstücke (sogenannte cavings) die auf den Rüttelsieben abgeschieden werden, sind die wichtigsten Indikatoren dafür und enthalten oft eine Fülle von Informationen. Beispiele dafür sind die Bewertung der Mikrofrakturen als auch die Wechselwirkung zwischen der Bohrspülung und dem erbohrten Tonstein. Derartige Schlüsselfaktoren sind einerseits entscheidend um mögliche Ursachen besser zu verstehen und andererseits Lösungen zur Vermeidung solcher Probleme zu finden.

In dieser Masterarbeit werden analytische Methoden vorgeschlagen um die Instabilitätsprobleme von Bohrungen besser zu verstehen. Dafür wurden Proben von anstehendem Gestein untersucht, die aus einem Ölfeld in Mexiko stammen.

Das in diesen mexikanischen Onshore-Bohrungen in dieser Masterarbeit vorgestellte Instabilitätsproblem ist mit mikrofrakturiertem Tonstein, anisotropem Versagen und labilen Schichtflächen verbunden. Dies wird durch das Auftreten von drei bis vier Zentimeter großen tafelförmigen Bruchstücken verdeutlicht, welche ein Hauptproblem bei der Kontrolle des Bohrlochs und der Handhabung der Bruchstücke übertage verursachen.

Diese Studie umfasst die Überwachung von Echtzeit Daten mit proNova, die geomechanische Analyse mit JewelSuite™, Mikro-CT-Scanning, Schiefercharakterisierung sowie einen experimentellen Aufbau der HPHT-Filterpresse (High Pressure High Temperature) für sogenannte „Permeability Plugging Tests“.

Mit dem vorgeschlagenen Aufbau der HPHT-Filterpresse sollen die Dichtheit des Filterkuchens in Tonstein sowie die Wechselwirkung zwischen der Bohrspülung und dem Tonstein analysiert werden. Dies wird erreicht, indem die herkömmliche Keramikscheibe durch die aus den Bruchstücken erhaltenen Schieferproben ersetzt wird. Eine Methodik zur Aufbereitung derartiger Scheiben für die Plugging Tests aus diesen Bruchstücken wurde entwickelt.

Die Ergebnisse der Labortests, der geomechanischen Analyse und der Schiefercharakterisierung vermitteln ein besseres Verständnis des Verhaltens des Tonsteins unter Bohrlochbedingungen, des In-Situ-Spannungszustands des Gebiets und der möglichen Ursachen des Problems. Die in dieser Arbeit angewandte Methodik kann von Vorteil sein, um die Auswahl des LCM (lost circulation material) durch Analyse der Mikrorissbreite in Bezug auf die Dichtheit des Filterkuchens zu optimieren.

Contents

Chapter 1 Introduction	1
1.1 General Information	1
1.2 Statement of the Problem.....	1
1.3 Thesis Structure.....	2
1.4 Scope and Delimitations	3
1.5 Importance of the Study	3
Chapter 2 Background Information	5
2.1 Shale: Sedimentary Rock.....	5
2.1.1 Definition	5
2.1.2 Properties / Characterization	6
2.1.3 Total Organic Carbon (TOC) Measurement	8
2.1.4 Source Rock Analysis (SRA)	9
2.1.5 Cleaning Methods	10
2.1.6 Micro CT and Medical CT Scanner	12
2.2 Geomechanics.....	12
2.2.1 Basic Concepts	12
2.2.2 Mechanical Rock Properties.....	17
2.2.3 Rock Strength Anisotropy	19
2.3 Pore Plugging Evaluation.....	20
2.3.1 Concepts.....	20
Chapter 3 Proposed Approach and Experimental Method	25
3.1 Methodology	25
3.1.1 When can we use the proposed methodology?	25
3.1.2 Workflow	25
3.2 Geological Background	26
3.3 Data Acquisition, Quality Control and Validation	29
3.4 Drilling Events Analysis	33
3.4.1 Integration of the Sensor Data into the Drilling Events Analysis.....	33
3.4.2 Drilling Events	37
3.5 Geomechanical Analysis.....	46
3.5.1 Input Data - JewelSuite™	46
3.5.2 Pore Pressure.....	51
3.5.3 Wellbore Stability	57
3.5.4 Validation of the Geomechanical Model.....	68
3.6 Shale Evaluation.....	71

3.6.1 Cleaning Methods.....	71
3.6.2 TOC and SRA Evaluation and Cleaning Methods Comparison.....	74
3.6.3 CT Scanner Images	75
3.7 Pore Plugging Analysis.....	76
3.7.1 Fluid invasion.....	76
3.7.2 Proposed PPT Set Up	79
Chapter 4 Shale Disks	81
4.1 Building the Shale Disks	81
4.2 Performing PPT with Shale Samples.....	85
Chapter 5 Results and Discussion.....	89
5.1 Results and Discussion.....	89
Conclusions.....	103

Chapter 1 Introduction

1.1 General Information

Wellbore instability is one of the main problems that cause high NPT (Non-productive Time) during drilling activities. It is a well-known and common challenge when drilling through shale formations. The instability can be caused by mechanical stresses or chemical and physical effects. Some of the causes that we must identify, study and understand to recognize the mechanism affecting a field are tension and compressive failure, shale hydration, pre-existing fractures and fluid invasion.

The main focus of this master thesis is to analyze the shale samples obtained from a caprock of an oil field in Mexico and perform a geomechanical model to better understand the root causes of the wellbore instability in this formation. This study includes geomechanical analysis, rock scanning, shale characterization, analysis of the interaction between the pore plugging material, drilling fluid and the shale using laboratory tests and specialized software.

1.2 Statement of the Problem

In existing onshore wells of Mexican oil fields, wellbore instability presents a common problem, especially during drilling operations in shale formations (intermediate sections, e.g., cap rocks). This is evident by the appearance of three to four centimeters large cavings, which can be observed in the shale shakers. This situation is a main problem when controlling the well and handling the cavings in the surface.

Although several recommended actions from different specialists have been applied in the past, the root of the problem has not been completely identified to date. Therefore, the NPT and related costs are still high. The company provided the samples and data of the affected fields, which will be analyzed focusing on three potential causes: weak bedding planes, micro-fractures and pore plugging effects.

There are two fields involved in this study, Field AM1 and Field AM2. They are 70 km apart from each other and present similar wellbore instability problems in the same section.

The data used to perform the geomechanical analysis were obtained from Field AM-1, which had more challenging wellbore instability problems according to the company. For this reason, in this study, it was decided to mainly focus on this field. Unfortunately, at the time of this analysis, there were no cavings available from these wells, so it was considered using a shale sample from an outcrop or cavings from another field. At the end, cavings from another well were used to research the pore plugging effect between the drilling fluid and shale using the High-Pressure High-Temperature filter press. Six months after this study started, well S-6081 from Field AM2 was being drilled in the shale formation and having cavings big enough to perform the tests proposed in this thesis. The cavings from well S-6081 were then chosen to research the pore plugging effects.

1.3 Thesis Structure

The proposed methodology in this MSc thesis integrates four main studies:

1. DDR/Real time cross-referenced data analysis
2. Geomechanical analysis
3. Shale and micro-fracture evaluation
4. Pore plugging test

DDR/Real-time cross-referenced data analysis

The current drilling events used to calibrate the geomechanical analysis were obtained just from the summary of the DDR (Daily Drilling Report). To have a stronger and solid starting point, it is important to have a deeper investigation into all the relevant drilling events such as tight hole, lost circulation, packed tool, etc., that occurred during drilling shale formations. To identify the specific intervals causing the wellbore instability issues, following information were cross-referenced:

- a. The complete and detailed DDR
- b. Real-time monitoring parameters
- c. Master-log parameters

The summary of the DDR provides the most relevant events during drilling, but not the entire picture. To really understand and determine each event at a specific depth mentioned in the DDR, it has to be correlated with the real-time drilling parameters and master-log at that specific time and depth. This thorough task must be carefully carried out in order to have a compelling starting point.

Geomechanical analysis

The geomechanical analysis was performed using the information of three development wells and one exploratory well, from field AM1, provided by the oil-company. All geophysical logs, well schematics, top formations, drilling events, caliper logs and trajectories were uploaded to JewelSuite™. From the set of data available, AM-1, AM-11 and AM-21 are the wells that have the most comprehensive information. Even though it was planned just to analyze the wells where the cavings were present, the decision to including AM-1 in this study was taken, in order to use and compare the information with the wellbore stability analysis.

The pore pressure, fracture gradient and horizontal stresses were calculated using the JewelSuite™ workflow. The model was calculated using the advanced mode that includes not only the rock properties but also bedding planes effects.

Shale evaluation and micro-fractures evaluation

The samples recovered in well S-6081 from Field AM2, are at first glance very brittle and highly reactive shales. From our observations, these don't look like classic pressure cavings but rock fragments that broke off due to shear slip along pre-existing bedding planes and formed anisotropic breakouts. Petrophysical analysis and rock evaluation, such as maturity, organic matter content, mineralogy, etc., were performed in collaboration with the Department of Applied Geology, to better understand the possible cause for overpressure and shear failure in this formation.

Due to the contamination of the shales with oil-based mud, different cleaning methods - Soxhlet and Dionex - were tested.

Pore plugging effects

An overlapping of the deep and shallow resistivity curves indicates filtrate into the formation during the drilling operations. Particularly, in well AM-8 we can observe filtrate from 3040- 4370m, reaching peak values at 4200-4330m depth. This will be further discussed in Chapter 3.

Making this observation, it was proposed to develop a setup and run pore plugging tests using the cavings recovered from the well S-6081, with the HPHT filter press that can be operated at pressure and temperature approximating those prevailing down-hole. It allows the use of a filtration media chosen to simulate exposed formations.

1.4 Scope and Delimitations

The MSc thesis is particularly focused on developing a methodology to better understand the root causes of the wellbore instability in caprock shale as well as the interaction between the drilling fluid and shale using the HPHT Filter Press at the Department Petroleum Engineering. The wellbore instability problem of the case study is related to anisotropy, micro-fractures and pore plugging effects. Therefore, it will be tackled by integrating real-time monitoring data analysis, shale characterization, HPHT filter press tests and geomechanical analysis. The latter will consider the wellbore trajectory, orientation and magnitude of in-situ stresses, poroelastic material, strength properties, bedding planes, shale composition and pre-existing fractures.

Due to the possible low permeability of the shale samples, the laboratory tests take long periods to fully evaluate the behavior of the lost circulation material. Nevertheless, the setup of the HPHT filter press will be tested at least with two samples.

1.5 Importance of the Study

When analyzing an instability problem, often the study is limited to a geomechanical analysis taking into consideration the shape of the cavings. In this thesis, in order to have a better comprehension of the problem, it is proposed to run tests on the cavings itself. The type and set up of the tests as well as the information that these studies will provide will be explained and integrated to have a deep insight into the problem.

Chapter 2 Background Information

In this chapter, the literature review, basic concepts, definitions and equipment specifications used during the development of the methodology described in Chapter 3 is outlined.

2.1 Shale: Sedimentary Rock

2.1.1 Definition

Shale is a sedimentary rock that according to Geologists is the most abundant on the Earth's crust, accounting for approximately 70 percent of sedimentary rocks. It is a fine-grain, often laminated and fissile rock, meaning that shale is build up by many thin layers and easily splits into thin pieces along the laminations (Bjorlykke, 2010). The grain size is generally less than 0.004 mm (Figure 2. 1). It main constitutes are either detrital or diagenetic (e.g., from the decomposition of feldspar) clay minerals. In addition, other minerals such as quartz, mica, pyrite and organic matter are present in shales (King, 2018).

Scheme for Sedimentary Rock Identification






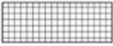


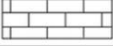

INORGANIC LAND-DERIVED SEDIMENTARY ROCKS					
TEXTURE	GRAIN SIZE	COMPOSITION	COMMENTS	ROCK NAME	MAP SYMBOL
Clastic (fragmental)	Pebbles, cobbles, and/or boulders embedded in sand, silt, and/or clay	Mostly quartz, feldspar, and clay minerals; may contain fragments of other rocks and minerals	Rounded fragments	Conglomerate	
			Angular fragments	Breccia	
	Sand (0.006 to 0.2 cm)		Fine to coarse	Sandstone	
	Silt (0.0004 to 0.006 cm)		Very fine grain	Siltstone	
Clay (less than 0.0004 cm)	Compact; may split easily	Shale			
CHEMICALLY AND/OR ORGANICALLY FORMED SEDIMENTARY ROCKS					
TEXTURE	GRAIN SIZE	COMPOSITION	COMMENTS	ROCK NAME	MAP SYMBOL
Crystalline	Fine to coarse crystals	Halite	Crystals from chemical precipitates and evaporites	Rock salt	
		Gypsum		Rock gypsum	
		Dolomite		Dolostone	
Crystalline or bioclastic	Microscopic to very coarse	Calcite	Precipitates of biologic origin or cemented shell fragments	Limestone	
Bioclastic		Carbon	Compacted plant remains	Bituminous coal	

Figure 2. 1. The scheme used for sedimentary rock identification (Mulroy, 2019).

2.1.2 Properties / Characterization

2.1.2.1 Mineralogy

Shale rocks are constituted by either allogenic or autigenic minerals. Allogenic are minerals brought into sedimentary shale basins from external sources, usually derived from rock weathering on land such as quartz, feldspars, mica and heavy minerals. Autigenic minerals are formed by sediment precipitation from water or changes such as cementation and recrystallization, carbonates are the most common autogenic minerals. Additionally, shale can also contain calcareous, siliceous or phosphatic remains from animal skeletons (Polish Geological Institute, 2014b).

By performing a petrographic analysis we can determine the mineral and petrographic composition of shale rocks and characterize the mineral composition, texture, structure, pore space (size, type, micro-fractures), and the origin of constituents.

The mineral composition is investigated using XRD (X-ray diffraction), petrographic thin section studies and SEM (scanning electron microscope) analyses.

The presence and percentage of specific minerals are determined by XRD analyses. It is very important to know the mineral composition of shale, because its mechanical properties and susceptibility to be fractured are depending on it.

Due to the very fine-grained mineral fractions, thin section studies are frequently not enough to achieve the desirable level of magnification. Thus, the SEM is the most useful equipment to examine the distribution of individual minerals, chemical and mineral composition of a micro-area and the distribution of elements using X-ray detectors or electro microprobe. The FIB (Focused Ion Beam) SEM has an even higher resolution which allows observations of micro-texture, micro-structure as well as micro- and nano-porosity (Polish Geological Institute, 2014b).

2.1.2.2 Petrophysical properties

In order to characterize a shale formation, two key parameters should be determined: Porosity and permeability.

Porosity

There are two types of porosity we need to distinguish: total and effective porosity. Total porosity refers to the total pore volume divided by bulk volume of the rock, while the effective porosity considers only the volume of interconnected pores divided by bulk volume of the rock.

The porosity in shale depends on micro-and nano-sized pore space, which is generally rather low. The effective porosity is normally a consequence of fracturing (Polish Geological Institute, 2014c).

Permeability and fracturability

The permeability of shale is normally associated with the presence of natural fractures in the rock. Shale is characterized by having very low permeability that does not allow the flow of hydrocarbons or water so easily, in most of the cases hydraulic fracturing is necessary to connect micro and nano pores or pre-existent micro-fractures (Polish Geological Institute, 2014c).

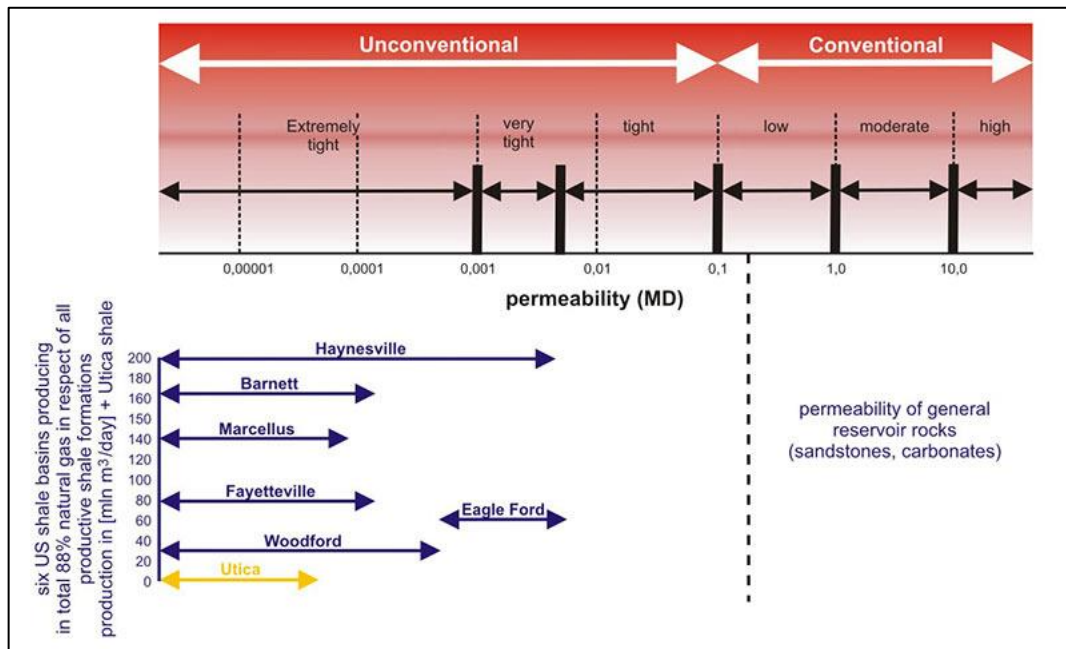


Figure 2. 2. Permeability diagram of conventional and unconventional reservoirs (based on: Faraj, 2012; Hughes, 2013; Jarvie, 2012).

These formations usually have permeability values in the range of nano-Darcy (Figure 2. 2). To use conventional steady-state techniques for measuring the permeability of shale is not efficient, due to the very low flow rates and long periods required to reach the steady state condition. Hence, other methods such as steady state GRI (Gas Research Institute) and pressure pulse decay have been used to determine the permeability of shale samples. This is a faster technique and can measure values as low as one nano Darcy. The GRI method was researched and developed by the Gas Research Institute, it is described in the GRI final report GRI-95/0496, "Development of Laboratory and Petrophysical Techniques for Evaluating Shale Reservoirs." The GRI method is a fast and inexpensive method to investigate the permeability based on crushed samples but cannot be applied under stress conditions. However, recent studies suggest that the method might be inconsistent due to particle size and pressure or volume conditions of the test. According to Core Laboratories, using the pulse decay method, the permeability of plug samples can be measured down to approximately 1 nD obtaining fast and accurate results. It can be applied under stress conditions and it is available for both gas and liquid flow. Nevertheless, there are also limitations or disadvantages such as: it is rather complicated to interpret the results and it is very sensitive to pore volume and compressibility measurements. Some studies report that the permeability values are 2-8 times higher than the values measured by steady-state techniques (Zamirian et. al., 2015).

Another way to measure the permeability in shale is by mercury injection due to a possible relationship between mercury injection curves and permeability. This method is limited because the sample can get contaminated and its pore structure changes during the high-pressure injection, as well as the inability of the mercury to flow through the smaller pores. In 2014, a new steady-state technique for measuring the permeability in shale core plugs was developed. The PPAL (Precision Petrophysical Analysis Laboratory) can measure porosity and permeability, the accuracy of the pore volume

measurements is 10^{-2} cm^3 . Instead of taking many hours or days as in the pulse decay method, the PPAL test can be performed in minutes up to hours depending on the characteristics of the sample. It doesn't need a gas sorption correction when adsorbent gases such as N_2 , CH_4 or CO_2 are used. The evaluation of this method showed that the permeability is very sensitive to stress (Zamirian et al., 2014).

2.1.2.3 Mechanical properties

The mechanical properties of shale rocks such as the elasticity coefficient, compressive and extensional strength are mainly depending on the mineral composition. Especially on the clay content which is a key factor of shale properties. A higher content in clay will lead to a higher plastic deformation and lower brittleness. When the clay content is higher than 40% it is considered to be a problem during fracturing procedures. While a high content of silica and diagenetic carbonates enhances brittleness due the fracturing process (Polish Geological Institute, 2014a).

2.1.3 Total Organic Carbon (TOC) Measurement

One of the key parameters for shale characterization as well as the source rock assessment is the total organic carbon (TOC) content. The TOC is the concentration of organic carbon present in a rock, it is represented by the weight percentage of organic carbon in the rock. Even though, organic carbon is associated with shales or silty shales, it can also be present in clean siltstone, sandstone and carbonate rocks (Crain, 2018). The minimum value to consider an effective source rock is approximately 0.5% wt TOC, but according to the Schlumberger glossary, a 2% wt TOC is already considered as the minimum for shales (Bjorlykke, 2010).

In collaboration with the Chair of Petroleum Geology at the Montanuniversität, measurement of the total organic carbon (TOC) content in our shale samples were performed.

The equipment used in this thesis is the ELTRA HELIOS CS-580A (Figure 2. 3), which measures carbon and sulphur contents. In the CS-580A the samples are weighed into crucibles, which are loaded in the furnace for combustion and burnt in an oxygen atmosphere; the temperature can be set in steps of 1°C to a maximum of $1,550^\circ\text{C}$. CO_2 , H_2O and SO_2 (combustion gasses) coming from the furnace pass through a dust filter and water vapor is chemically absorbed and the dried CO_2 and SO_2 are detected in the infrared cells. (ELTRA GmbH 2019). TOC is measured by decarbonizing the samples in advance with hydrochloric acid.

TIC (total inorganic carbon) and calcite equivalent are calculated as follows:

Total inorganic carbon: $\text{TIC} = \text{TC} - \text{TOC}$

Calcite equivalent = $\text{TIC} \times 8.34$



Figure 2. 3. Eltra CS-580A analyzer used to measure TC, S and TOC on shale samples placed at the Chair of Petroleum Geology.

2.1.4 Source Rock Analysis (SRA)

As we stated previously, the TOC is one of the important parameters to indicate the amount of hydrocarbon generation. In order to have a complete source rock analysis we have to consider other parameters such as: S1 (free oil), S2 (kerogen yield) and T_{max} (maturity). Additionally, the AI (adsorption index), OSI (oil saturation index), HI (hydrogen index), OI (oxygen index), PI (production index), GOC (generative organic carbon) and NCOG (non-generative organic carbon) can be calculated.

The Rock Eval pyrolysis measurement is carried out in a pyrolysis oven with an inert atmosphere. A small sample (around 80 mg) is used to quantitatively and selectively determine the free hydrocarbon and kerogen contained in the sample.

The equipment used to analyze these parameters is the Vinci Rock-Eval 6 (Figure 2. 4). The Rock-Eval 6 is used in the petroleum industry to estimate the S1 and S2, which in turn are used to determine the type of organic material (e.g. HI and kerogen type) and maturity of the source rocks. It gives a better understanding of the thermal cracking of sedimentary organic matter, hydrocarbons generation, expulsion, storage and retention mechanisms. It has two micro-ovens that reach up to 850 °C. The FID detector measures the hydrocarbon gas released during the pyrolysis while the infrared cell measures the quantity of CO and CO₂ generated during the pyrolysis and oxidation of the sample (Vinci Technologies, 2019).

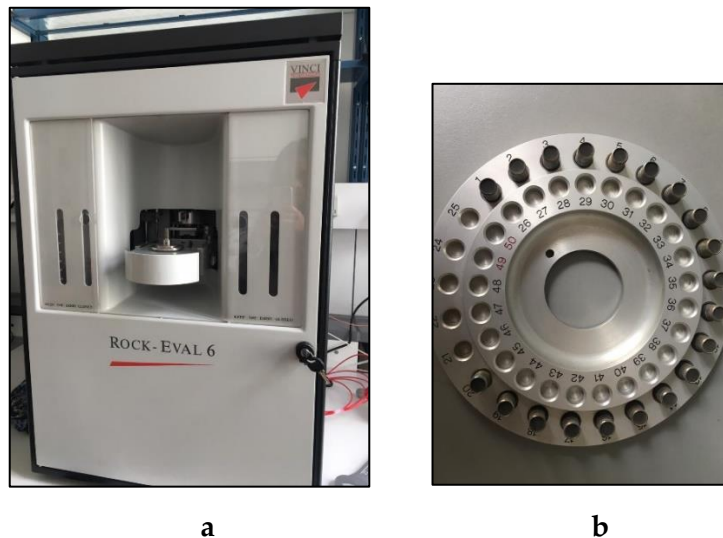


Figure 2. 4. a) Rock-Eval 6 apparatus from the Chair of Petroleum Geology at Montanuniversität. b) Samples carousel with prepared samples.

2.1.5 Cleaning Methods

During the drilling operations and transport; the samples get contaminated with oil base mud or drilling mud in general. Before TOC and RockEval measurements can be made, the samples must be cleaned of the oil-based mud in order to get correct values.

2.1.5.1 Soxhlet

In collaboration with the Chair of Reservoir Engineering, the Soxhlet extraction method to clean the shale samples from the oil-based mud was performed after Gupta et al., 2017. The results are discussed in Chapter 5.

The Soxhlet extractor (Figure 2. 5) is an apparatus in the laboratory which is used for the extraction of lipids or other molecules from a solid sample (the cavings in this case). It has three main parts: a round bottomed flask, the Soxhlet extractor and a condenser. There are several applications such as pharmaceuticals, environmental analysis of soils, biofuels, food testing. In this case, it was used to remove the impregnated oil-based mud in the pores and micro-fractures in the shale cavings before TOC and SRA (Source Rock Evaluation) measurements as well as pore plugging testing was conducted (Labcompare, 2019).

A solid sample containing desired or undesired material is placed in the main chamber of the Soxhlet extractor in a thimble made of thick filter paper. The solvent is heated to reflux considering the azeotropic mixture data, the solvent will evaporate and the vapor will travel up through the sample. In the condenser, the vapor will change to a liquid phase and drips back down to the sample in the main chamber. This chamber will slowly fill and the desired or undesired compound will dissolve in the warm solvent. When this chamber is full, it will automatically empty via the siphon side arm. This process may run over hours or days (Fernandes, 2015).

An azeotropic mixture occurs when the composition of a solution of two or more liquids remains the same in both vapor and liquid phase. In other words, the composition of the liquid at the boiling point is identical to the vapor in equilibrium. In Chapter 3 and 4, the

procedure and results of using Toluene-Methanol (12 to 88 vol%) as solvent to remove the oil base mud in the Soxhlet extractor will be described (Gupta et al., 2017).

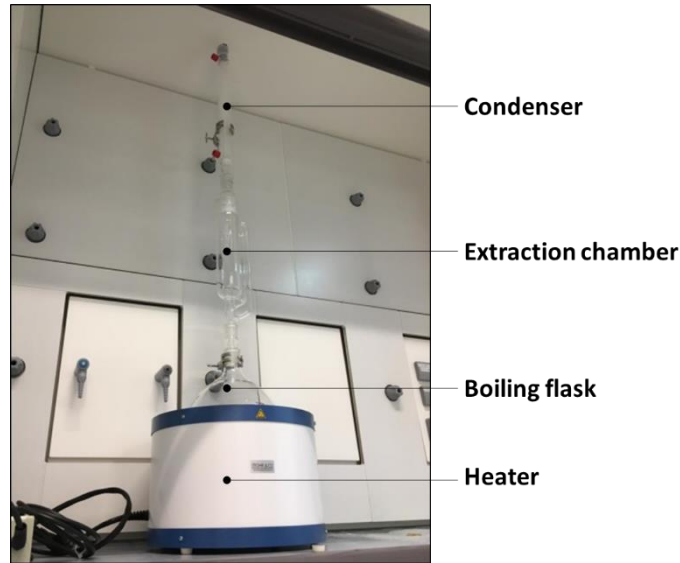


Figure 2. 5. Soxhlet extractor at DPE – Chair of Reservoir Engineering.

2.1.5.2 Dionex

A second method to clean the shale samples before testing them will be evaluated and compared to the previous one in Chapter 5. This is the Accelerated Solvent Extraction (ASE) method, this apparatus uses organic acids and aqueous solvents or acids at high temperatures and pressures. The one at the Chair of Petroleum Geology is the Thermo Scientific™ Dionex™ ASE™, Figure 2. 6, which extracts compounds from solid samples in just about 20 minutes and uses 50 to 90% less solvent compared to other methods such as the Soxhlet extractor. The Dionex system can clean samples up to 100 g at temperatures up to 200 °C and 1500 psi of pressure. The high temperature increases the extraction efficiency of the analyte while the high pressure keeps the solvent in a liquid state as the temperature increases above the boiling point (Life Technologies, 2019).

Both methods Soxhlet and Dionex will be used and their efficiency will be compared in Chapter 5.



Figure 2. 6. Thermo Scientific™ Dionex™ ASE™ at the Chair of Petroleum Geology.

2.1.6 Micro CT and Medical CT Scanner

In order to investigate the fracture width of the cavings, it was proposed to scan the samples with both, Micro and Medical CT Scanners available at the Chair of Reservoir Engineering. Both use the same method, X-ray imaging in 3D slice by slice, but the different between them is that the Micro-CT is on a much smaller scale with greatly increased resolution. The Medical CT is limited to a resolution of 1 millimeter while the Micro-CT scanner can operate at the level of one micron or smaller (Micro Photonics, 2018).

The Micro-CT scanner used in this study is a CT-ALPHA system from Procon X-ray GmbH. It can be equipped with different X-ray powers, from 160kV for nanometer resolution through 225 kV, 320 Watts to the highest power of 450 kV, 1500 Watts (ProCon X-ray GmbH, 2014).

The Medical CT scanner is a Siemens Definition DS (Dual Source); it is called dual-source because it has two Straton MX tubes. This feature makes the scanning time more efficient without sacrifices in the image quality.

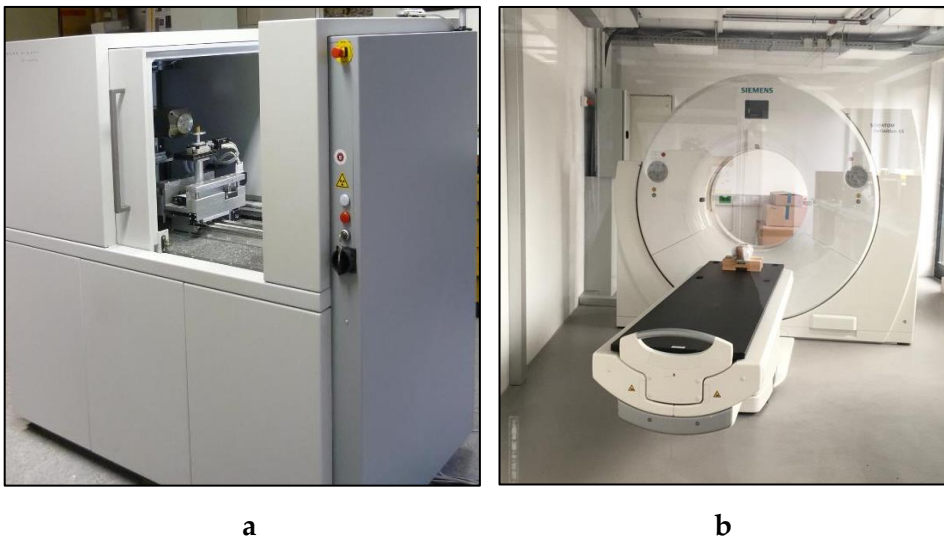


Figure 2. 7. a) Micro and b) Medical CT scanners at the Chair of Reservoir Engineering.

2.2 Geomechanics

2.2.1 Basic Concepts

One of the main parts of this thesis refers to the geomechanical analysis and how to improve the results of it by integrating tests ran in the laboratory. This is why it is important to explain the basic concepts of geomechanics in this chapter.

Because the earth's surface is in contact with a fluid, air or water, that cannot support shear tractions, we have a principal stress plane. Therefore, there is a principal stress that is generally normal to the earth's surface and two principal stresses acting in a horizontal plane. According to a compilation of earthquake focal mechanism data and other stress indicators, this generally applies in the upper crust at about 15-20 km depth. Assuming this is true, we can describe the state of stress at any depth by defining four parameters:

the magnitude of the principal stresses, S_v , S_{Hmax} and S_{hmin} and the orientation of one of them, mostly used the azimuth of the S_{Hmax} (Zoback, 2010).

Following the scheme originally proposed by E.M. Anderson, it is defined three faulting regimes depending on the magnitude of the principal stresses: Normal ($S_v > S_{Hmax} > S_{hmin}$), strike-slip ($S_{Hmax} > S_v > S_{hmin}$) and reverse ($S_{Hmax} > S_{hmin} > S_v$), Figure 2. 8.

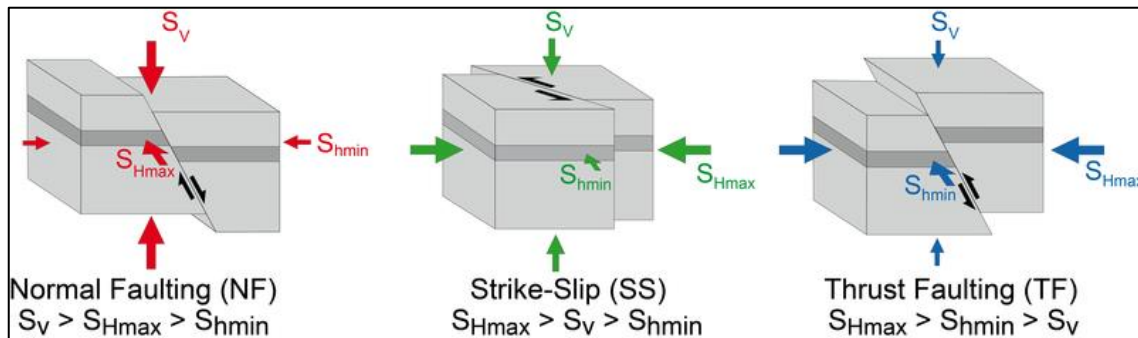


Figure 2. 8. Illustration of the different stress regimes (World Stress Map, 2019).

2.2.1.1 Vertical Stress, S_v

The vertical stress, S_v , corresponds to the weight of the overburden. In other words, the magnitude of S_v is equals to the integration of the rock densities from the surface to the depth of interest:

$$S_v = \int_0^z \rho(z)g \, dz \approx \bar{\rho}gz$$

Equation 2. 1

S_v : Vertical stress, Overburden

$\rho(z)$: Density as a function of depth

g : Gravitational acceleration

2.2.1.2 Horizontal Stresses. Magnitude and Orientation

We can determine the magnitude of the least principal stress, S_3 , meaning, S_{hmin} in normal and strike-slip faulting environment and S_v in reverse faulting environment, through direct measurements or empirical equations. The most reliable method is taking direct measurement of the least stress in wells and boreholes. This can be achieved when performing leak-off tests (LOT's), extended leak-off tests (XLOT's) or mini-fracs. Other direct methods but not too accurate could also be when we observe significant mud losses which infers that we accidentally fractured the formation or when we notice wellbore ballooning effects that indicate that the wellbore pressure is very close to the least principal stress.

When the direct measurements are not available, we can find in the literature several empirical methods to calculate the least principal stress. It is important to mention that most of the empirical methods predict S_3 when the pore pressure is hydrostatic, in other words, at shallow depths. However, in the study case in this thesis, the formation presenting the wellbore instability problems is over-pressurized shale. In his book, Reservoir Geomechanics, Zoback (2010) discusses and compares different empirical

methods applied in the Gulf of Mexico and points out that the frictional faulting theory tends to underpredict measured values of S_3 in overpressure formations. His explanation to this might be because it has been observed that the coefficient of friction in smectite-rich shales is lower than 0.6, different to most of the rocks which values have been proven to range between 0.6-1 (Zoback, 2010).

On the other hand, the magnitude of the maximum horizontal stress, S_{Hmax} , is not that straightforward to estimate because it cannot be measured directly. However, there have been developments of different approaches to estimate it. Some of them derivate from multi-arm caliper data and the Kirsch equations published in 1898 by German engineer Ernst Gustav Kirsch. In their paper, Dobroskok and AL Zadjali (2016), applied this method in vertical wells in Oman, they concluded that it is relatively accurate and can be strongly affected by tool rotation or alteration of the borehole shape (Dobroskok and AL Zadjali, 2016). Another approach is using hydraulic fracturing (Hubbert and Willis, 1957; Haimson and Fairhurst, 1969), which has been proven to be successful at shallow depths where stress and temperature are low (less than 2 kms) and relatively strong rocks. Since the oil fields are normally deeper than that, the application in the oil and gas industry is limited (Zoback, 2010). Barton et al. (1988), assuming that the breakout width remains stable, proposed a methodology based on it to determine S_{Hmax} when the rock strength is known (Barton et al. , 1988). It can be calculated with the following equation:

$$S_{Hmax} = \frac{(C_0 + 2P_p + \Delta P + \sigma^{\Delta T}) - S_{hmin}(1 + 2\cos 2\theta_b)}{1 - 2\cos 2\theta_b}$$

Equation 2. 2

where $2\theta_b = \pi - W_{bo}$

S_{Hmax} : Maximum horizontal stress

S_{hmin} : Minimum horizontal stress

P_p : Pore pressure

$\sigma^{\Delta T}$: Thermal stresses (mud and formation temperature difference)

W_{bo} : Breakout width

2.2.1.3 Pore Pressure

The pore pressure can be defined as the pressure of the fluid trapped in the pore space of rock formations. It is usually hydrostatic unless there is a different mechanism acting on the formations which leads to abnormal pressures, less or higher than the hydrostatic pressure; underpressure and overpressure respectively. In our case study, it is clear that there is an overpressure zone. There are several causes of overpressure, Figure 2. 9. In his review of all of them, D. Grauls (1999) concluded that the main overpressure mechanisms are mechanical, thermal stresses and dynamic transfers in the petroleum systems (Grauls, 1999). In this thesis, we will evaluate the possible compaction disequilibrium, kerogen cracking, oil generation and cracking as the cause of the overpressure in the shale.

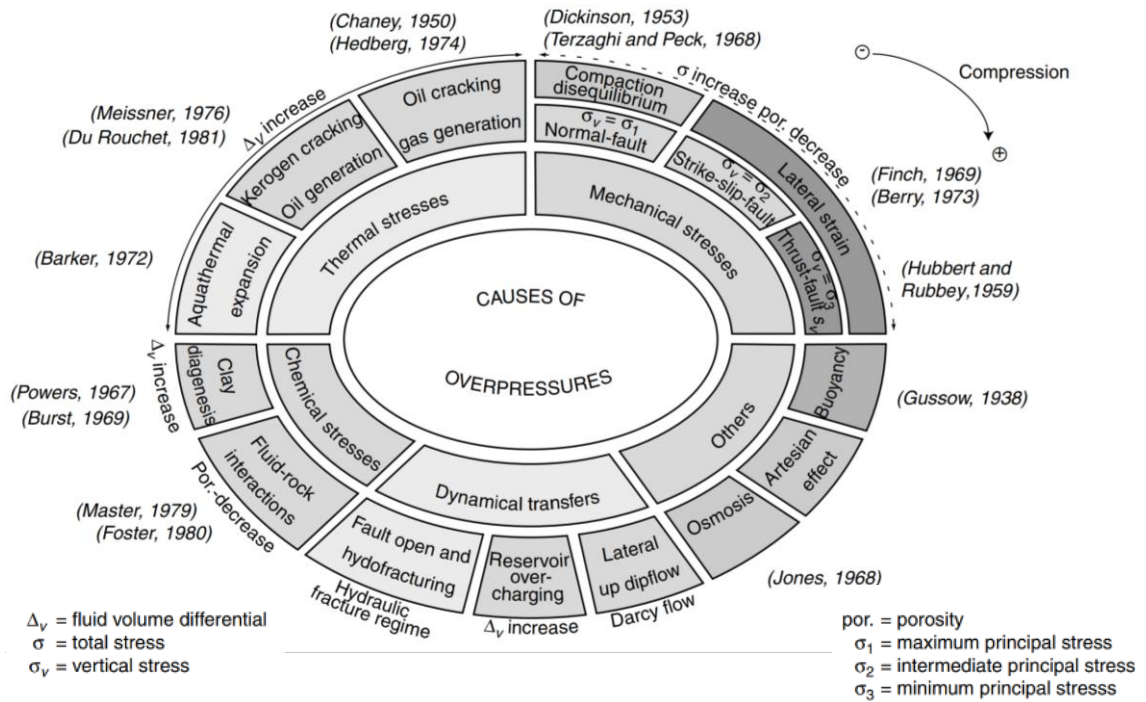


Figure 2. 9. Diagram of the main overpressure causal mechanisms (Grauls, 1999).

There are a number of methods to calculate the pore pressure, most of them based on Terzaghi’s effective stress principle (Terzaghi, 1943):

$$P_p = S_v - \sigma'$$

Equation 2. 3

P_p : Pore pressure

S_v : Total stress

σ' : Effective stress

Some of these methods are:

Pore pressure prediction from resistivity

- Eaton’s method (Eaton, 1972)

Pore pressure prediction from interval velocity and transit time

- Eaton’s method (Eaton, 1975)
- Bowers’ method (Bowers, 1995)
- Miller’s method (Zhang, 2011)
- Tau model (Lopez et al., 2004) (Gutierrez et al., 2006)

Adapted Eaton’s methods with depth-dependent normal compaction trendlines

- Eaton’s resistivity method with depth-dependent normal compaction trendline
- Eaton’s velocity method with depth-dependent normal compaction trendline

Other theoretical models of pore pressure prediction

- Pore pressure prediction from porosity
- Pore pressure prediction from transit time or velocity

The review and evaluation of these methods were performed and published by J. Zhang (2011).

2.2.1.4 Fracture Gradient

The pressure required to fracture the formation can be defined as the fracture gradient in the oil and gas industry, especially in drilling operations. It is obtained by dividing the true vertical depth and the fracture pressure (Zhang et al., 2017). In other words, the fracture gradient is the pressure gradient required to induce fractures in the rock at a given depth (Schlumberger Oilfield Glossary, 2019). Based on this definition, we can state that the fracture gradient is the maximum mud weight that a formation can hold without mud losses or induced tensile failures.

It is commonly confused with the minimum horizontal stress because there hasn't been an agreement on a method to calculate it. Some specialists use the minimum horizontal stress as the fracture gradient, others, the maximum leak-off pressure gradient (the peak value in the LOT test), Figure 2. 10, or the fracture initiation pressure gradient (Zhang et al., 2017).

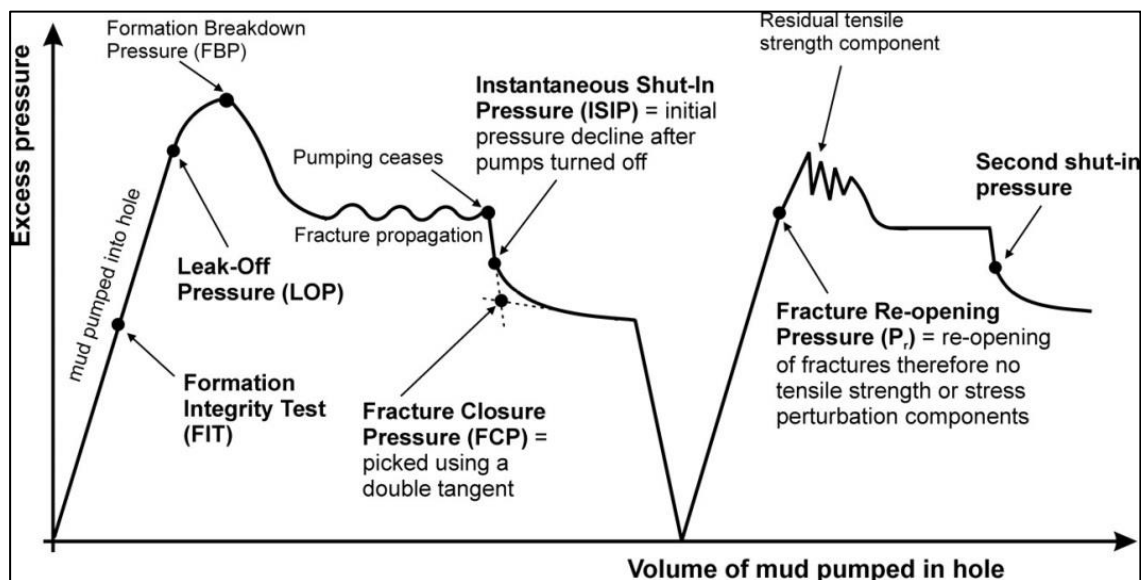


Figure 2. 10. The use of leak-off tests as means of predicting minimum in-situ stress (White et al., 2002)

Some methods to calculate the fracture gradient, FG, are listed below (Jincai Zhang and Yin, 2017),

- Hubbert and Willis' method (Hubbert and Willis, 1957)
- Matthews and Kelly's method (Matthews and Kelly, 1967)
- Eaton's method (Eaton, 1969)
- Daines' method (Daines, 1982)

Fracture gradient from wellbore tensile failure

- Haimson and Fairhurst, 1967
- Detournay and Cheng, 1988

- Zhang, 2013

Upper and lower bounds of fracture gradient

- Zhang, 2011

2.2.2 Mechanical Rock Properties

The mechanical rock properties are divided into dynamic and static properties. The dynamic properties are calculated from petrophysical logs in a continuous manner while the static properties are measured throughout laboratory tests using core samples in a deterministic way.

2.2.2.1 Unconfined Compressive Strength (UCS)

The unconfined compressive strength (UCS) is the measurement of the strength of the material under confined conditions, in other words, when the confining stress is zero. It is determined in the laboratory with a uniaxial compressive test where the application of the stress is just along one axis. The value of the UCS is then, the maximum axial compressive stress that the sample (cylindrical) can withstand.

2.2.2.2 Young's Modulus (E)

The Young's Modulus is deduced from the theory of linear elasticity. Assuming that the sample is 1) homogeneous, 2) isotropic and 3) elastic, in the following equation, the Hook's law, the constant E is the Young's modulus.

$$\varepsilon_z = \frac{1}{E} \sigma_z$$

Equation 2. 4

Hence, as it can be seen in Figure 2. 11, the Young's modulus is the ratio of the stress to strain considering a uniaxial stress applied, F. In other words, the higher is the value of the Young's modulus, the more resistant is the material to be deformed.

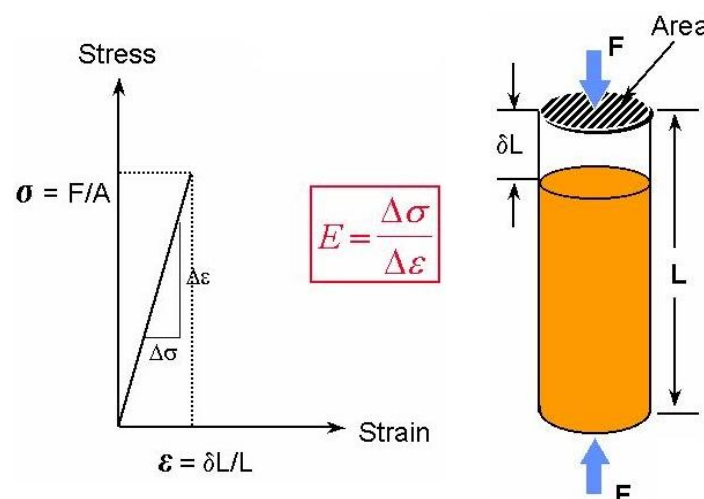


Figure 2. 11. Illustration of the concept of the Young's Modulus. Ratio of the stress to strain considering a uniaxial stress applied, F.

2.2.2.3 Poisson's Ratio (ν)

The ratio of the increase of the lateral deformation to the length contraction of a material is called the Poisson's ratio, ν . When we apply a force in an axial direction, this force is then laterally transmitted (Figure 2. 12). The higher value of the Poisson's ratio will imply a higher lateral deformation of the material. It is dimensionless and usually ranges between 0.18 and 0.35.

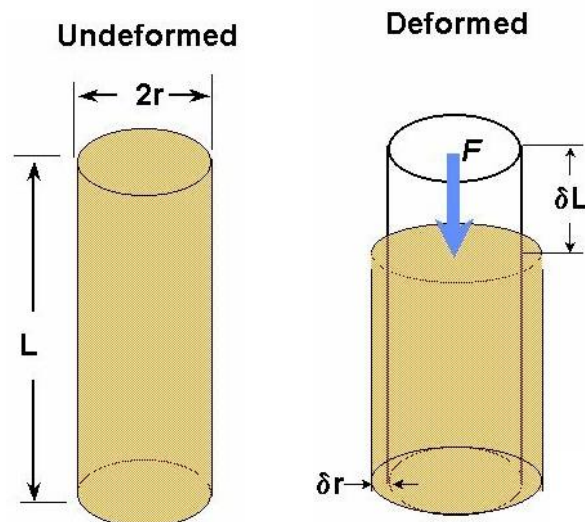


Figure 2. 12. Illustration of the concept of the Poisson's ratio. The ratio of the increase of the lateral deformation to the length contraction of a material.

2.2.2.4 Biot's Constant (α)

The Biot's constant, also known as poroelastic constant, gives an indication of the efficiency of the fluid to counteract the total overburden stress. This value will depend on the pore geometry and properties of the rock. It is described by the theory of poroelasticity (Biot, 1962), assuming: 1) interconnected pore system uniformly saturated with fluid, 2) the total volume of the pore system is small compared to the volume of the rock and, 3) considering the pore pressure, total stress acting on the rock and stresses acting on individual grains in terms of statistically averaged uniform values (Zoback, 2010). The values range between 0 and 1 where zero indicates there is no porosity in the rock.

2.2.2.5 Internal Friction Angle (ϕ) and Cohesion (S_0)

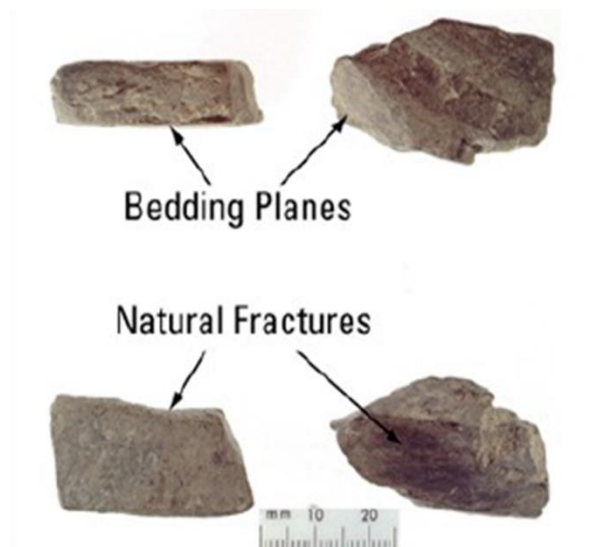
The internal friction angle in rock mechanics is the angle on the Mohr's Circle graph of the shear stress and normal effective stresses at which shear failure occurs. In other words, it is the ability of the rock to withstand a shear stress. The angle is measured between the normal and resultant force that is obtained when failure occurs. It can be determined in the laboratory by the Direct Shear Test or the Triaxial Stress Test (Geotechnicalinfo, 2012).

Cohesion (S_0) is simply the intercept on the τ axis at zero normal stress. In rock mechanics, true cohesion happens when cemented surfaces are sheared. However, in many practical applications, the term cohesion is used for convenience and it refers to a mathematical quantity related to surface roughness.

2.2.3 Rock Strength Anisotropy

During the analysis of the cavings' shape of the case study presented in this thesis, it was concluded that the relatively large and tabular cavings are a sign of failure in anisotropic formations. According to the Schlumberger Oilfield Glossary, an anisotropic formation is a formation with directionally dependent properties, normally permeability and stress (Schlumberger Oilfield Glossary, 2019). The stress anisotropy is very often greatest between overburden stress and horizontal stress in the bedding plane. And it is common that happens in tectonically active regions. Both, permeability and stress anisotropy can sometimes be related to each other.

The rock strength can be affected by the presence of weak bedding planes in shaley rocks. This influence can be defined as rock strength anisotropy. There are two important points to take into consideration, the relative weakness of the bedding plane and the orientation of the plane with respect to the applied stress. As shown with two case studies that the effect of strength anisotropy on the wellbore instability is very important in Zoback's book, the analysis of the wellbore instability in this thesis considers the possibility as well of having rock strength anisotropy, thus weak bedding planes were analyzed. Breakouts can give an indication of this problem when the width is not symmetric but with different angles, Figure 2. 13, this will also be analyzed in the following chapters (Zoback, 2010).



Key Characteristics:

- Majority of caving surfaces represent preexisting planes of weakness
- One or more parallel surfaces are common
- Surfaces tend to be relatively smooth and planar
- Failure initiates on high side of wellbore when well is nearly parallel to a plane of weakness

Figure 2. 13. Key characteristics of cavings bounded by preexisting planes of weakness (Schlumberger, 1998).

2.3 Pore Plugging Evaluation

2.3.1 Concepts

2.3.1.1 HPHT Filter Press

The equipment used during the methodology of this thesis is the Fann High-Pressure, High-Temperature Filter Press (Figure 2. 14). This apparatus is used to determine the filtration properties of drilling muds, cement as well as fracturing fluids. The filtrate is the liquid, usually water that passes through the filter cake and the filter medium, which can be a filter paper, ceramic discs of different porosities and screens of different mesh sizes, under differential pressure conditions. To evaluate this parameter is very important when it comes to treatment and control. The filtration behaviour can be affected by type of fluid, particle sizes, lost circulation materials, temperature and pressure.

The filter press simulates the filtration against a permeable formation at borehole conditions. Fann has two sizes available, 175 ml and 500 ml. In our case, we use the 500CT model which operates up to 500 °F (260 °C), 1800 psig on the cell and 750 psig in the back-pressure receiver. The pressurization can be achieved with carbon dioxide, bottled nitrogen, or an in-house gas supply (Tomlin, 2017).

The development of a new filter medium and set up of the filter press will be shown in Chapter 3 and 4. Using the cavings from the shale formation and an epoxy as a glue material, several discs will be built and tested.

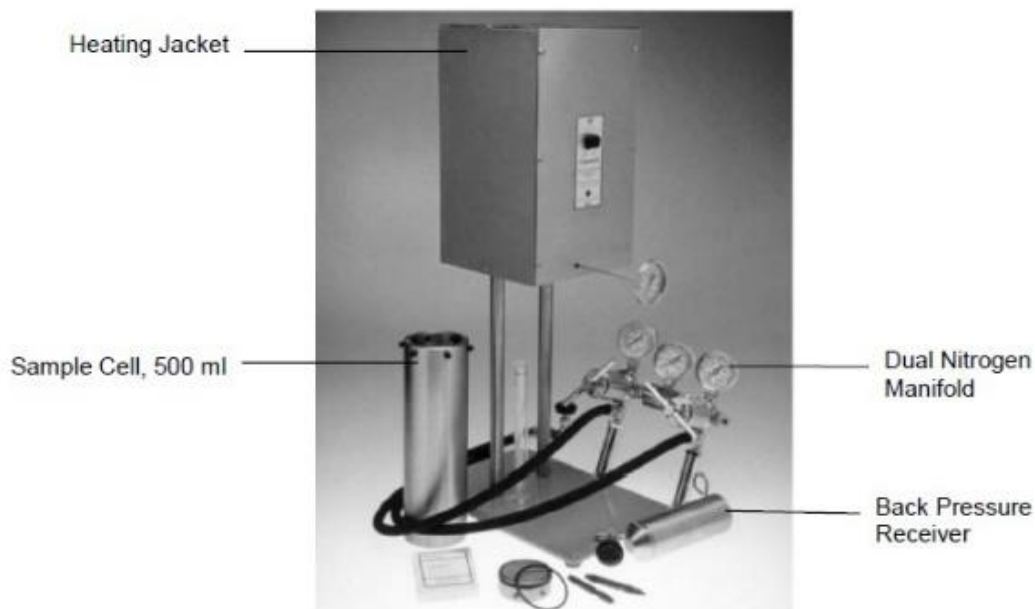


Figure 2. 14. HPHT Filter Press, 500ml. Model used at the Chair of Drilling and Completion Engineering.

2.3.1.2 Fracture Width

The fracture width is a very important parameter when selecting the optimum lost circulation material (LCM) due to the assumption that the shale formation might be micro-fractured, it was necessary to review the literature about this parameter.

To study the fracture width, distribution and network in shales started to be one of the main concerns with the boom of gas shale. It is known that the natural micro-fracture system increases the permeability of the rock matrix, especially in shale rocks. The challenge is to measure and determine the actual width of this micro-fractures. Since the beginning of the '70s, the Oil and Gas Institute – National Research Institute (NRI) has been performing analyses of micro-fractures on cores. The NRI performed 3D imaging (CT), 2D imaging (RTG) and PulsDecay method on 40 samples from the Baltic Basin. In order to distinguish the natural micro-fractures from the fractures generated from the core decompression they used a petrographic microscope to identify the fractures generated by decompression. Those are normally associated with very fine laminations. From their study, they obtained values of micro-fracture width range between 0.939 and 5.478 μm Table 2. 1(a) and mentioned that these values can be compared to the average size of the pores in conventional sandstones reservoirs. They also carried out the sensitivity analysis of the overburden pressure Table 2. 1 (b) with one sample at different confining pressures (Leśniak, 2015).

Sample number	Permeability [μD]	Fracture width [μm]	Permeability – matrix permeability [μD]	Fracture width [μm]
1	2	3	4	5
7	1.511	1.112	0.911	0.939
10	1.619	1.137	1.019	0.975
33	2.991	1.399	2.391	1.299
2	3.495	1.472	2.895	1.382
35	4.363	1.598	3.763	1.521
14	4.569	1.607	3.969	1.534
12	6.789	1.861	6.189	1.805
4	10.522	2.134	9.922	2.093
3	11.018	2.161	10.418	2.121
31	22.036	2.727	21.436	2.702
32	24.898	2.863	24.298	2.840
38	31.156	3.065	30.556	3.045
34	88.423	4.356	87.823	4.346
42	111.287	4.734	110.687	4.726
1	138.160	5.021	137.560	5.014
46	173.012	5.485	172.412	5.478

a

Confining pressure [psi]	Permeability [μD]	Width of microfracture [μm]
900	174.615	5.459
1125	118.762	4.798
1225	79.109	4.187
1400	60.083	3.817
1600	43.847	3.432
1800	30.474	3.034
2000	18.084	2.538
2500	7.765	1.885
3000	5.030	1.606

b

Table 2. 1. a) Results of calculation of the microfracture width (for 1 microfracture in a sample). b) Result of permeability measurements, the microfracture width calculated for various confining pressures (Leśniak, 2015).

2.3.1.3 Lost Circulation Material

Lost circulation or bridging materials are solids that are added to the drilling mud to create a bridge or blockage across the fractures or high permeable formations to prevent or minimize fluid loss or excessive filtrate. In the reservoir the LCMs are also used with

Background Information

the characteristic of being removable by acid, water or oil, in such manner that it can be clean after drilling and the permeability of the production zones are not affected (Schlumberger Oilfield Glossary, 2019).

These additives have been used in the oil and gas industry to prevent and remediate a problem of drilling fluid loss. It is applicable on different scenarios such as natural fractured formations, depleted reservoirs, wellbore instability, high permeable formations, induced fractures, wellbore strengthening, drilling pore pressure regressions and others. The selection of the proper lost circulation material (LCM) depend on different factors such as fracture size, Young's modulus, Poisson's ratio, stresses in the wellbore, well pressure (ECD), hole diameter, length of fracture and other wellbore conditions.

An analysis of the size distribution of the LCM and fracture width has to be carried out before just pumping the LCM into the well to plug the fractures or problematic zones. Different size particles have to be pumped in a specific sequence to create what is known as an effective bridging strategy. Modeling software can be used to determine or predict the required materials and the particle size distribution, Figure 2. 15.

Nowadays, many service companies have developed different types of LCM from different materials, structure, shape, size, etc. The most common are calcium carbonate (CaCO_3) in different particle sizes, resilient graphitic carbon material, different kind of fibers, normally ranging between 5 and 1200 μm . In very severe cases of fluid loss even coconut shell, mica or nutshell have been reported to be used as a common practice when it is required (Whitfill, 2008).

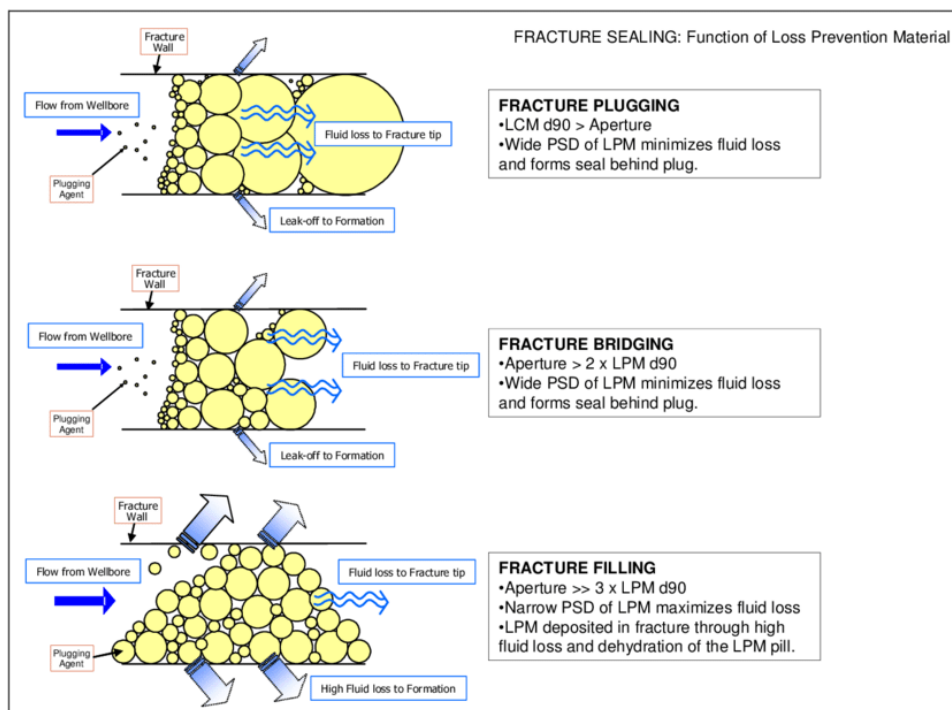


Figure 2. 15. Illustration of the fracture sealing: Function of Loss Prevention Material (Kageson-Loe et al., 2009).

As it has been previously mentioned in the first Chapter, during the drilling operations in wells of both fields AM1 and AM2, the resistivity logs were being analyzed and an overlapping on the shallow and deep curves was observed indicating a possible filtration into the formation during drilling. They normally use lost circulation material as a preventive measurement, CaCO₃ in different particle sizes from fine to medium and graphite. The effectiveness of the selection of this material is being questioned because filtrate has been still observed in the resistivity logs. One of the main concerns is to figure the fracture width of these formations, since it has been established in the previous topic "Fracture width" that the range of the fracture width in shales might be between 0.939 and 5.478 μm ; then it will be likely that a LCM in this range should be used. This process, analysis and results will be described in Chapter 3 to 5 once the micro CT scanner and pore plugging test have been described.

Chapter 3 Proposed Approach and Experimental Method

The descriptions of the methodology, main analyses and laboratory tests carried out in this master thesis are presented in this Chapter.

3.1 Methodology

3.1.1 When can we use the proposed methodology?

The following methodology applies to fields where wellbores present an instability problem in overpressured and potentially micro-fractured shale formations; cavings must be available for its analysis and proper characterization. It is important that the size of the cavings exceeds 3cm for the test to work properly.

3.1.2 Workflow

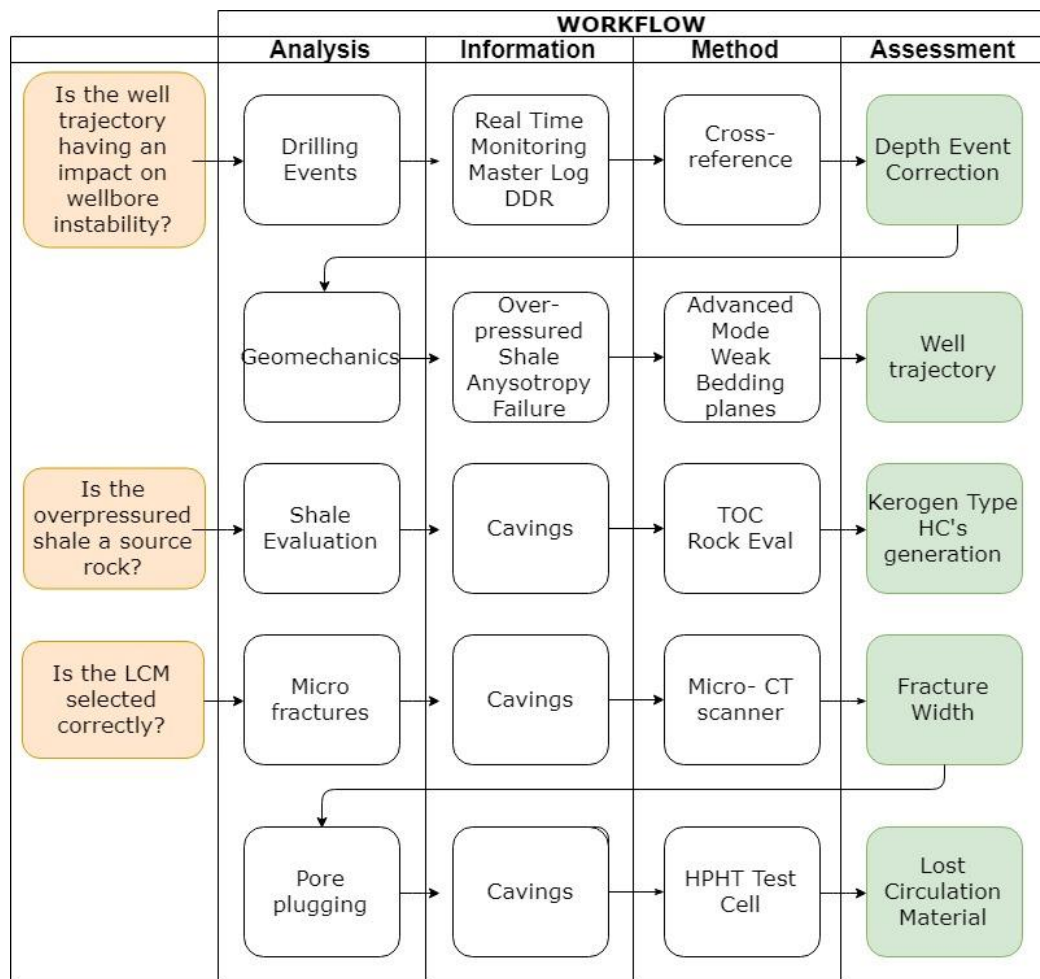


Figure 3. 1. Workflow followed in this study.

3.2 Geological Background

The company provided the information, figures and all the geological data mentioned in this section; some figures were modified, name tags deleted or changed, in order to comply with the requirements of the company.

The target of the wells drilled in the AM1 Field is the carbonate rocks of the Middle Cretaceous. The structure where the wells AM-1, AM-11, AM-21, AM-5 and AM-8 were drilled corresponds to an asymmetric anticline oriented NW-SE, limited to the NSW&E by inverse faults, F1, F2, F4 and F5, Figure 3. 2.

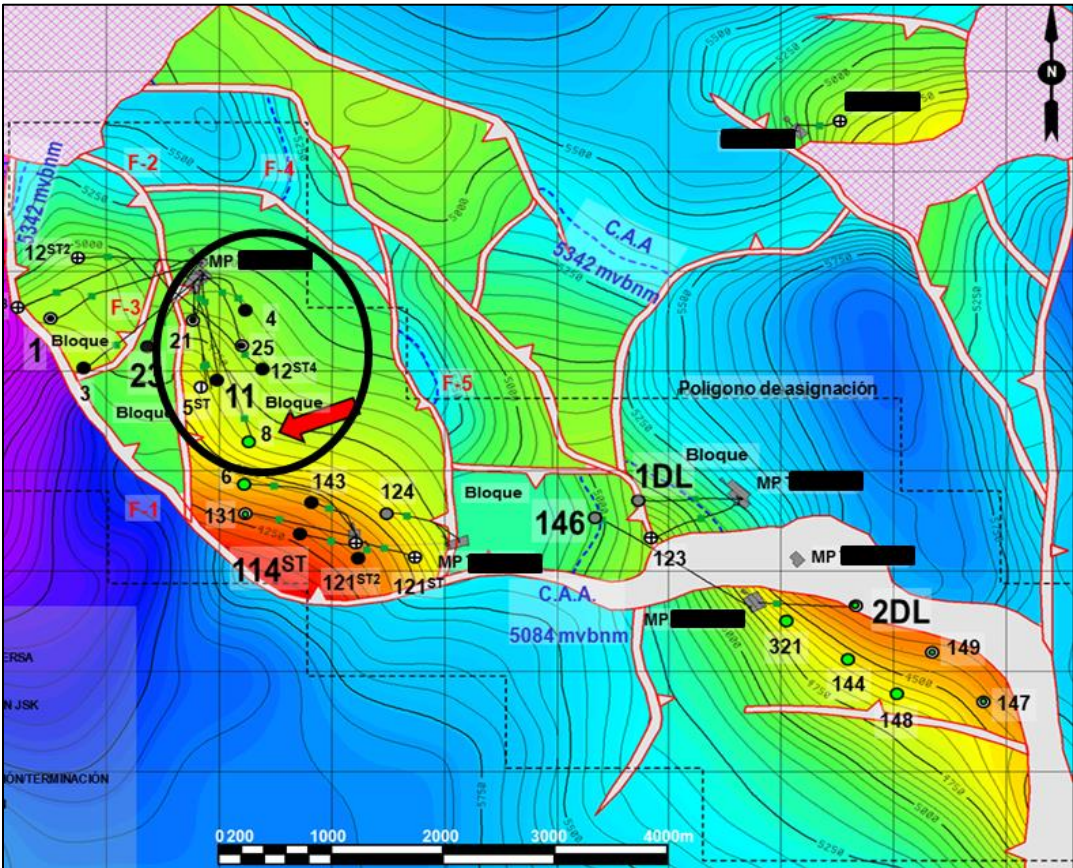


Figure 3. 2. Contour map of the reservoir of the field AM1, the circle area shows the area analyzed in this study. Company courtesy.

According to the company, the quality of the seismic information is from regular to good. In Figure 3. 3, the seismic section \overline{AB} shows a structure of an anticline resulted from compressive tectonic stresses, two inverse faults, F1 and F4, are present with a W - E orientation.

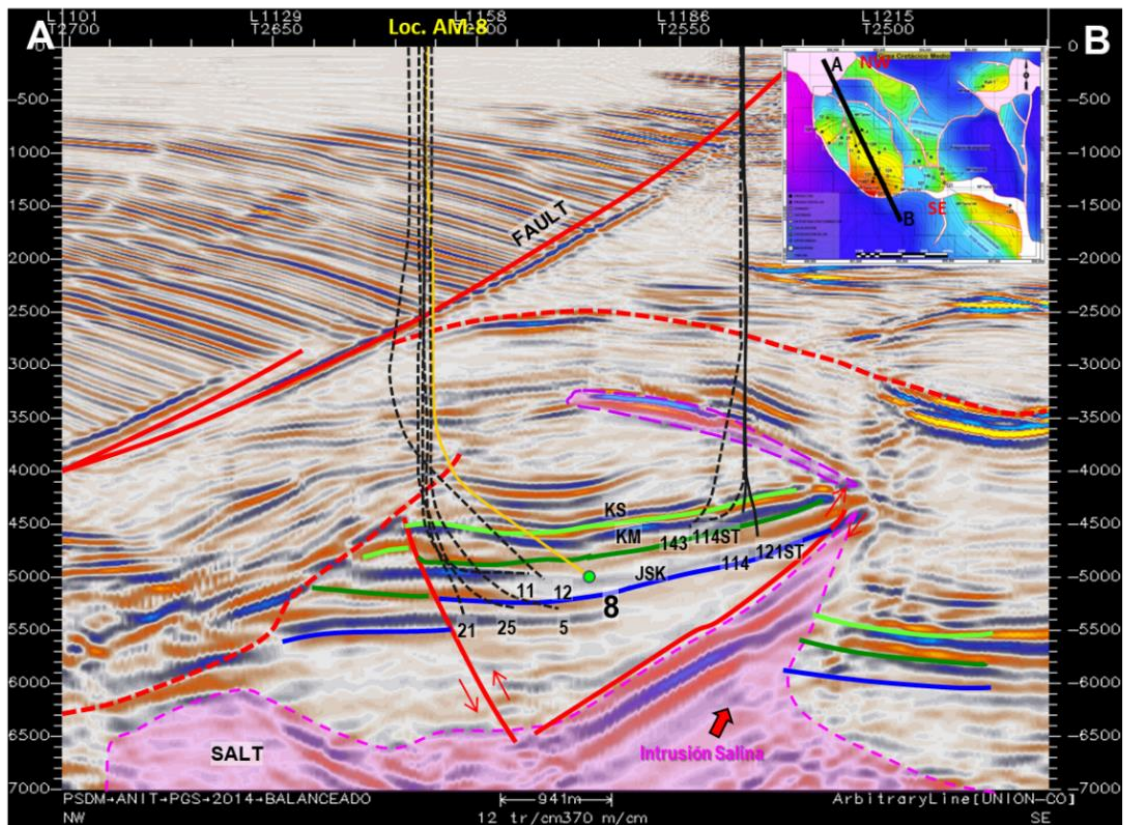


Figure 3. 3. Seismic in depth of field AM1. The seismic line is shown in depth domain with NW-SE orientation where the trajectories and targets of the analyzed wells are shown, two discontinuities are marked as red dash lines. Company courtesy.

The geological model of the AM1 Field can be observed in Figure 3. 4. The structural complexity of this play is the result of the interaction of tectonic stresses due to severe salt intrusion and compressive stresses, which is a characteristic of the naturally-fractured reservoirs of the region.

Proposed Approach and Experimental Method

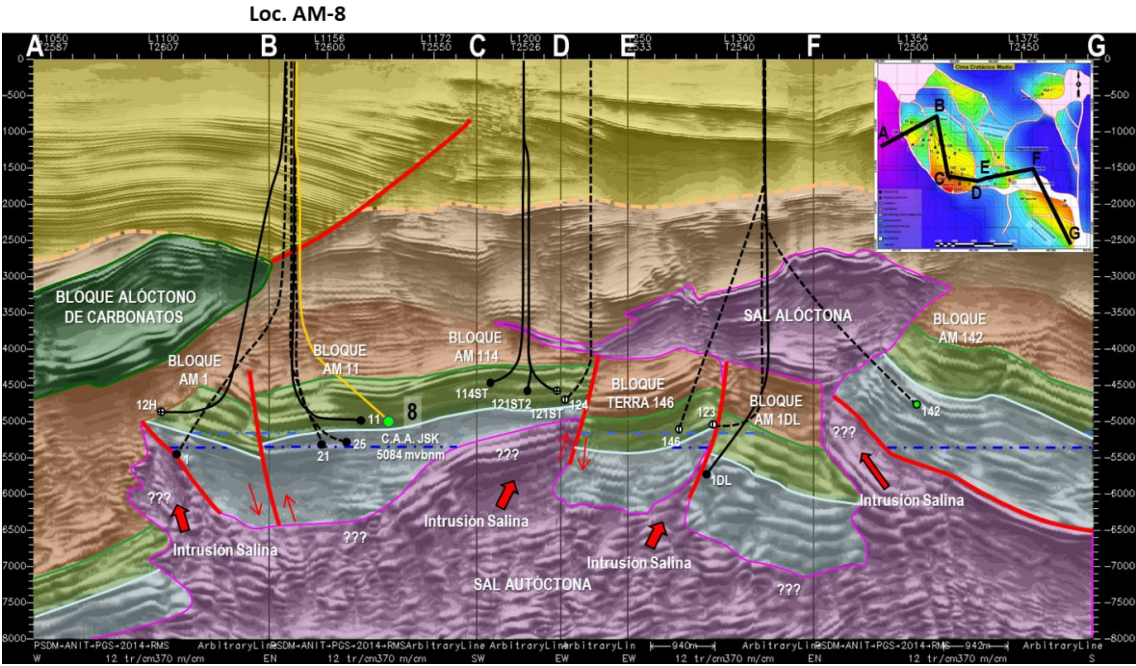


Figure 3. 4. Seismic in depth of field AM1 with RMS attribute. Company courtesy.

The geological column that the wells included in this analysis cross during the drilling activities comprises from the Plio-Pleistocene to the Middle Cretaceous ages.

The problem of the high volume of cavings occurred in the Cenozoic. The Cenozoic is the geological period from 66 million to 2.6 million years ago. It is divided into the Palaeocene Epoch (56 – 66 million years BP), the **Eocene Epoch (33.9 – 56 million years BP)**, the Oligocene Epoch (23 – 33.9 million years BP), the Miocene Epoch (5.3 – 23 million years BP) and the Pliocene Epoch (2.6 – 5.3 million years BP). In *Table 3. 1*, the geological column of this area (AM-1 site) is shown along with the description of each formation. The Tertiary corresponds to formations A1 to B3 while the Mesozoic to formations C1 to C5.

The formation B2 is the one that is being analyzed in this thesis. This formation corresponds to the Eocene Epoch where all the instability problems occurred. It is important to mention that not all the wells drilled from site AM-1 (exploratory well) presented the problem of cavings. In following sections, the drilling events and details of these wells will be explained.

Description of B2: Light gray and greenish gray shale, bentonite appearance, some calcareous and sandy parts. Traces of white mudstone.

Formation	Description
A1	White quartz sand, medium to coarse grained, angular, poorly classified, with light gray sandstone traces, fine to medium grained, cemented in calcareous clayey material.
A2	
A3	
A4	Light gray and greenish gray shale with traces of sandy shale and mudstone light brown and cream.
A5	
A6	
B1	Light gray, dark gray and gray greenish shale. Traces of green olive bentonite and white to cream mudstone.
B2	Light gray and greenish gray shale, bentonite appearance, some calcareous and sandy parts. Traces of white mudstone.
B3	Brown reddish and greenish gray shale. Reddish brown marl and traces of white to cream mudstone.
C1	Mudstone
C2	Mudstone
C3	Mudstone
C4	Mudstone - Wackestone
C5	Mudstone - Wackestone

Table 3. 1. Geological column and description of the formations of the wells drilled in the AM1 field. Company courtesy.

3.3 Data Acquisition, Quality Control and Validation

The information acquired from the company had to be reviewed and validated in order to have a better understanding of the problems, be acquainted with the field and to verify if the information was consistent.

The data requested to the company were the following:

General Information: Drilling Program, Schematics (planned and actual), Trajectory (planned), Survey (actual), Rig Data Sheet, KB, Coordinates surface and target (actual), Coordinates System, Template (Domino)

Geophysics: Logs (Gamma Ray, Resistivity, Density, Sonic Compressional, Sonic Shear, Sonic Stoneley, Porosity, FMI, Caliper), Seismic (Interpretation/General Information)

Geology: Geologic Column (Planned and actual), Geological Model (Interpretation / General Information, Isopach map, Contour map, Shale characterization)

Drilling: Fluids (Mud Properties, Drilling mud test), Bit (Bit Record), BHA's (Reports), Formation Tests (LOT, FIT, MDT), Drilling Events

Proposed Approach and Experimental Method

Monitoring: DDR, Real Time Monitoring Parameters, Mud Logging, Observations in Shakers, Photos (Cavings/Cuttings)

Samples: Fluid (Drilling mud, Formation fluid), Shale (Cuttings, Cavings, Core)

As expected, not all the information requested was available but most of the information was provided (see Appendix B).

Regarding QC, the quality control of the well logs can be performed by a rigorous control of depth, calibrations, signal processing and operating procedures. All these processes were not covered in this thesis' purpose. The logs were obtained from the petrophysicist specialist and were taken as valid.

Well selection

At the beginning of this analysis, the selection of the wells to be included was performed according to the distance with each other, specifically from well AM-8 - which was the last well to be drilled - and the one that according to the company presented the biggest issues during the drilling operations in the 12 ¼" section.

While reviewing the information, a power point slide showing the cavings in other wells came to my attention, and I decided to use at least two wells where the cavings were present and the photos were available, for comparison and analysis purposes. Another well where cavings were present and the caliper was completely available for calibration. In addition, one well where no cavings were reported. For the latter, it was decided to select the exploratory well due to the extensive information that this one was able to provide. It is important to mention that even though it is going in a different direction, the stratigraphic column that crosses it is the same one as the other three wells and it is built from the same template or drilling site.

This field has one exploratory well, AM-1, and two appraisal wells, AM-1DL and AM-2DL. After a successful recovered oil production, the company started the development of the field. As it can be seen in Figure 3. 2, the field is divided by a reverse fault system, and four drilling sites were located to cover the whole area. As it was explained by the company specialists, in this field, just wells drilled from the AM-1 drill site presented the problems of cavings and not all of them as mentioned before.

The wells drilled from other drilling sites such as AM-1DL and AM-2DL and their correspondent development wells present other kinds of problems and cross different geological columns. The reason for this is the presence of a salt dome in the southeast area of the field. Having said that, the wells located in the drill site AM-1 are the ones taken into account for this analysis.

From AM-1 drill site, the following wells were drilled: AM-1, AM-3, AM-4, AM-5, AM-8, AM-12, AM-21, AM-23, AM-25. The trajectories of every well and their respective sidetracks are displayed in Figure 3. 5.

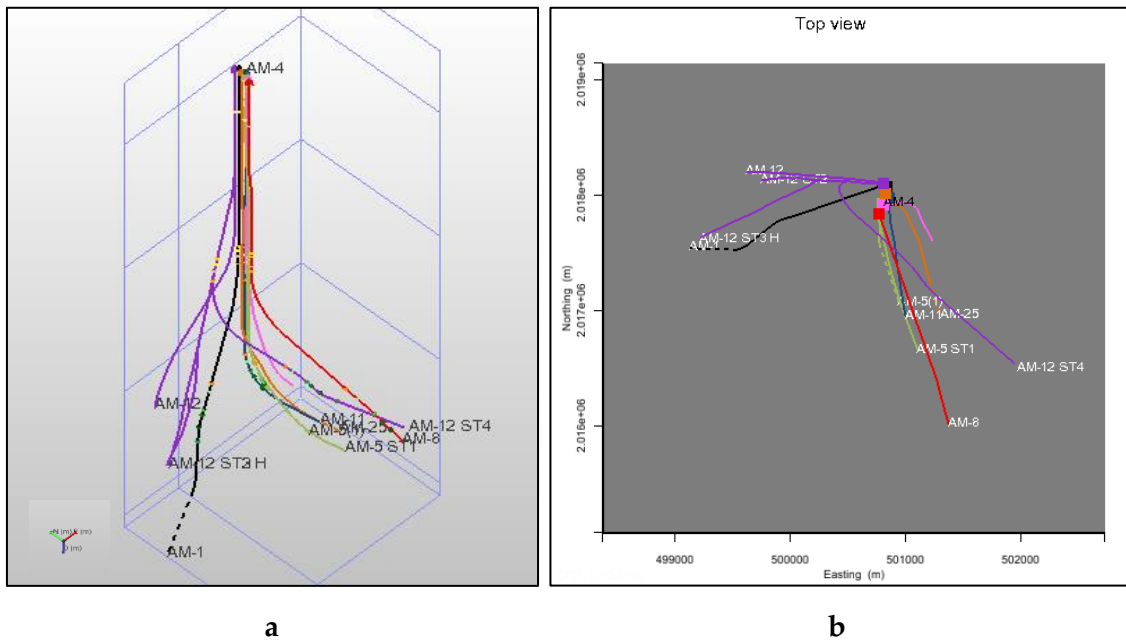


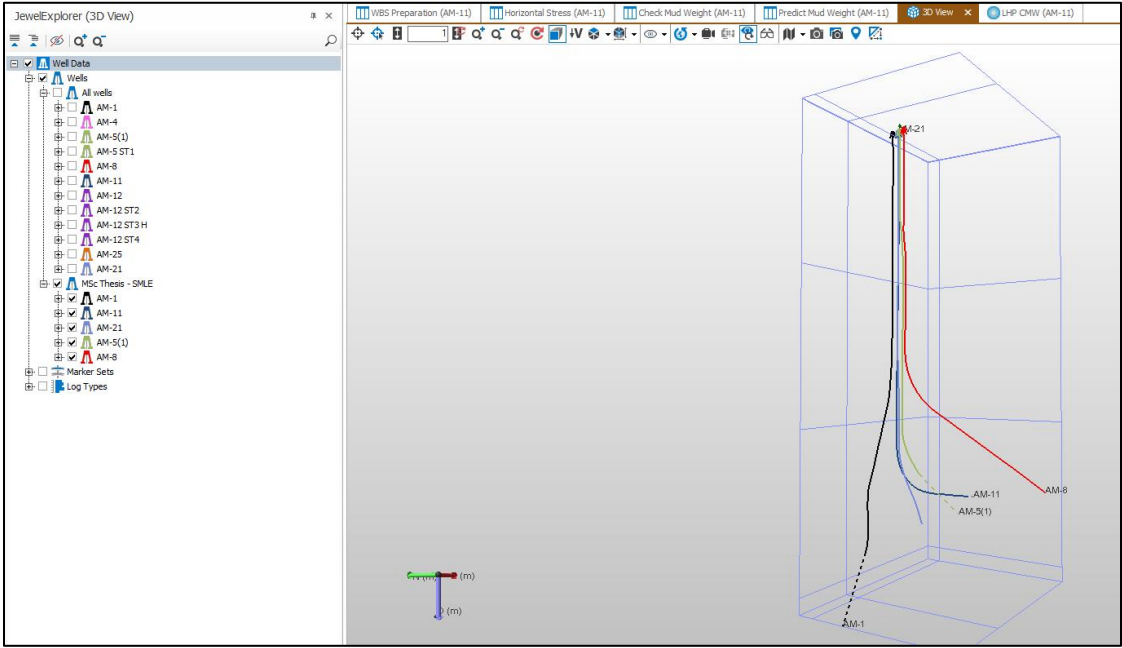
Figure 3. 5. a) 3D and b) 2D views from JewelSuite™ showing all the wells drilled from drill site AM-1.

As mentioned before, due to the workload and time of analysis, it was decided to select four wells including the exploratory well AM-1, Figure 3. 6.

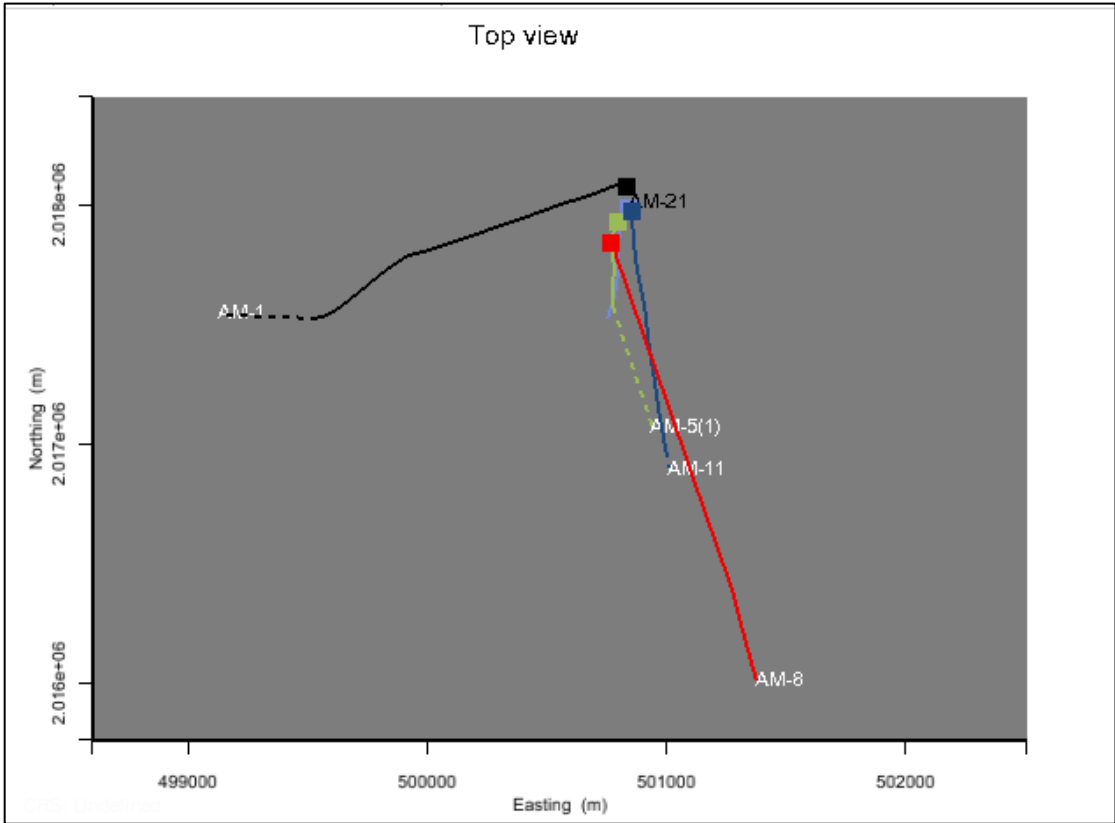
The wells selected and analyzed in this thesis are:

- **AM-1:** Exploratory well, no cavings reported
- **AM-11 or AM-21:** Complete data set, caliper log and photos, cavings reported
- **AM-5:** Complete caliper log, cavings reported
- **AM-8:** Last well drilled, cavings reported

Proposed Approach and Experimental Method



a



b

Figure 3. 6. a) 3D and b) 2D view of the selected wells for this analysis.

The wells in this field were drilled in the period 2008-2017. The selected wells for this analysis were drilled in the following order: AM-1, AM-11 or AM-21, AM-5 and AM-8. The timeline is important to mention in order to have a better understanding of the drilling learning curve and the influence of the knowledge acquired with every well

drilled. For this reason, the data presented and analyzed will be displayed in chronological order.

3.4 Drilling Events Analysis

3.4.1 Integration of the Sensor Data into the Drilling Events Analysis

An important task to properly assess an instability problem in a well is the complete understanding and detailed analysis of the drilling events and their causes. Most of the time, the drilling events are just taken from the Daily Drilling Report (DDR) and used to calibrate our geomechanical model. There are other sources that can provide useful and reliable information, such as the master log or sensor data (real-time monitoring).

In this master thesis, a methodology is proposed to analyze and cross-reference the data obtained from the DDR, master log and real-time monitoring using the available data from one of the wells of the case study field. Fortunately, the latest drilled well in field AM1, well AM-8, has the data of real-time monitoring from 850md (20" casing seat) to 5803md (total depth) available. With the support of TDE Thonhauser Data Engineering GmbH and its software, proNova, it was possible to analyze the data in a very detailed manner, especially the section where the cavings and wellbore instability issues were worsening the most.

In Figure 3. 7, the sensor data of well AM-8 are being displayed as follows:

- In the first horizontal track: Bit and hole depth over the full drilling and completion time (time vs depth navigation track) / blue square shows the selected time period for detailed analysis in the tracks below
- Second: Rotation (RPM) and torque, selected period
- Third: Pump pressure and mudflow, selected period
- Fourth: Hook load, block position and weight on bit (WOB), selected period
- Last track: Bit and hole depth, selected period

Proposed Approach and Experimental Method

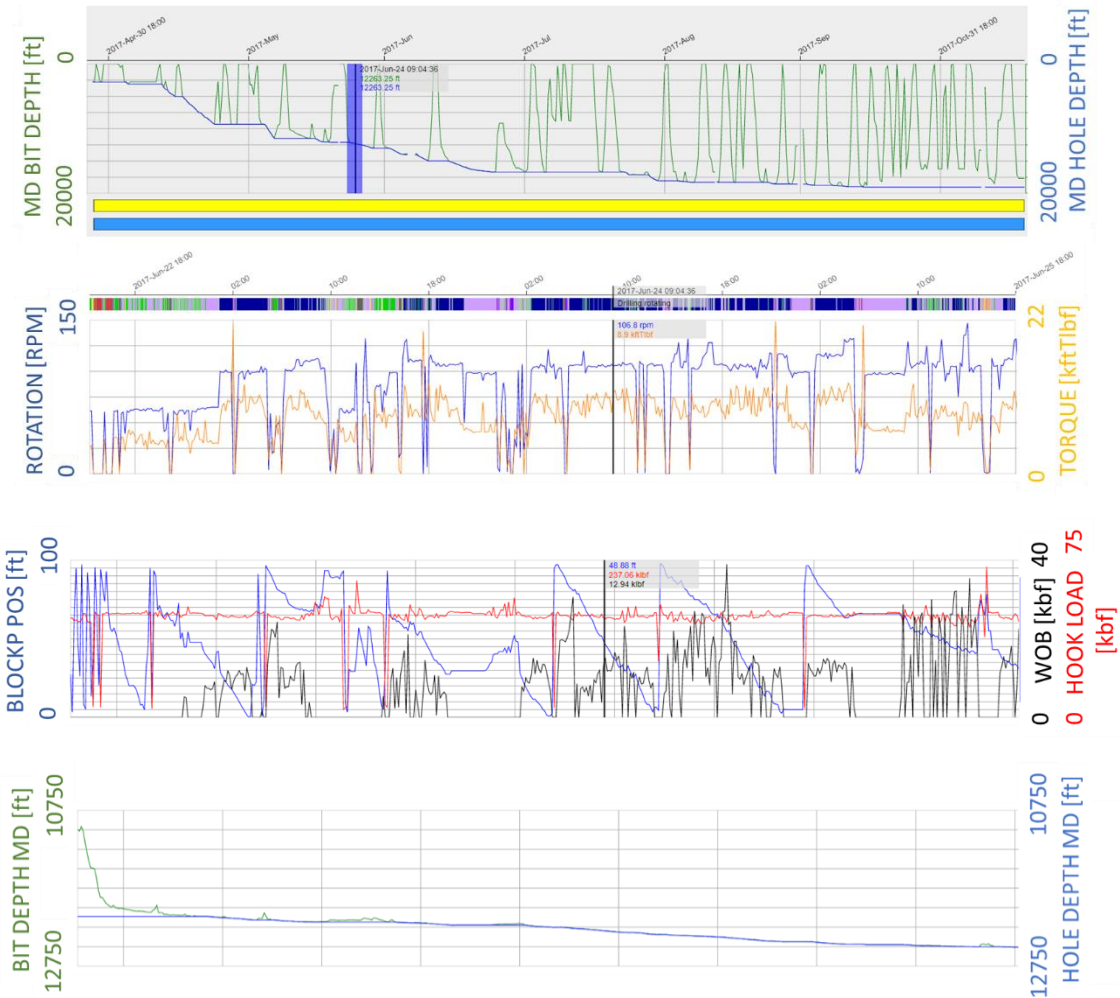


Figure 3. 7. Overview of the drilling parameters using the proNova software by TDE, well AM-8.

In order to identify each drilling event at a certain depth, the sensor data have to be correlated with the DDR and the drilling parameters at these time and depths should be thoroughly analyzed. To perform this task in an efficient manner, the ideal is to have at least two or three monitors to be able to navigate, manipulate and visualize the information simultaneously.

First of all, it is important to read the detailed DDR instead of just reading the summary because in the daily summary, only the major activities or problems that occurred are mentioned. It is necessary to categorize and define every event such as a tight hole, stuck pipe, pack off, ballooning, etc. When a drilling event is found in the DDR, the exact date and time have to be selected in the proNova software for a detailed visualization. The symptoms of the problems related with the wellbore instability, depending on the event of course, will be normally associated with a change in torque, rotation and pump pressure. The rig site indications are being added in Appendix A.

Once the time and date have been selected and zoomed on proNova, the description of the activities has to be understood and related to the values of the different parameters. For example, Figure 3. 8, on 15th of June, from 8:00 to 12:00hrs, a stuck pipe event was reported. In the text the crew mentioned: *“With 12 ¼” bit and directional BHA it was drilled*

to 3523m ... drilling parameters ... where the activities were suspended because it was observed four times stuck pipe." If only this information is taken, the geomechanical model would be calibrated with an event of stuck-pipe at 3523m. But if the sensor data are cross-referenced with this event, then it can be seen that the four events mentioned, occurred at different depths: 3512m, 3521m, 3517m and 3522m.

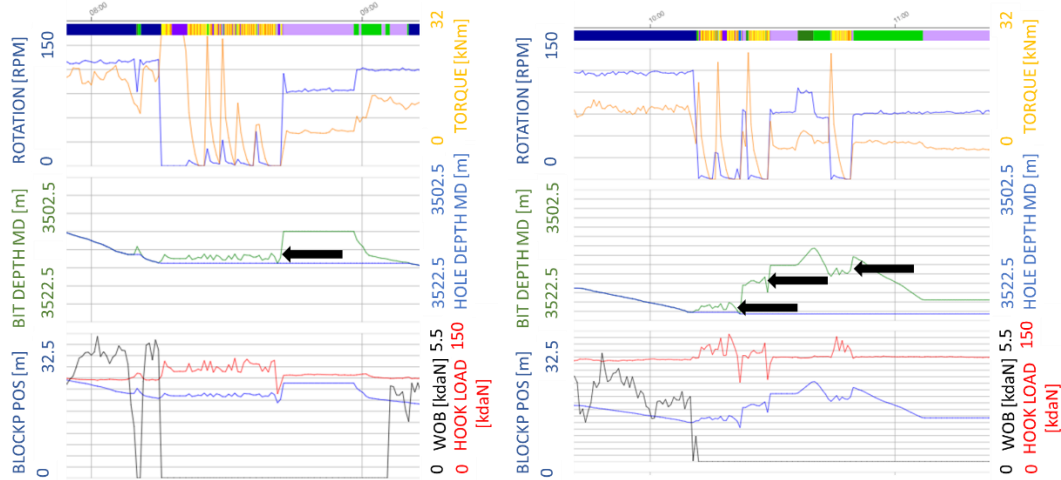


Figure 3. 8. Example of a stuck pipe event corrected by the real-time monitoring data, AM-8.

The result of integrating the real-time monitoring into the analysis of the events, for the 12 ¼" section, is shown in Figure 3. 9. There are some events, marked in black in the last track that were reported during trips using a higher density (1.84 g/cc).

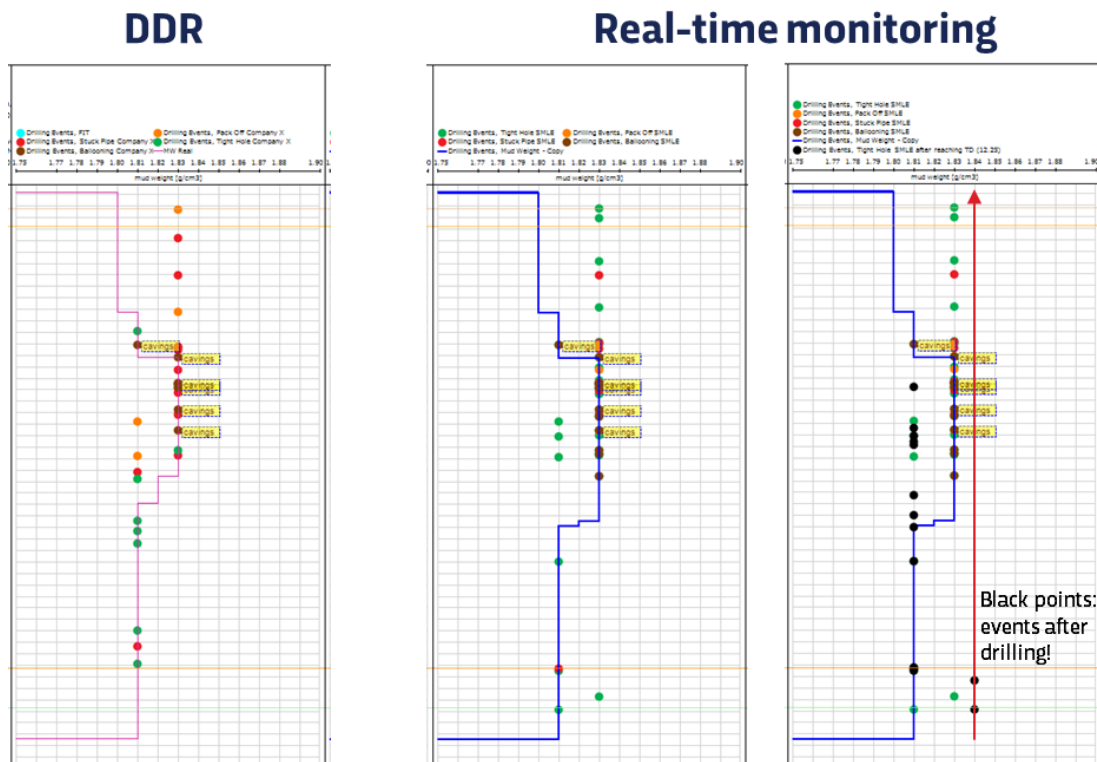


Figure 3. 9. Comparison of the drilling events obtained just from the DDR and real-time monitoring, well AM-8.

Proposed Approach and Experimental Method

It is important to have a record of the events including the crucial information that will provide a better understanding of the problems. A suggested heading for an Excel spreadsheet includes:

1. Date
2. Time
3. Formation
4. Type of drilling event
5. Bit depth (at the moment of the event)
6. Hole depth
7. Schematics
 - a. Hole section (bit size)
 - b. Previous casing size and depth
8. Fluid
 - a. Type of drilling fluid (OBM/WBM)
 - b. Inlet mud weight (static and dynamic)
 - c. Control mud weight (static and dynamic)
9. Shale shakers observations
10. Lithology
11. Interpreted cause/mechanism associated with the drilling event
12. Relation between the geological aspects and the drilling event
13. Summary of the drilling activity

Finally, it is recommended to plot the drilling events, actual mud weight and ECD (if available) in terms of time and depth. Since some events occur during not only drilling operations but also during trips, running in or pulling out, in this type of plots (Figure 3. 10), it can easily be observed in what conditions each kind of problem occurred.

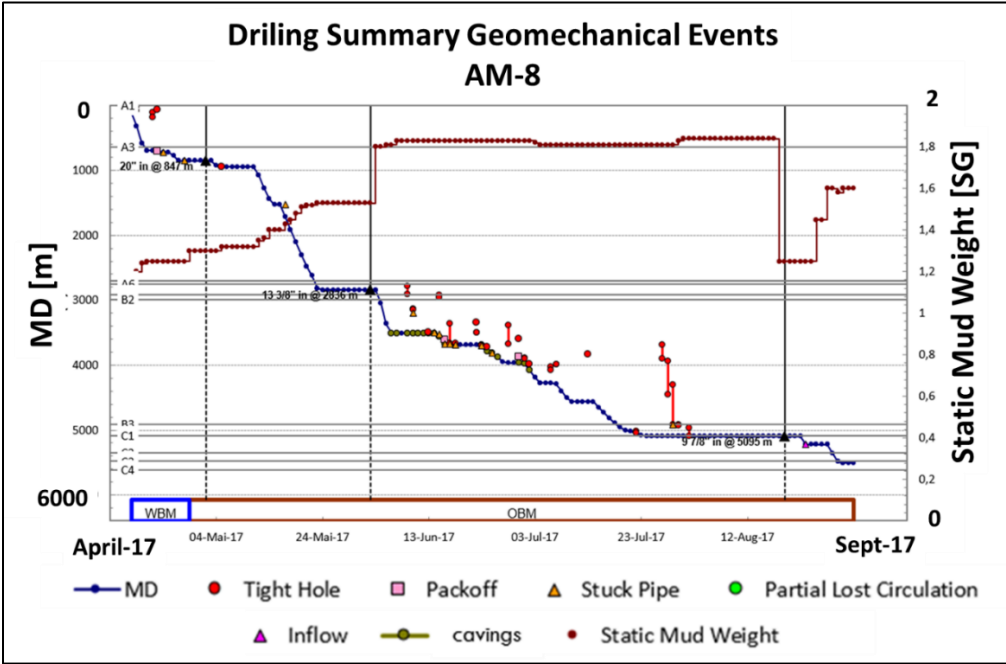


Figure 3. 10. Example, plot of drilling events, mud weight, casings and top formations in terms of time and depth, AM-8.

3.4.2 Drilling Events

The methodology explained in point 3.4.1 was applied only to analyze the drilling events in well AM-8 because it was the only one provided by the company that had the real-time monitoring data of the complete 12 ¼" section and that was drilled from the AM-1 site (area of study). The DDRs of wells AM-5 and AM-11 were thoroughly read and analyzed. At the beginning, AM-1 (exploratory well) was not contemplated to be added in this analysis because it didn't present cavings during the drilling operations. Furthermore, it has a different direction than the analyzed area. However, after reviewing the information of the wells involved, it was decided to include well AM-1 in the analysis for the information that it could bring being the exploratory well, as well as to be compared it with the wells that presented the cavings. For these reasons, the events of this well were taken from the company files.

The summary of the drilling events including the mud weight, the schematics and caliper logs available, is displayed in Figure 3. 11 and Figure 3. 12 . In well AM-1, the first well drilled in the area (exploratory well), there were no cavings reported even if an enlargement of the caliper log is observed.

During the drilling operations of wells AM-11, AM-5 and AM-8, there were cavings reported several times at different depths but most of them are reported between 3300md and 4100md in the unit B2, which corresponds to the overpressured shales. Nevertheless, the cavings are reported at the interval mentioned before, the caliper log shows the enlargement in diameter slightly shifted, overlapping the reported cavings, from 3000 to 4000md, units A6 to B2. This might be shifted due to the lag time that is the time required to pump cuttings or, in this case, cavings, from each particular depth to the surface.

Proposed Approach and Experimental Method

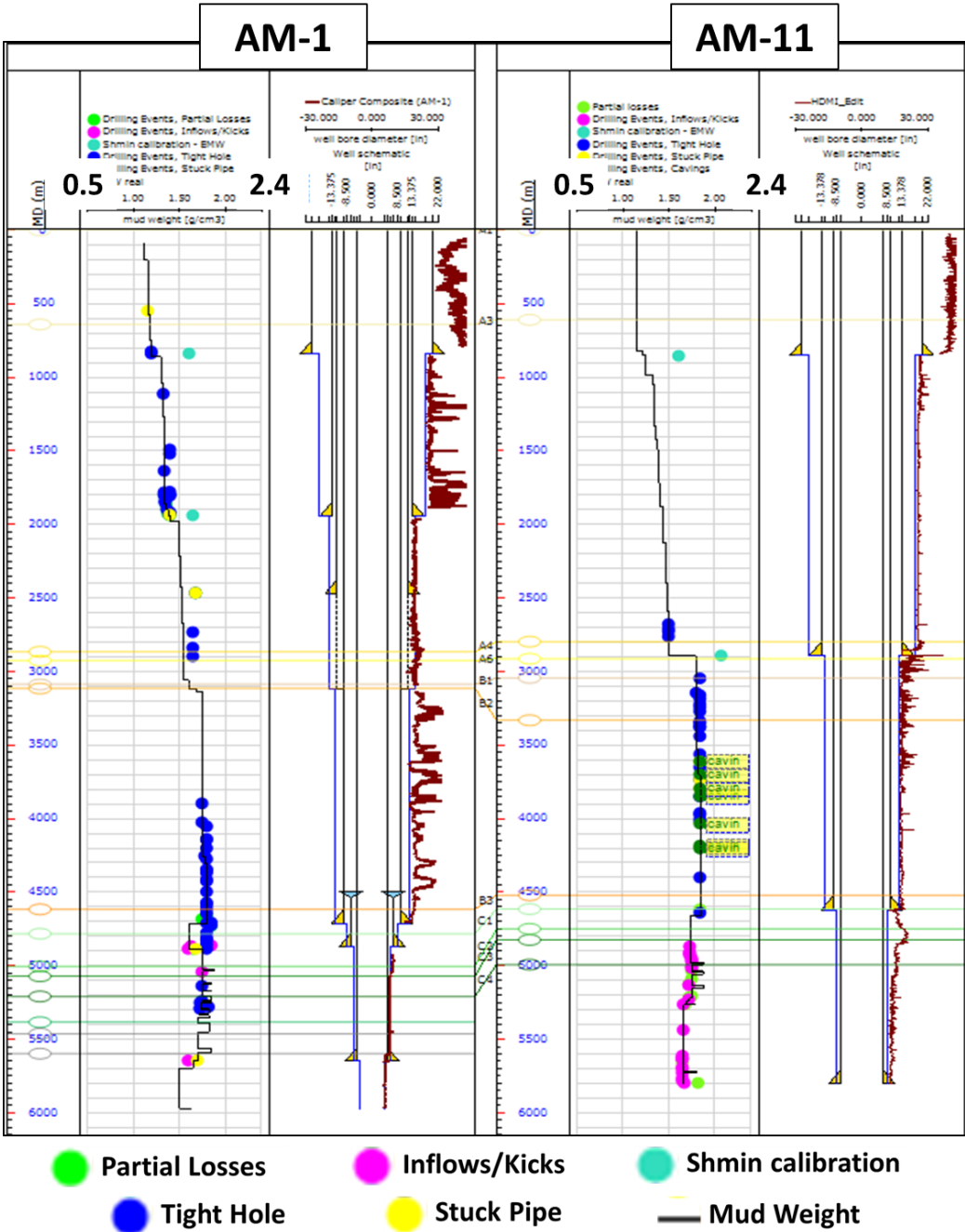


Figure 3. 11. Overview of the drilling events, actual mud weight, schematics and caliper logs of wells AM-1 and AM-11.

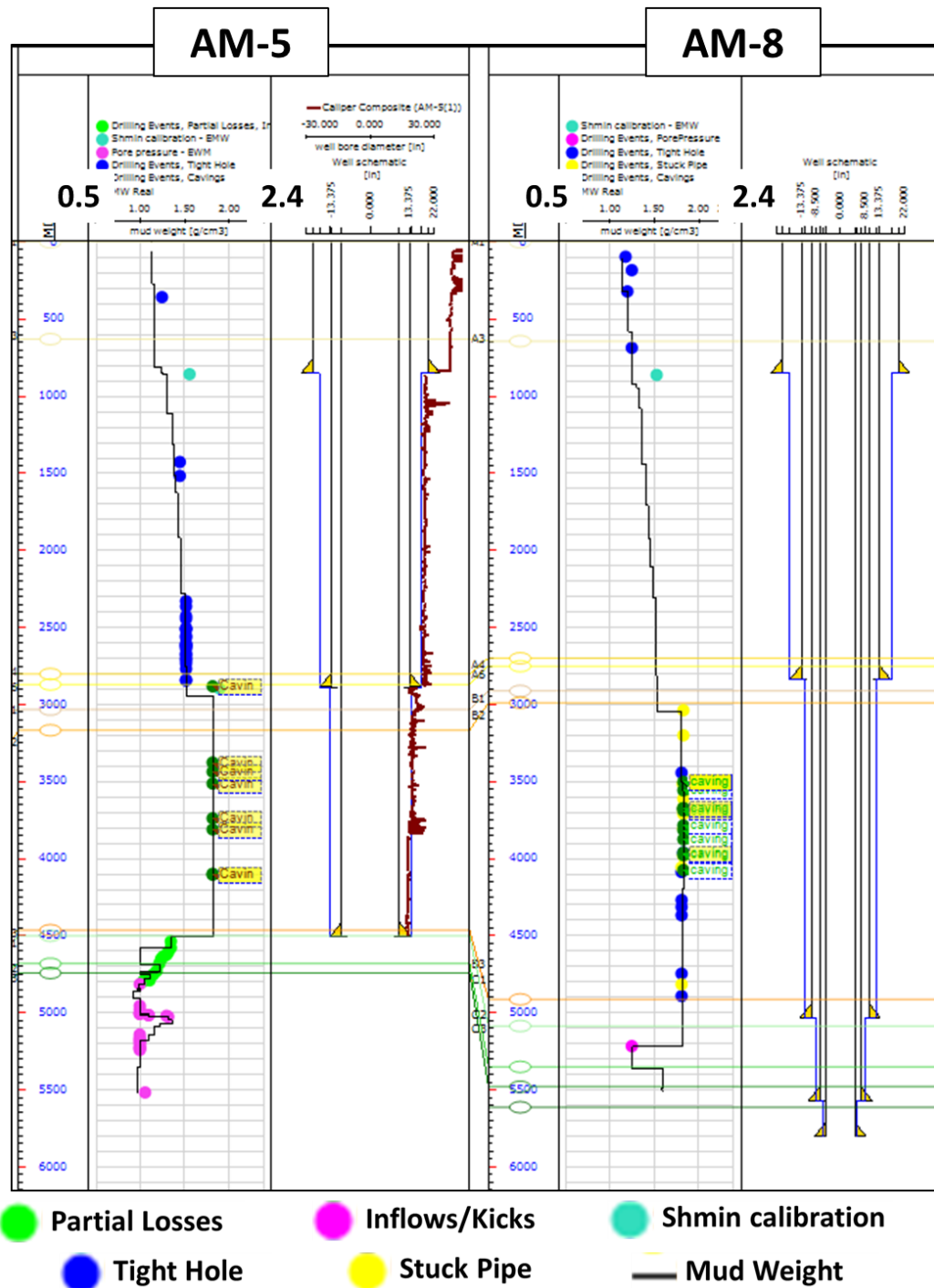


Figure 3. 12. Overview of the drilling events, actual mud weight, schematics and caliper logs of wells AM-5 and AM-8. The caliper log of the last one was not available even though it was requested.

The cavings from wells AM-21, AM-11, AM-25, AM-4 and AM-8 recovered at the surface are shown in Figure 3. 13 to Figure 3. 15. From these images, one can analyze their morphology. The morphology analysis of these cavings was a critical aspect for the geomechanical model in this case study since their size, shape and appearance were giving the indication of the failure mechanism.

Proposed Approach and Experimental Method

There are two main failure mechanisms: shear failure (isotropic rock failure) and failure along pre-existing weak planes like fractures or bedding planes (anisotropic rock failure) (Edwards et al., 2004). As mentioned before, each type of failure mechanism can be identified by analyzing the morphology of the cavings. The three main shapes of cavings are tabular or blocky, angular and splintered.

Looking at the shape of the cavings in Figure 3. 13 to Figure 3. 15, we were able determine that most of them presented the similar tabular shape with parallel and planar surfaces and some of them were eroded due to the friction against the borehole while travelling to the surface. According to Osisanya (2011) and Bradford et al. (2000), these tabular cavings may originate from weak bedding planes or unstable natural fractures and they might be also caused by the invasion of drilling fluids into the weak planes or fractures. They also mention that the cavings present flat faces and are often induced by selecting a low mud weight. Therefore, the failure mechanism predicted from the morphology of the cavings in this analysis was an anisotropic rock failure due to micro-fractures and weak bedding planes. In addition, Zoback et al. (2010) states that due to the permeable nature of these shear-induced cracks, they present a plane of weakness that allows the drilling fluid to go into the formation, which was also observed in the resistivity logs of the analyzed wells. They added that a preventive measure would modify the mud weight or change the trajectory of the well to provide additional support to the wellbore wall.

Seeing the photos and the information just mentioned, it was determined to use the advanced mode on JewelSuite™, which considers weak bedding planes calculations based on bedding dip, azimuth, cohesion and friction. The bedding dip and azimuth parameters were obtained from the seismic sections in terms of depth along well AM-11. While the bedding cohesion and friction were determined according to the type of rock, shale in this case, and a trial and error approach.

The Modified Lade criterion was chosen because unlike Mohr Coulomb, it considers the magnitude of the intermediate stress. Additionally, the Modified Lade criterion shows a better fit in rocks behaviour when comparing both models and still similar to Mohr-Coulomb, it considers cohesion and internal friction as rock properties (Zoback, 2010).

The mud weight used in this section (bit size 12 ¼"), azimuth and inclination of each well is shown in Table 3. 2:

Well	Depth [m]	Mud weight [g/cc]	KOP [m]	Inclination [°]	Azimuth [°]
AM-1	3140 - 4714	1.75 - 1.80	3180	1.6 - 36	0 - 250
AM-11	2897 - 4661	1.79 - 1.84	4320	2 - 27	0 - 170
AM-5	2940 - 4498	1.82	4110	2.8 - 28	0 - 177
AM-8	3050 - 5030	1.80 - 1.83 - 1.81	3037	2.3 - 55	0 - 160

Table 3. 2. Mud weight used during drilling the problematic area and inclination and azimuth from the top to the bottom of section 12 ¼" bit size.

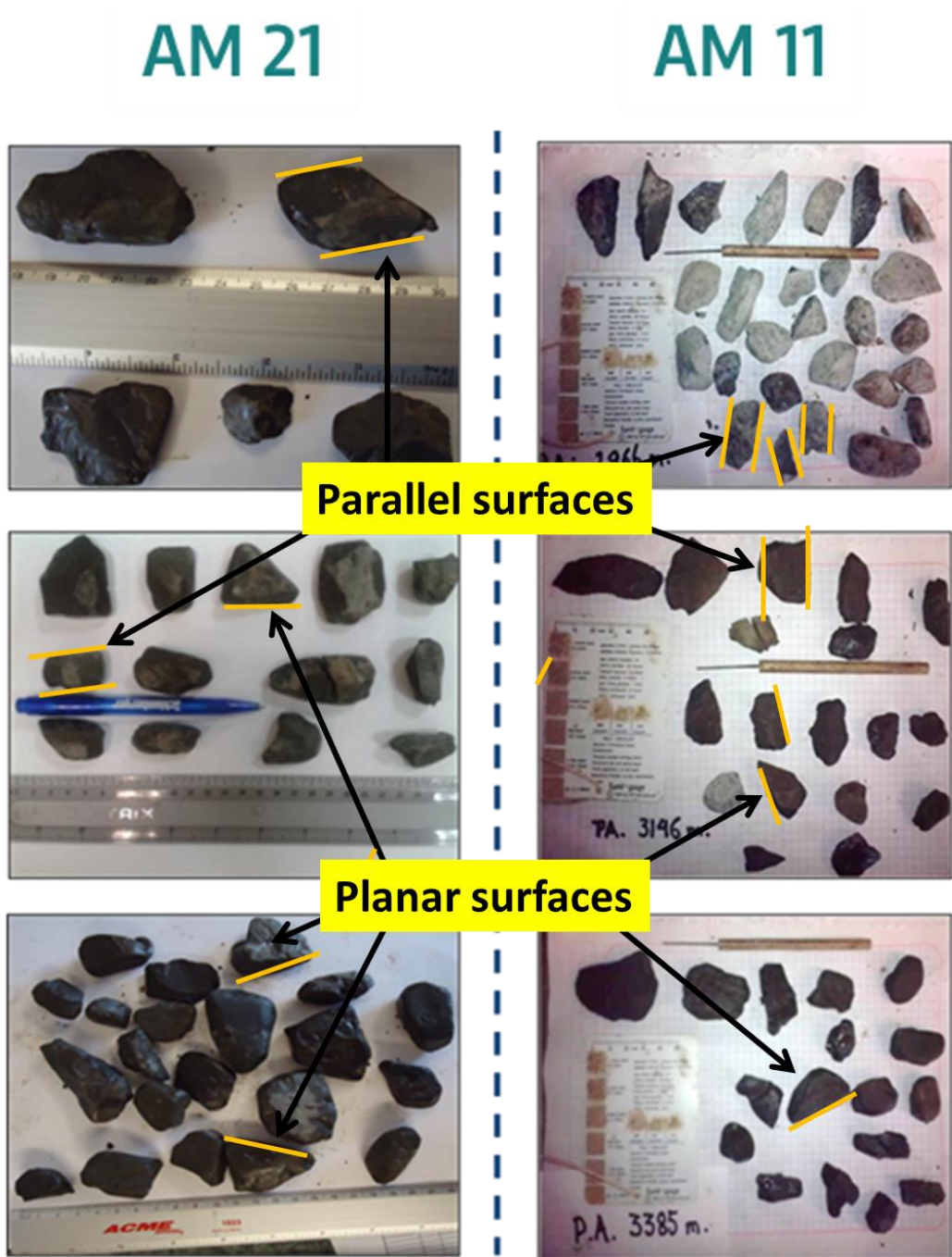


Figure 3. 13. Cavings from wells AM-21 and AM-11. Company courtesy.

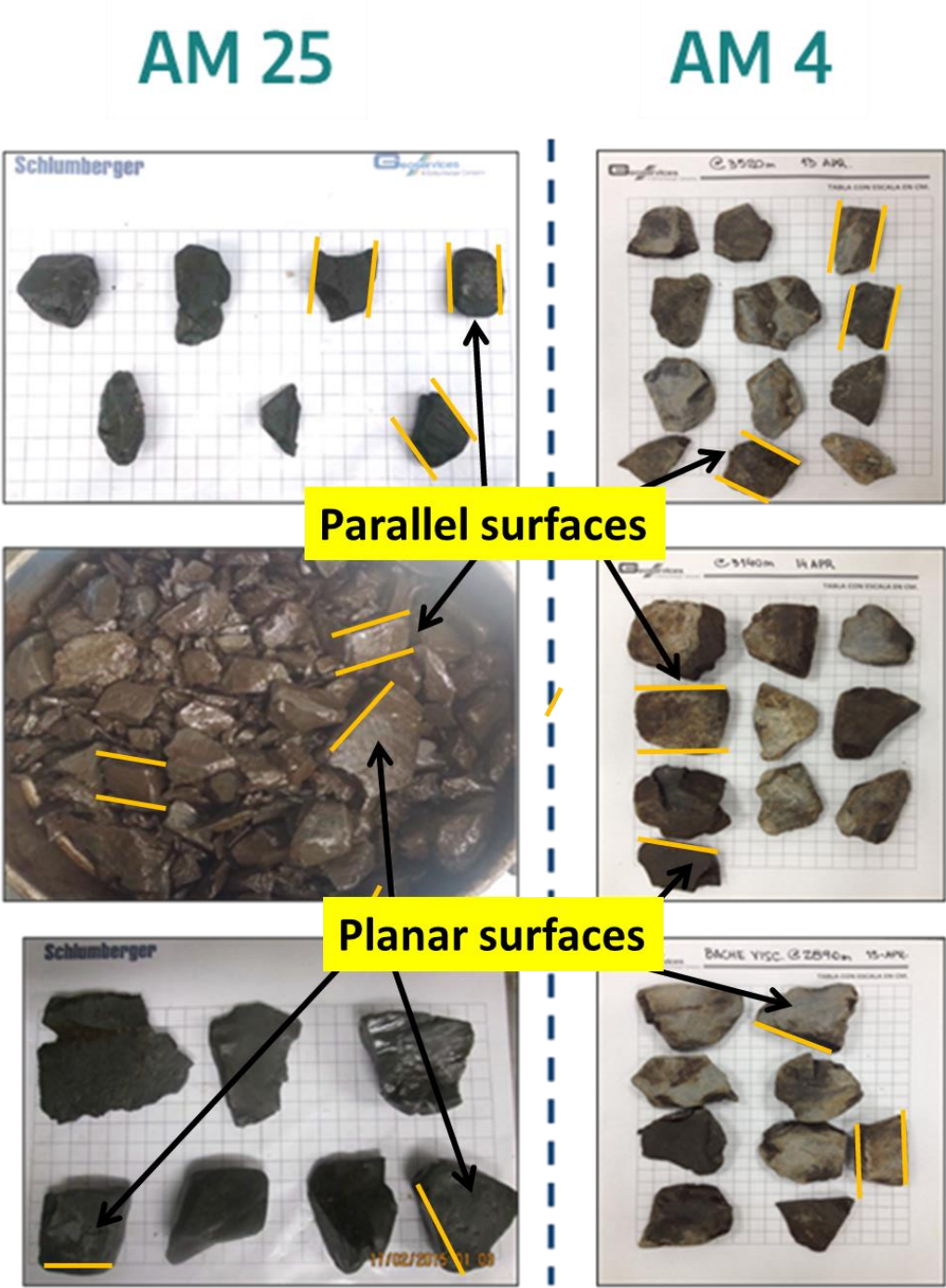


Figure 3. 14. Cavings from wells AM-25 and AM-4. Company courtesy.

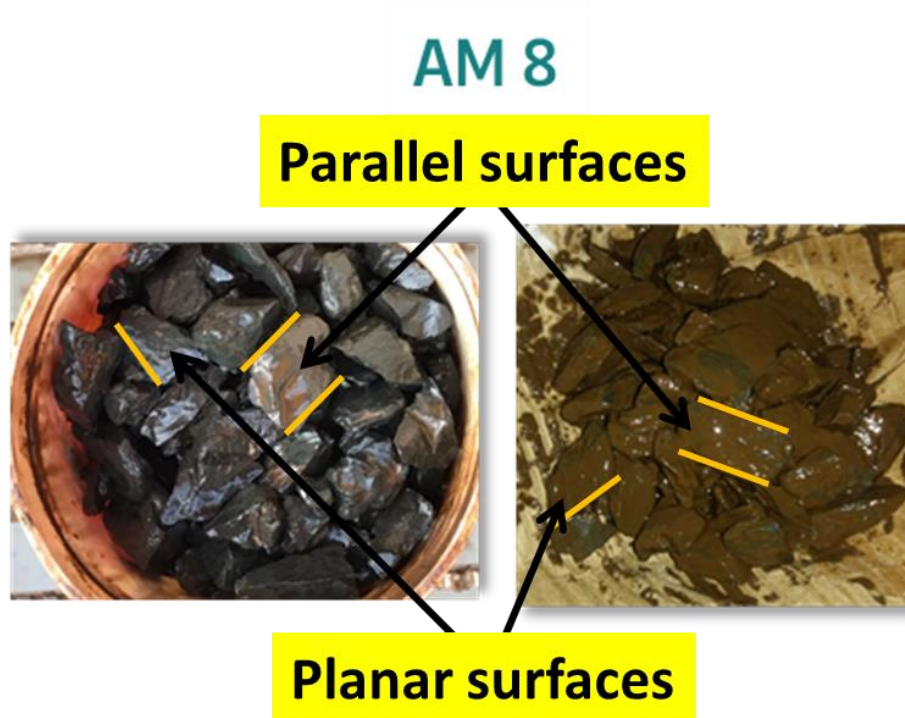


Figure 3. 15. Cavings from well AM-8. Company courtesy.

Regarding kicks or gas inflow events, all of them are observed only in the reservoir - formations C1, C2, C3 and C4 - which corresponds to naturally-fractured carbonates. It can be seen that in the last well drilled AM-8, there is just one kick event, the explanation is that the reservoir has been exploited and the pressure has been decreasing over a period of 8 years, Figure 3. 16. Partial losses are also being reported in the reservoir, probably due to the naturally-fractured formations.

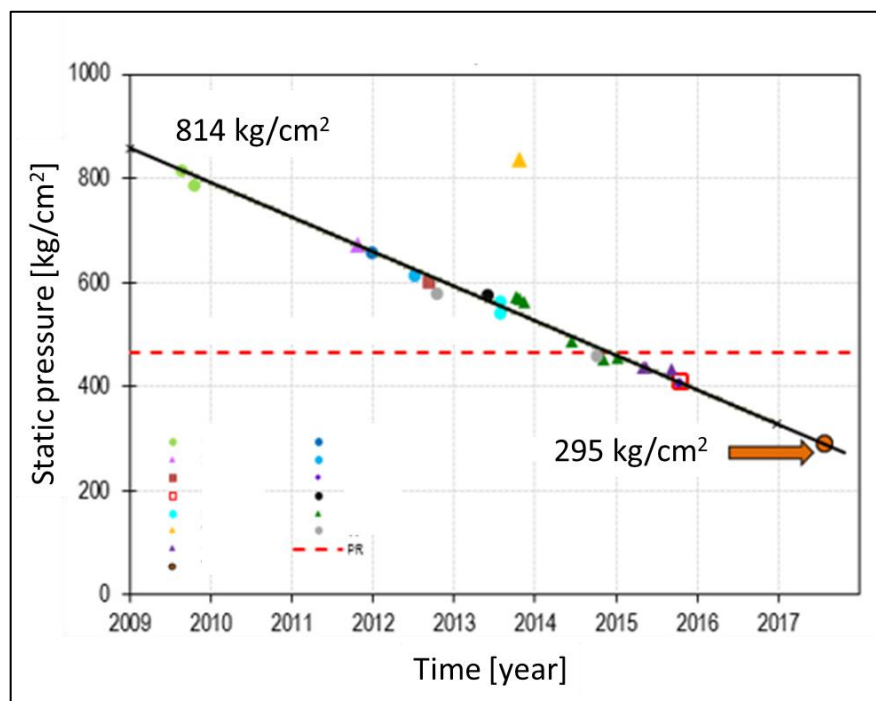


Figure 3. 16. Reservoir pressure of field AM1. Company courtesy.

Proposed Approach and Experimental Method

In Figure 3. 17, one can see the drilling events that occurred in well AM-11. There are two FITs at 987m (casing shoe 20") and 2895m (13 3/8") with an equivalent density value of 1.61 g/cm³ and 2.07 g/cm³ / 2.25 g/cm³, respectively. There is uncertainty about the value of the FIT at 2895m because in the DDR they reported it as 2.25 g/cm³ but in one of the analysis of the company, they mention that they took 2.07 g/cm³ to calibrate the S_{hmin}. Unfortunately, the FIT plot was not provided to be analyzed. Thus, both values were considered in the calculations.

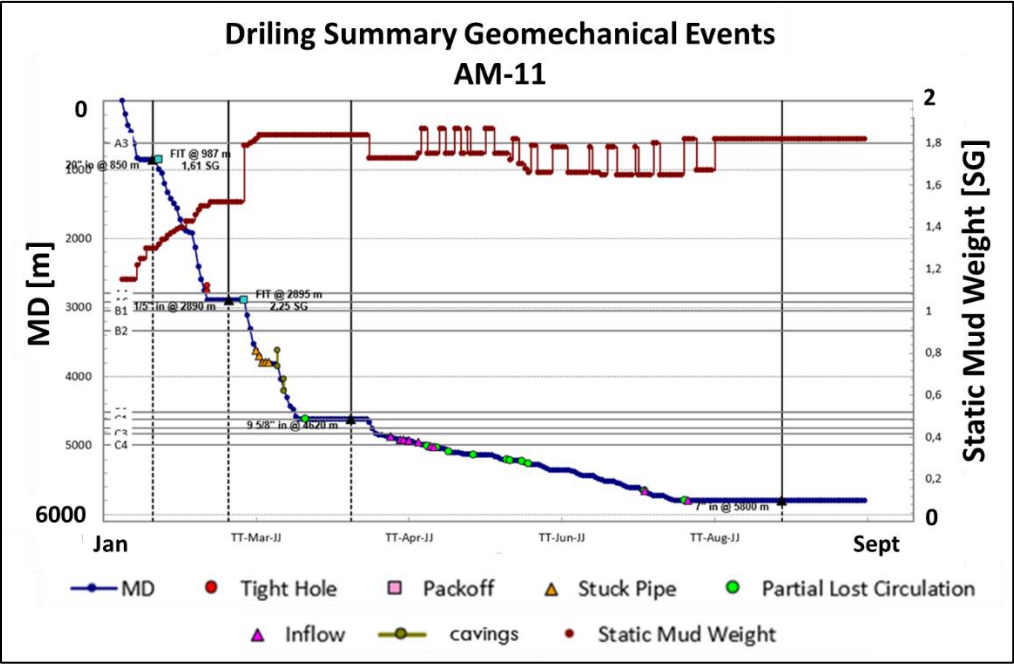


Figure 3. 17. Drilling summary, AM-11.

Regarding the events of AM-11, the instability problems started at ~3000m with few tight hole events. After cementing the 13 3/8" casing, they started to increase the mud weight from 1.79 g/cm³ to 1.84 g/cm³ and started to have stuck pipe problems in the interval 3600m - 3800m. Keeping the MW of 1.84 g/cm³ constant for the rest of the section until 4620m, they encountered cavings and tight hole events between 3615m and 4190m.

In Figure 3. 18 , we can observe the events of well AM-5. The information that was taken for this thesis from this well were just the one corresponding to the main hole. The sidetracks occurred in the carbonates which was not in the scope of this study. Slightly similar to well AM-8, this well presented a few tight hole events from ~300m to ~2500m. After cementing the 13 3/8" casing at 2883m, they kept the MW of 1.82 g/cm³ constant until TD at 4502m. During this section they observed cavings on the shale shakers coming from different intervals from ~3400m to ~4200m. After that, they had two sidetracks in the carbonates.

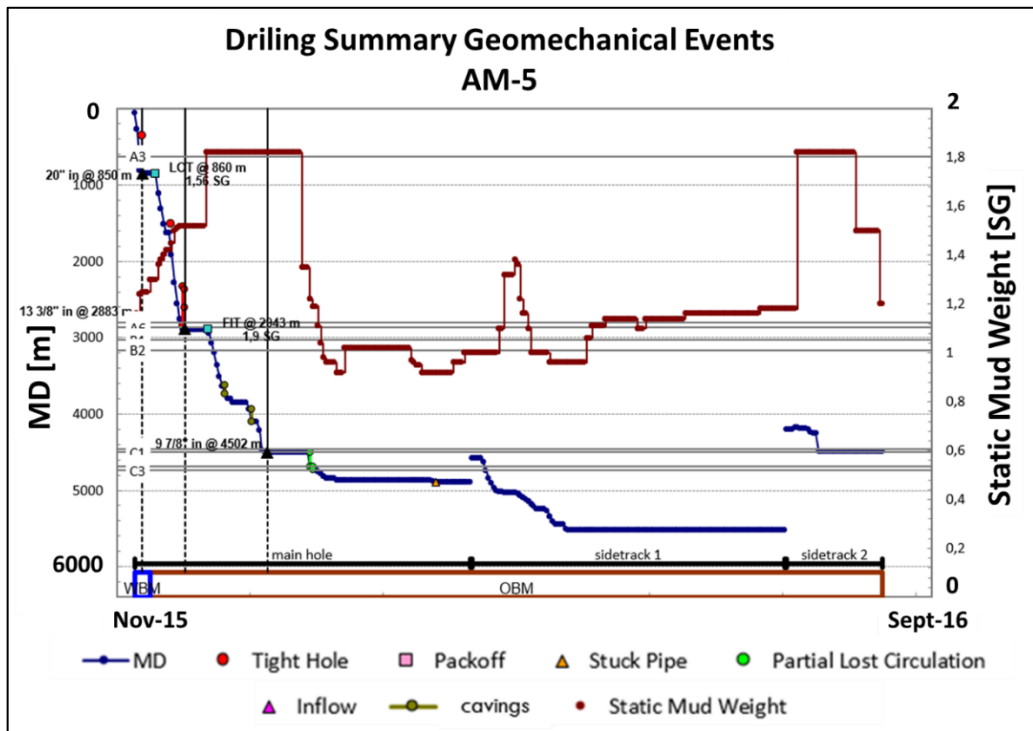


Figure 3. 18. Drilling summary, AM-5. Just the main hole is being analyzed.

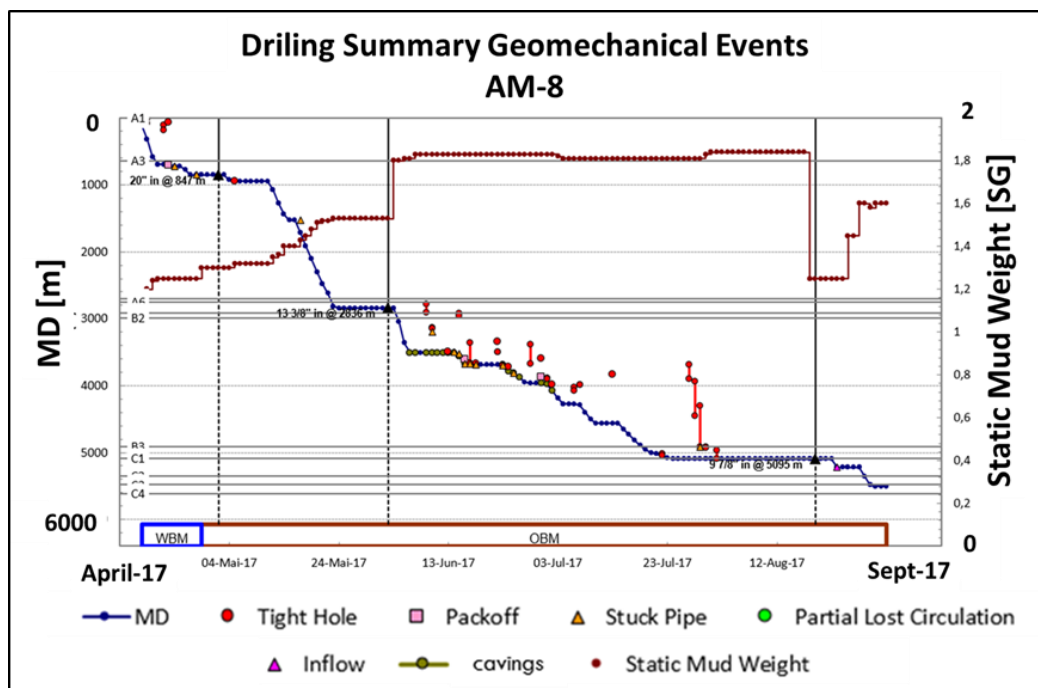


Figure 3. 19. Drilling summary, AM-8.

Figure 3. 19 shows the drilling events of well AM-8, last well drilled in this area. This well showed instability problems in the first section (26" bit size), events of tight hole, pack off and stuck pipe were encountered. After cementing the 13 3/8" casing at 2836m, the MW was increased from 1.80 g/cm³ to 1.83 g/cm³, after increasing the mud weight to 1.83 g/cm³ they started to see cavings on the shale shakers. They kept 1.83 g/cm³ until ~4270m observing several events of cavings, tight hole (especially during tripping) and pack off. They decided to reduce the MW to 1.81 g/cm³ from ~4270m to TD, which

Proposed Approach and Experimental Method

seemed to reduce the events until they finished to drill this section; but, during the preparation (cleaning, run in hole and pull out of hole trips) to run the casing, they started to have problems (tight hole events) again. By increasing the MW to 1.84 g/cm³, the problems were mitigated again.

To sum up the events observed in the analyzed section, the cavings were encountered in wells AM-5, AM-11 and AM8 at similar depth, between ~3500m and ~4200m. At this depth, AM-11 and AM-5 are vertical wells, their KOP started ~4320m and ~4110m, respectively. The KOP of AM-8 started at ~3037m with an inclination from ~2.3° to ~55°. Nevertheless, it is important to point out that these three wells had the same direction with an azimuth between 160° and 177°. On the other hand, AM-1, did not present cavings in this section, it was already deviated there and was drilled towards a different direction: ~250°. AM-1 was the exploratory well and had several events related with wellbore instability, probably due to the lack of information in this area at that time.

3.5 Geomechanical Analysis

3.5.1 Input Data - JewelSuite™

In the following pages, the logs available from the four wells were uploaded on the specialized software JewelSuite™, sponsored by Baker Hughes, and displayed next to each other for comparison purposes:

Resistivity and Gamma Ray logs, Figure 3. 20 and Figure 3. 21, are showing the space between the wells and tops of each formation. Fortunately, both GR and Resistivity logs were taken in all the wells. For the resistivity logs, we can observe both curves, the deep and shallow ones: this information will be crucial when analyzing the possible filtration of the mud into the formation, in further steps.

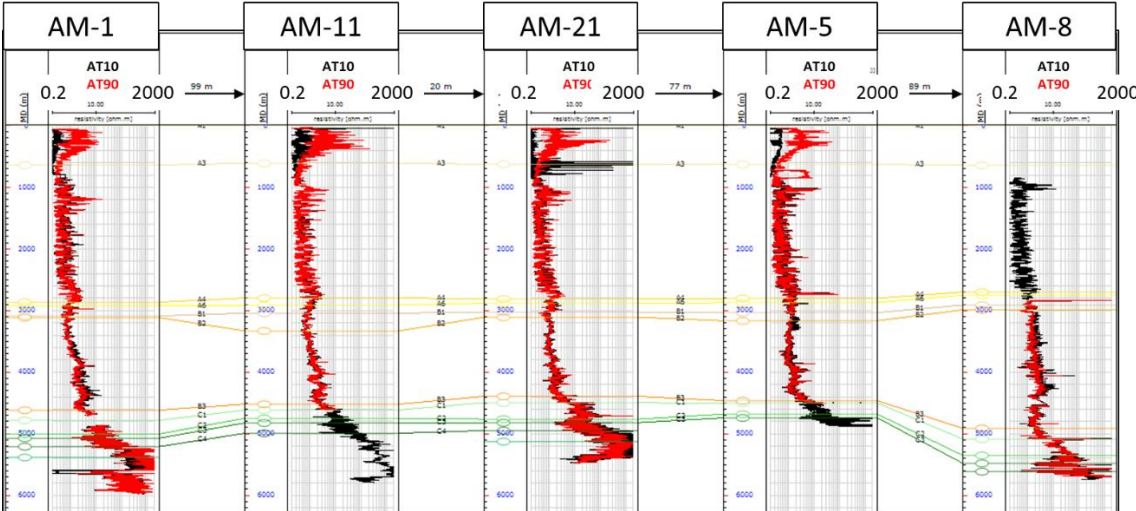


Figure 3. 20. Resistivity logs of wells AM-1, AM-11, AM-21, AM-5 and AM-8. AT10 in black and AT90 in red.

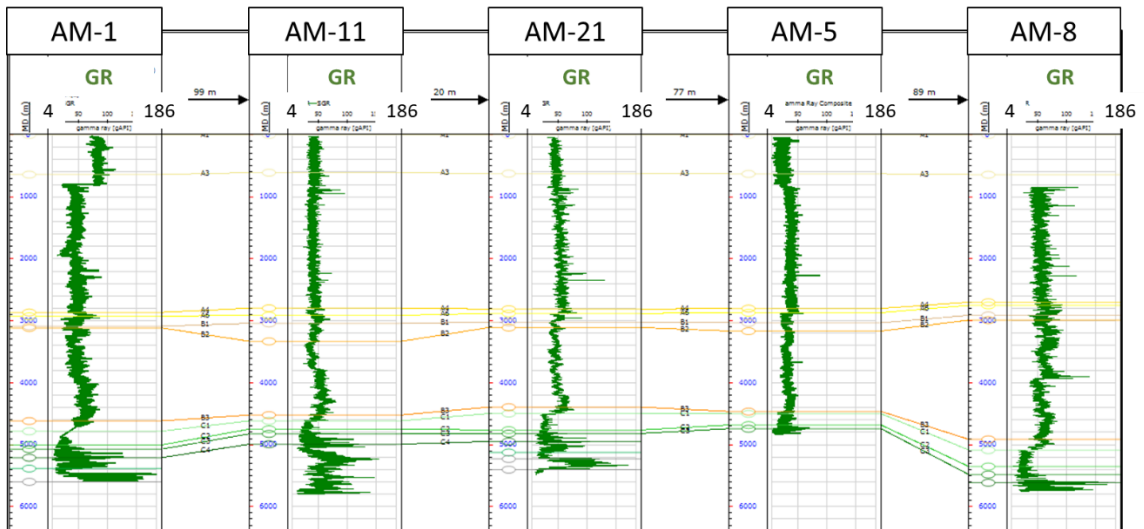


Figure 3. 21. Gamma Ray logs of wells AM-1, AM-11, AM-21, AM-5 and AM-8.

It is important to mention that the exploratory well, AM-1, due to operative complications, does not have the complete set of logs from bottom to top, as it was expected at the beginning of this analysis. Reviewing the data provided, I realized that the complete set of logs were ran in AM-11 and AM-21, which is close to the analyzed wells and had the cavings as well. Thus, some of the logs at a certain depth, when they were missing, were obtained from AM-11 or AM-21, by the depth-stretching methodology. One can distinguish between actual and depth-stretched logs by the color and data displayed.

Having said that, in Figure 3. 22, it is observed that the density logs of wells AM-11 and AM-21 are almost complete (pink = real log). Therefore, the density log of well AM-11 was used and depth-stretched to complete the missing parts in wells AM-1, AM-5 and AM-8 (light turquoise = depth stretched log).

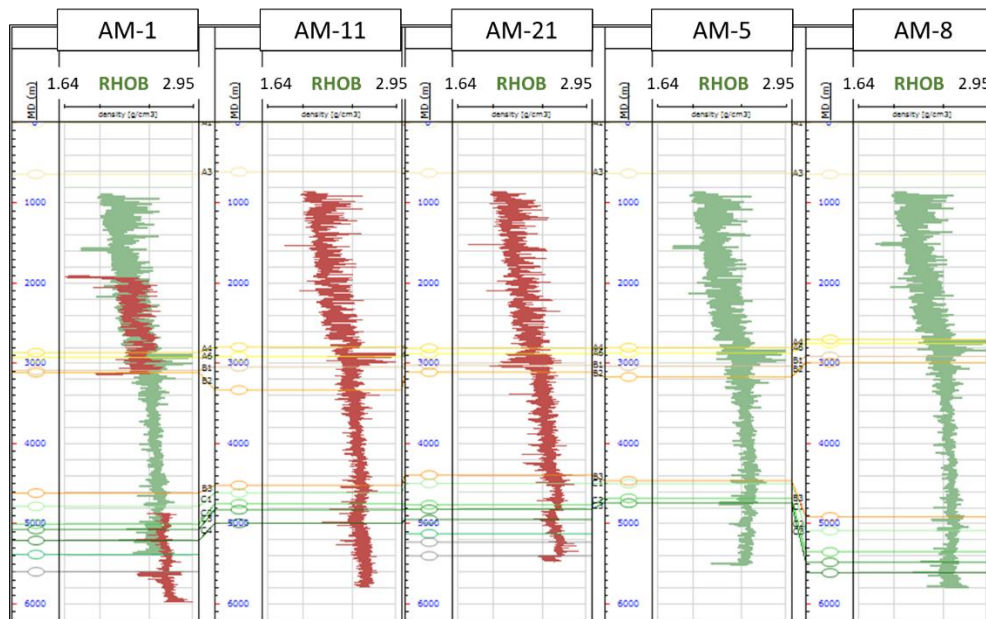


Figure 3. 22. Density logs of wells AM-1, AM-11, AM-21, AM-5 and AM-8.

Proposed Approach and Experimental Method

For the porosity logs (Figure 3. 23), the logs found within the files have a name of SPHI that might be indicating that these logs are calculated from the sonic log. Again, it is observed that the porosity logs of AM-11 and AM-21 are almost complete (brown = real log). Therefore, the porosity log of AM-11 was used and depth-stretched to complete the missing parts in wells AM-1, AM-5 and AM-8 (light orange = depth stretched log).

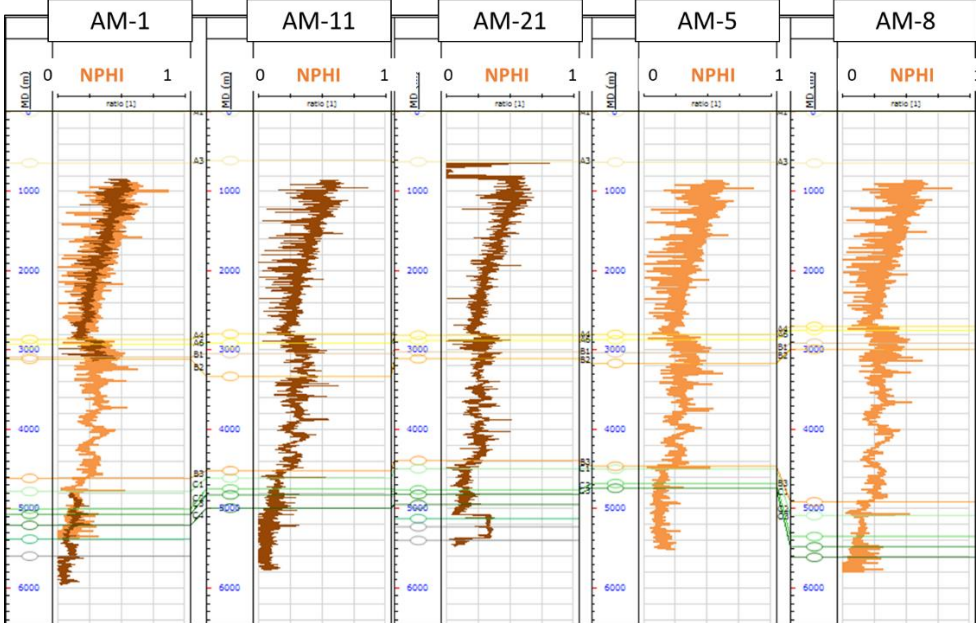


Figure 3. 23. Porosity logs of wells AM-1, AM-11, AM-21, AM-5 and AM-8.

Regarding the compressional sonic logs (Figure 3. 24), the sonic log of wells AM-11 and AM-21 are almost complete (dark blue = real log). Therefore, the sonic log of AM-11 was used and depth-stretched to complete the missing parts in wells AM-1, AM-5 and AM-8 (light blue = depth stretched log).

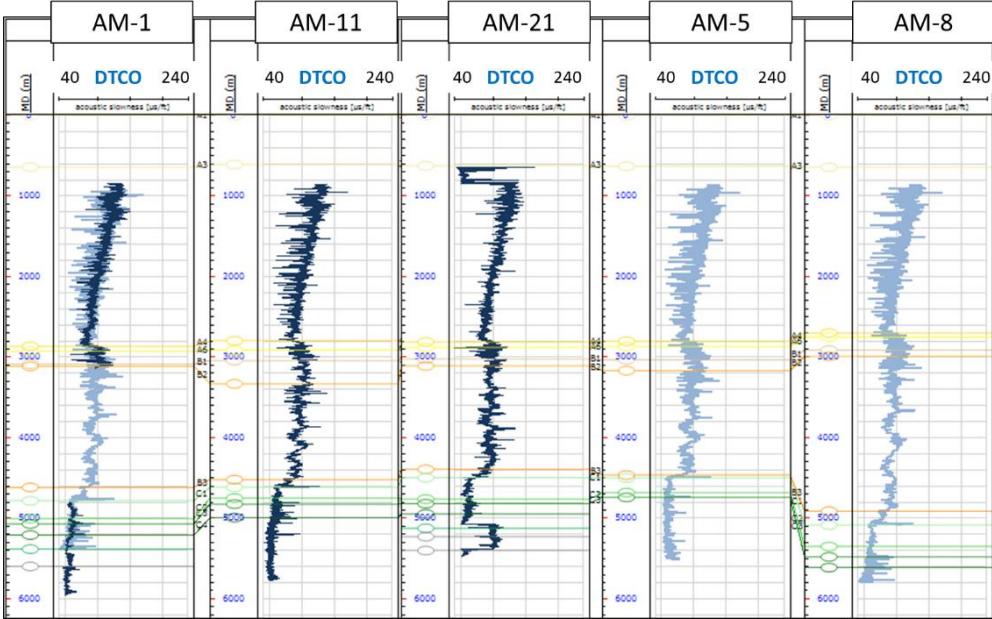


Figure 3. 24. Sonic Compressional logs (DTCO) of wells AM-1, AM-11, AM-21, AM-5 and AM-8.

In the case of the shear sonic log, Figure 3. 25, it was a little bit more complicated since none of the wells has a complete log from bottom to top. A composite from wells AM-1 (upper part) and AM-11 (lower part) had to be created in order to depth-stretch it to wells AM-21, AM-5 and AM-8. The results will be shown in following steps. At the moment, it was depth-stretched from AM-11 to AM-1(lower part) and from AM-1 to AM-11 (upper part). Dark purple = real log and light purple = depth-stretched log.

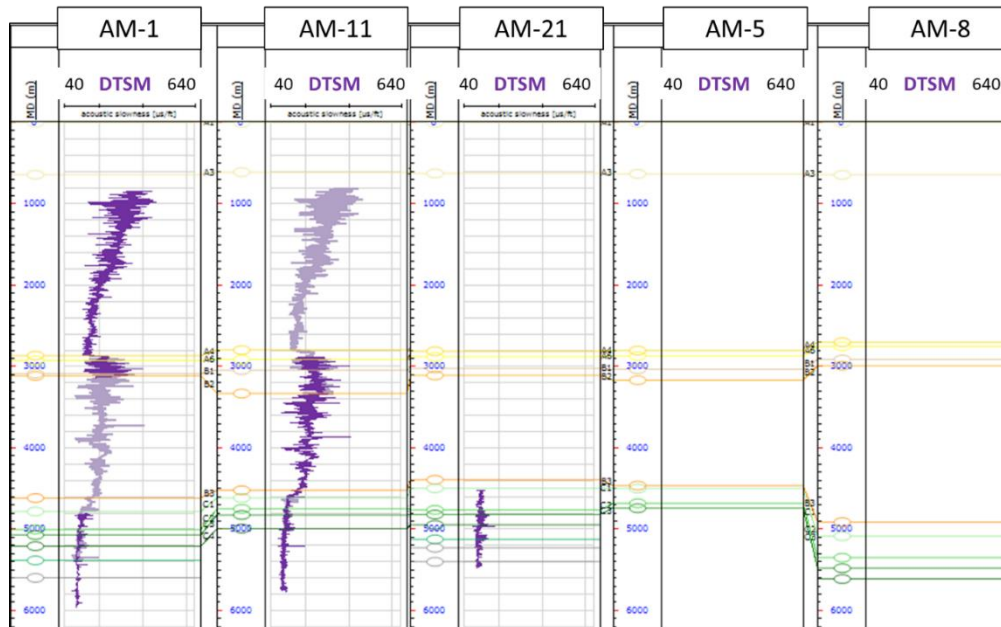


Figure 3. 25 Sonic Shear logs (DTSM) of wells AM-1, AM-11, AM-21, AM-5 and AM-8.

Unfortunately, the sonic stoneley log was not available for any of the wells. This log, in the problematic area, could have had provided important information regarding the micro-fractures or fractures in the formation.

In the porosity and sonic logs, one can see a regression in the data. This might be due to the presence of a fault and the start of the overpressure zone. With the results of the TOC and Rock Eval, it was investigated whether or not this formation was a source rock and whether or not the hydrocarbons generation was the mechanism of overpressure in this area. The results indicated that it could not be a source rock because of the low values of maturity. Thus, it is believed that the mechanism of overpressure is under compaction. High rates of sedimentation do not let the water scape and when buried, due to temperature and pressure effects, the water expands and the porosity increases. The sonic log is affected in the same way, when the volume of water trapped into the rock rises, the water decreases the velocity or increases the acoustic slowness of the rock.

The image logs were taken only in the reservoir (units C1 to C7), and the interpretation of the direction of the fractures were provided by the company, Figure 3. 26. When the four arms caliper or image logs are not available in the study area, the direction of the fractures in the reservoir might give an indication of the S_{Hmax} azimuth in upper layers, although this is not completely reliable.

Figure 3. 26 shows the density, direction and dip of the fractures in the reservoir: it can be observed that there are opened and closed fractures showing different directions. This

Proposed Approach and Experimental Method

could have happened during different geological time caused by different events. The direction of the fractures in wells 21, 11 and 8 are mostly consistent with and azimuth of $\sim 140^\circ$ and well 114 shows a different azimuth of $\sim 300^\circ$.

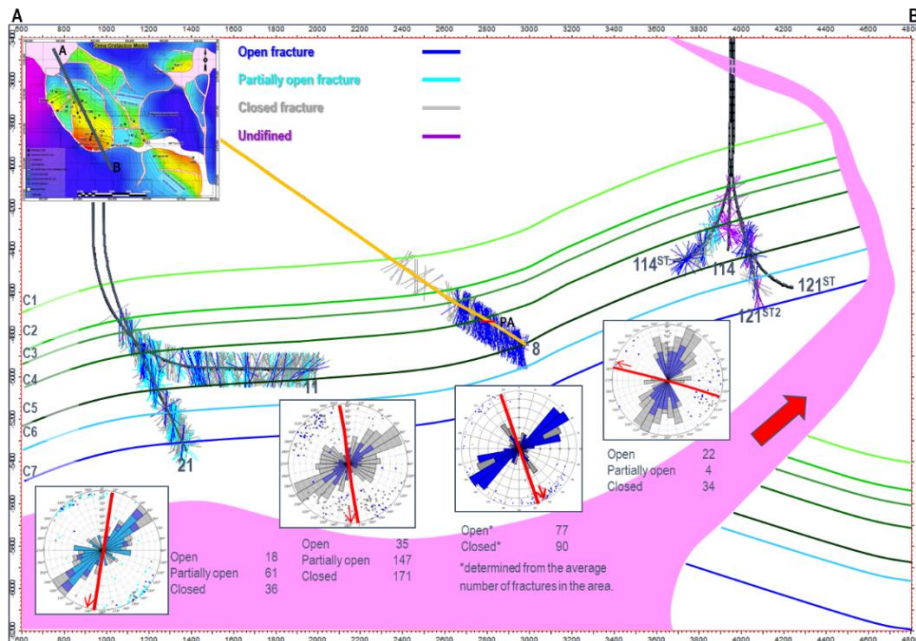


Figure 3. 26. Density, direction and dip of the fractures in the reservoir according to the information from image logs of wells 11, 4, 21 and 114. Company courtesy.

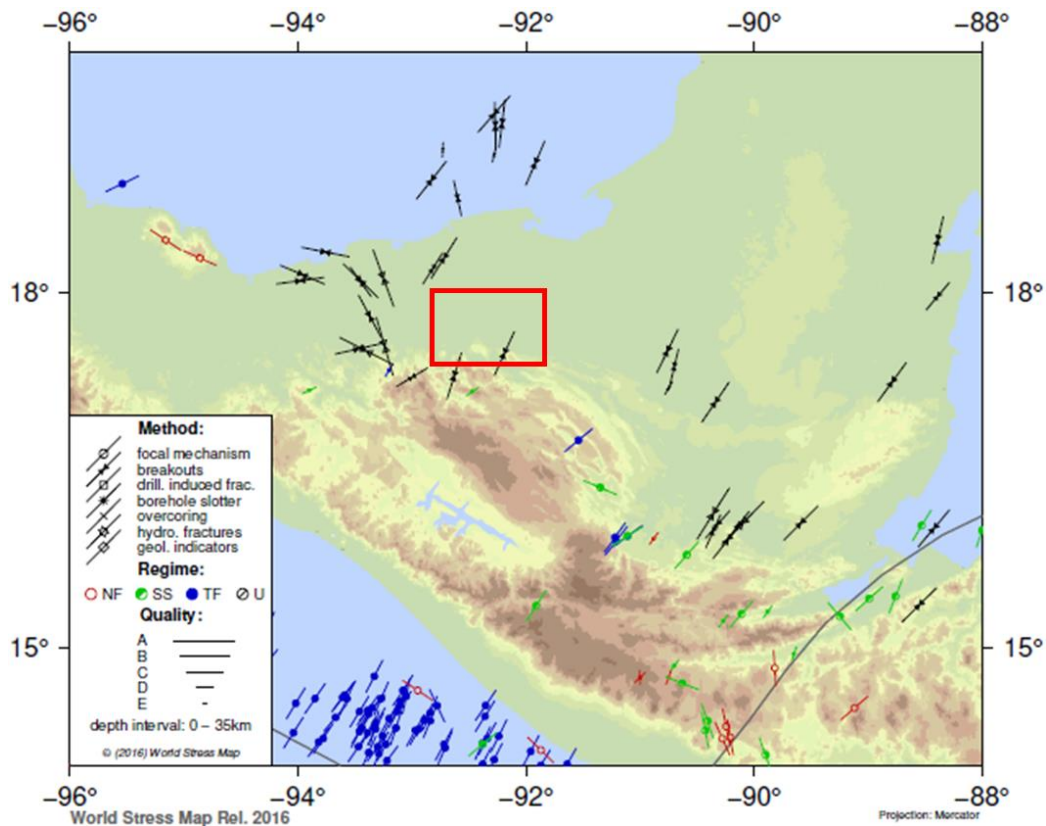


Figure 3. 27. Azimuth of the S_{Hmax} around the area of interest obtained from the World Stress Map. (World Stress Map: Data 2016)

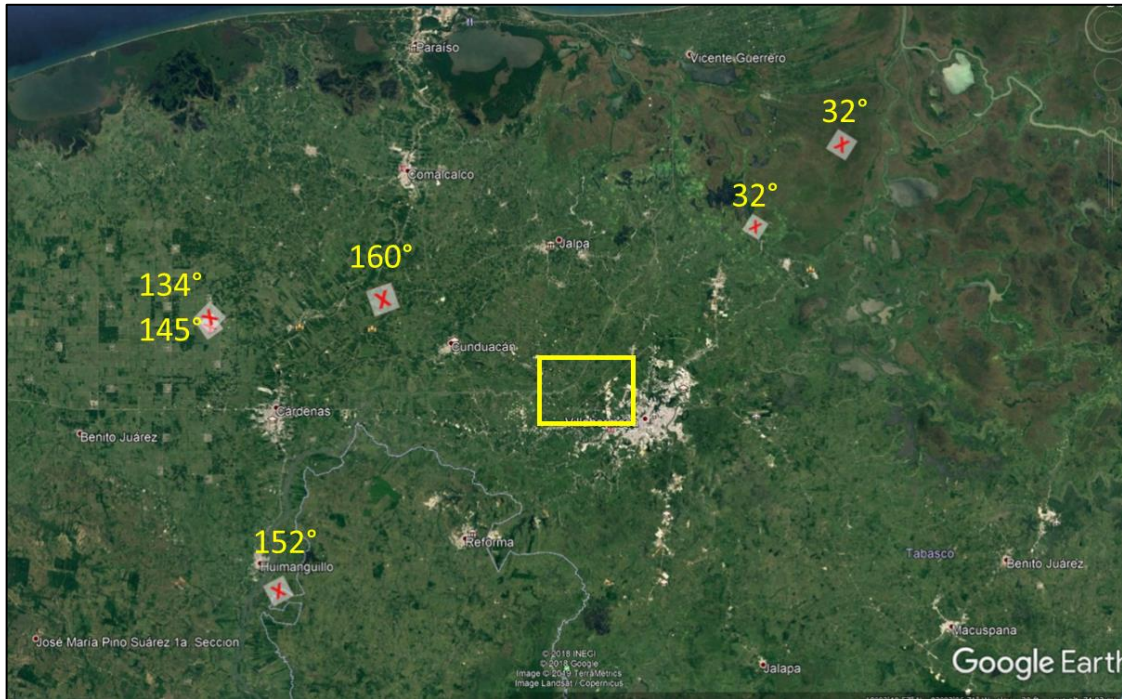


Figure 3. 28. Azimuth of the S_{Hmax} in wells near the area of interest (yellow square), data obtained from the World Stress Map. (World Stress Map: Data 2016)

Additionally, the World Stress Map (WSM) gives us useful and certain information regarding the direction of S_{Hmax} and the stress regime of the area. The data obtained from the WSM are shown in Figure 3. 27 and Figure 3. 28. Figure 3. 27 shows all the data obtained from breakouts, focal mechanism, drilling induced fracture, etc., and Figure 3. 28 shows the data available closer to the field. Based on these two maps and overall information, it was decided to use a S_{Hmax} azimuth of $\sim 30^\circ$.

3.5.2 Pore Pressure

The process to calculate the pore pressure will be described in this chapter just for two wells. Firstly, AM-1 because it is the exploratory well, it has the complete caliper and mostly all real logs, and no cavings were reported. Secondly, AM-11 because there are photos of the shape of the cavings and it has the complete caliper and mostly all real logs.

The complete set of logs of the well AM-1 (Figure 3. 29), the exploratory well, are shown from left to right in each track as follows: Gamma Ray, Shallow and Deep Resistivity, Density, Porosity, Compressional Sonic, Shear Sonic, Well Schematics, Bit Size and Caliper.

Proposed Approach and Experimental Method

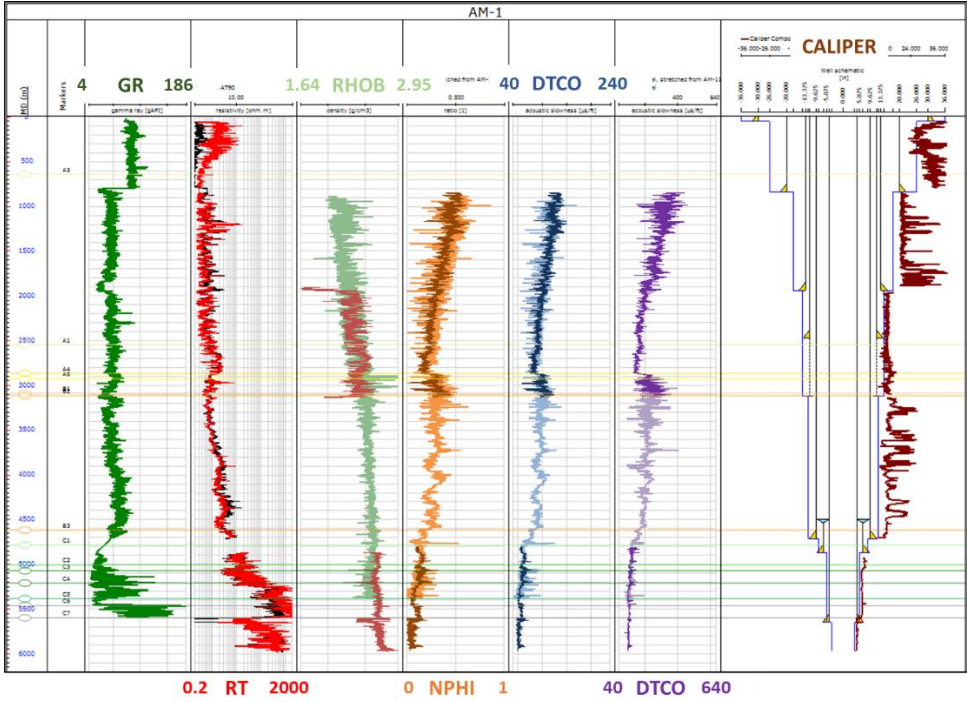


Figure 3.29. AM-1, actual and depth-stretched logs.

The composite of each log was selected using the real logs of the well AM-1 and adding the depth-stretched logs obtained from AM-11 for the missing parts. The upper part of the gamma ray log was moved using the “calculator” tool to make it match with the rest of the log, shifted probably due to a calibration issue. Additionally, the velocity logs, acoustic and shear, were calculated from the sonic logs through the “log conversion” tool from JewelSuite from slowness to velocity. All logs used for further calculations are shown in Figure 3.30.

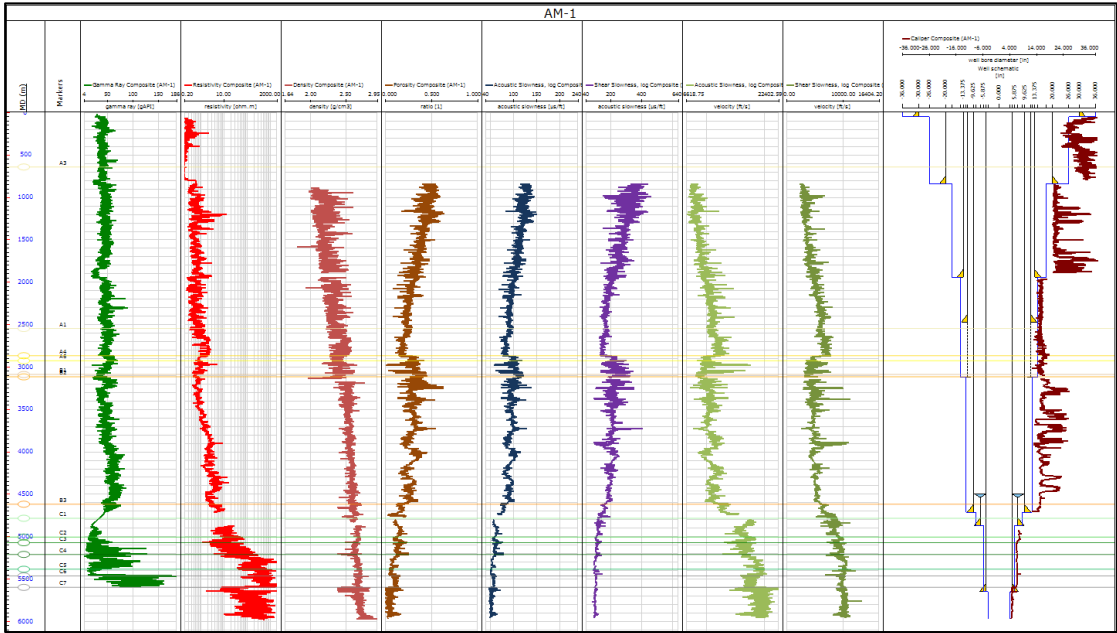


Figure 3.30. AM-1, final logs used for the geomechanical analysis.

Proposed Approach and Experimental Method

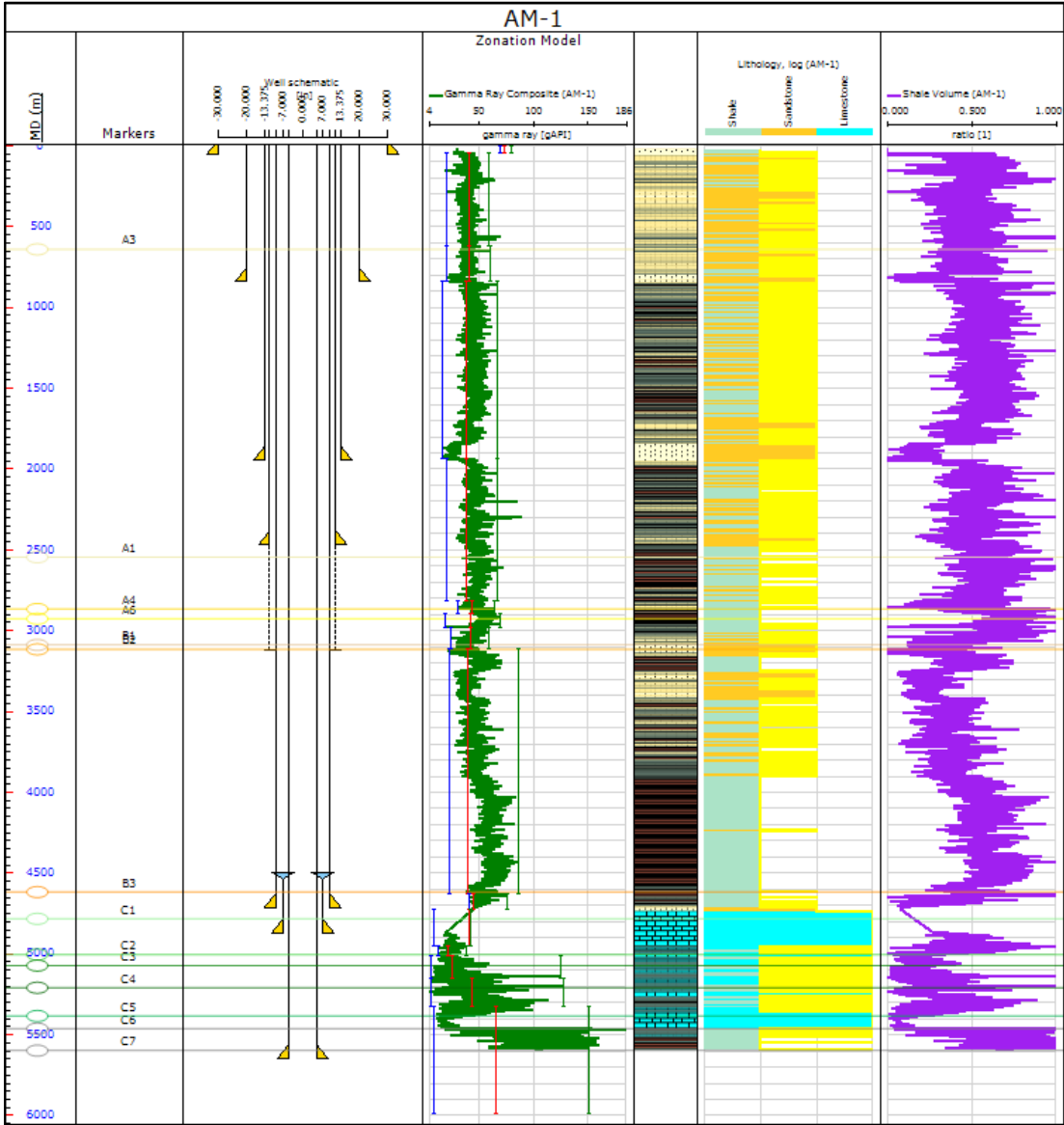


Figure 3.32. Zonation and lithology models calculated in AM-1.

The calculation of the overburden or vertical stress was performed using the density composite obtained in previous steps. Normally, at shallow depth, from 0 to 1000m, the density log is being affected by the diameter of the borehole and the values are usually not reliable information. Thus, a trend line starting from around 1.95 g/cm³ (on ground floor) until the first density datum was used to calculate the overburden; the data were not available in this case. In Figure 3.33, it is observed from left to right: the lithology, tops, caliper log, both density logs - the one from the composite and a second density log calculated from the sonic log using Gardner equation - and the trend line mentioned before. Finally, in green, the overburden composite used to calculate the overburden stress. The higher value for the overburden stress at the end of the well is 2.37 g/cm³.

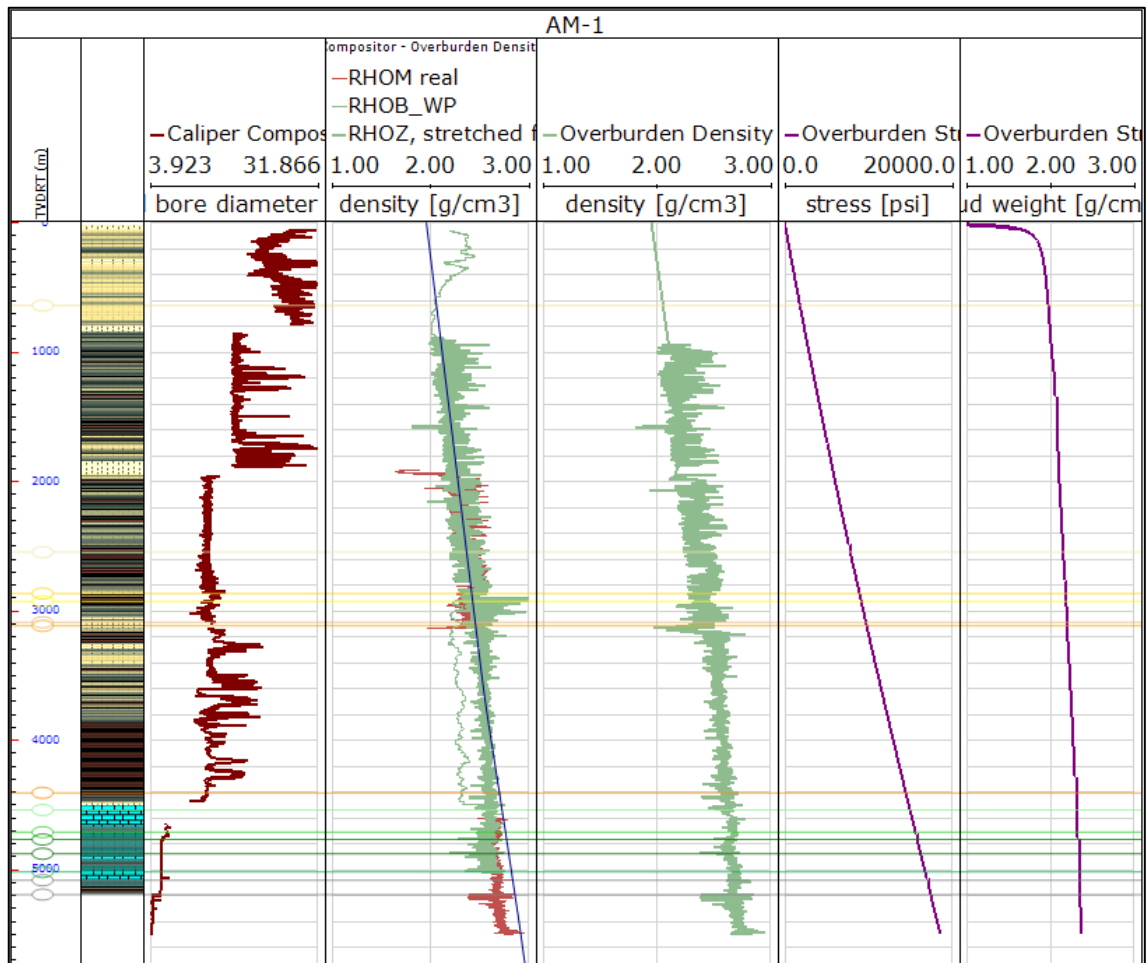
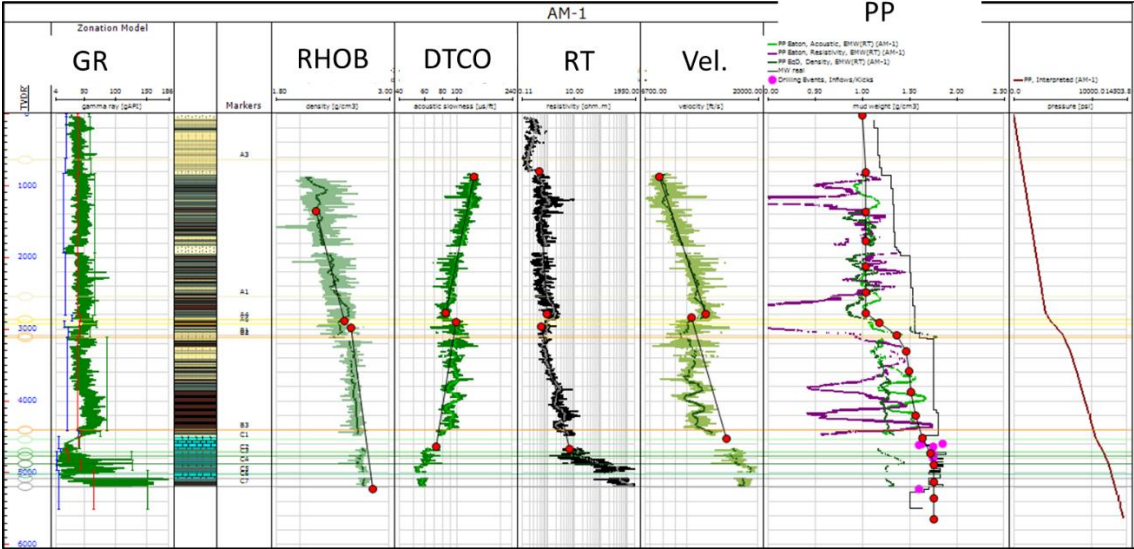


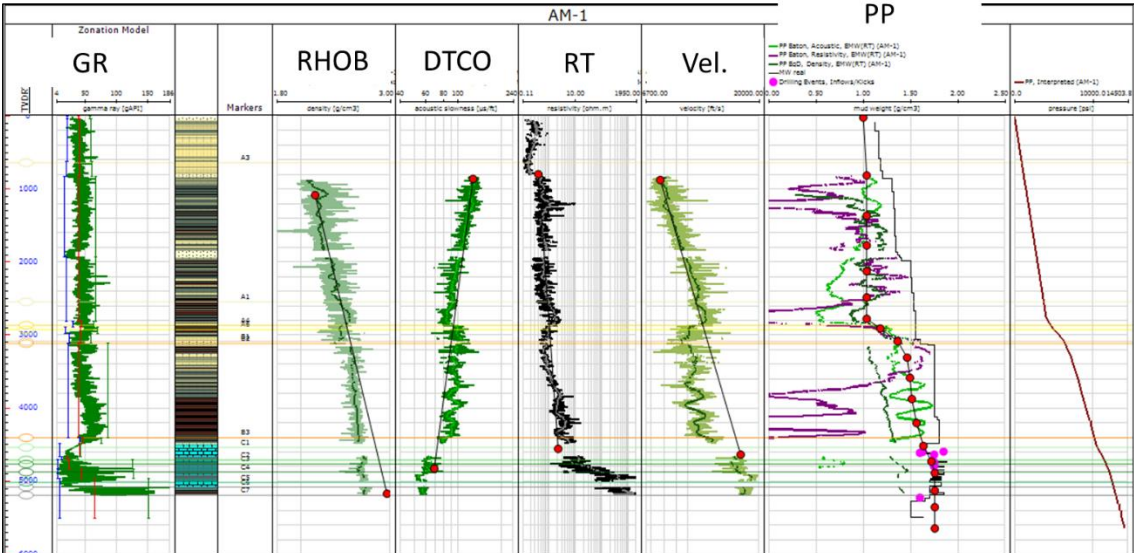
Figure 3. 33. Calculation of the overburden gradient in well AM-1

Once the overburden was defined, the next step was to estimate the pore pressure. For this calculation, the Eaton’s method and two different Normal Compaction Trend (NCT) lines were used in order to compare the results from both assumptions. The reason to verify both assumptions is that from the geological view point, it was learnt (Figure 3. 3 and Figure 3. 4) that there is a discontinuity at the beginning of the overpressure zone. The comparison of using different trend lines can be observed in Figure 3. 34. It seems to be slightly better matching when using two different slopes but using just one slope gives also similar tendencies. Unfortunately, MDT or formation tests were not taken during the drilling operations. Kicks and gas influxes were reported starting at 4865 md, corresponding to C1, the top of the Naturally-Fractured Carbonates (NFC) reservoir.

Proposed Approach and Experimental Method



a



b

Figure 3. 34. Pore pressure calculation of well AM-1. a) Pore pressure using two different slopes b) Pore pressure using just one trend line.

Fracture Gradient

After having defined the interpreted pore pressure, the calculation of the fracture gradient was performed using the following methods:

- Hubbert Willis; constant: 0.55
- Matthews Kelly; constant: 0.55
- Eaton; using the Dynamic Poisson’s Ratio obtained from sonic logs

The default value for the constants used in HW is 0.5 and M&K, 0.6. Fortunately, it was possible to calibrate this data with the reported LOT’s. There were two leak off test in this well at 841m and 1942m, the results are shown in Table 3. 3. With these data, the constants were changed until they matched.

MD [m]	TVDSS [m]	MW [g/cc]	LOT [g/cc]	LOT [psi]
841	832	1.30	1.61	1925.8
1942	1933	1.50	1.65	4557.5

Table 3. 3. Data of the LOTs taken in well AM-1.

All methods matched both LOTs with the mentioned constants values and data. In Figure 3. 35, one can observed both LOT's in terms of pressure and equivalent mud weight overlying the results (light blue dots).

Following the workflow of JewelSuite, the FG was also calculated from the sonic, density and resistivity logs. For this step, the method Matthew and Kelly with the 0.55 same constant was used. In Figure 3. 35, the red curve corresponds to the fracture gradient calculated using the sonic log, which, in my opinion, it is the best match for both LOTs.

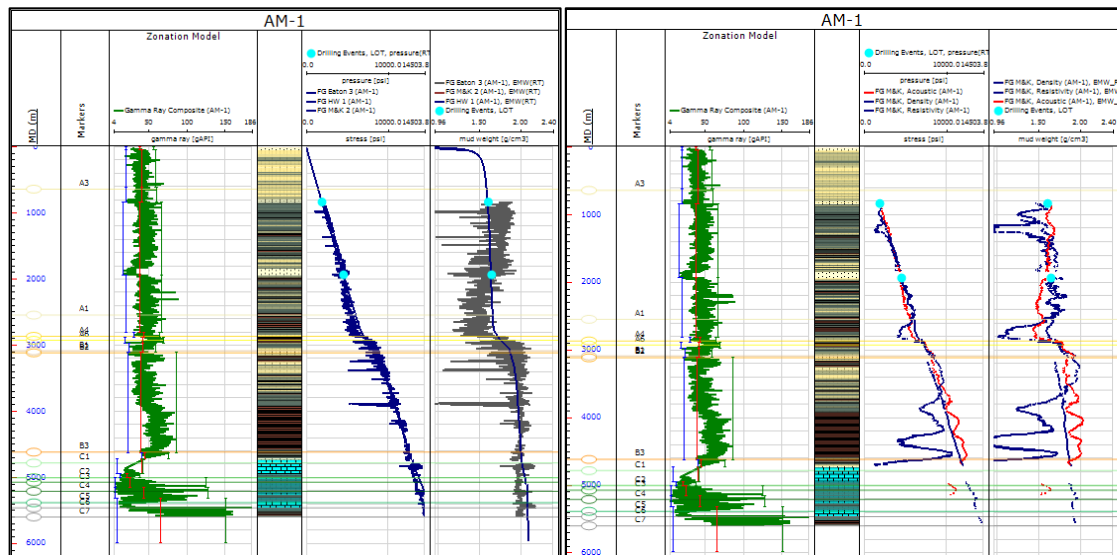


Figure 3. 35. Fracture gradient calculated with six different equations and calibrated with LOTs available, AM 1.

3.5.3 Wellbore Stability

In order to start with the wellbore stability analysis, firstly, it is important to define the rock properties. As mentioned in Chapter 2, there are two values for each property, one dynamic and the other one, static. The dynamic values are calculated through different equations from the literature, while the static values are the ones obtained from laboratory results. Unfortunately, there are no cores available in the problematic shale formations in this case study. Thus, it will have to be relied on data from the literature and regional values provided by the company.

The data provided by the company were collected from logs of wells in the area, and the literature. These data will be used to calibrate the model as well as the properties values obtained from the logs and different methods available on JewelSuite. The values of UCS and Friction Angle Coefficient for each formation are listed in Table 3. 4.

Proposed Approach and Experimental Method

Unit	UCS [psi]	FA* [°]	Φ*
	Hosrud Vp / GOM Shale		
A6	3133 / 2269	34	0.36
B1	3057 / 3057	33	0.37
B2	3766 / 2687	39	0.35
B3	5961 / 4247	42	0.33

Table 3. 4. Rock properties data provided by the company. The UCS was calculated with histogram in each formation, using two methods for comparison. *Company courtesy.

As mentioned before, the rock properties were also calculated using different equations for shales, sandstones and carbonates listed in Table 3. 5. These parameters might be changed when the collapse pressure is being calibrated with the observed breakouts or drilling events reported.

	UCS	Internal Friction	D. Young’s Modulus	Vp to Vs
Shale	Hosrud Vp	Lal Vp	$E_{dyn} = \rho V_s^2 \frac{(3V_p^2 - 4V_s^2)}{2(V_p^2 - V_s^2)}$	Shale-Castagna
Sandstone	McNally	Lal Vp	D. Poisson’s Ratio	SST Castagna
Carbonates	Golubev-DT	Lal Vp	$\nu = \frac{(V_p^2 - 2V_s^2)}{2(V_p^2 - V_s^2)}$	Limestone Castagna

Table 3. 5. Methods used to calculate the rock properties, AM-1.

In Figure 3. 36, the rock property curves calculated with the methods mentioned above are displayed from left to right as follows: Gamma Ray (green), UCS (black), Internal Friction Coefficient (dark blue), Dynamic Young’s Modulus (light blue), Dynamic Poisson’s Ratio (brown) and the well schematics including the Caliper log (brown).

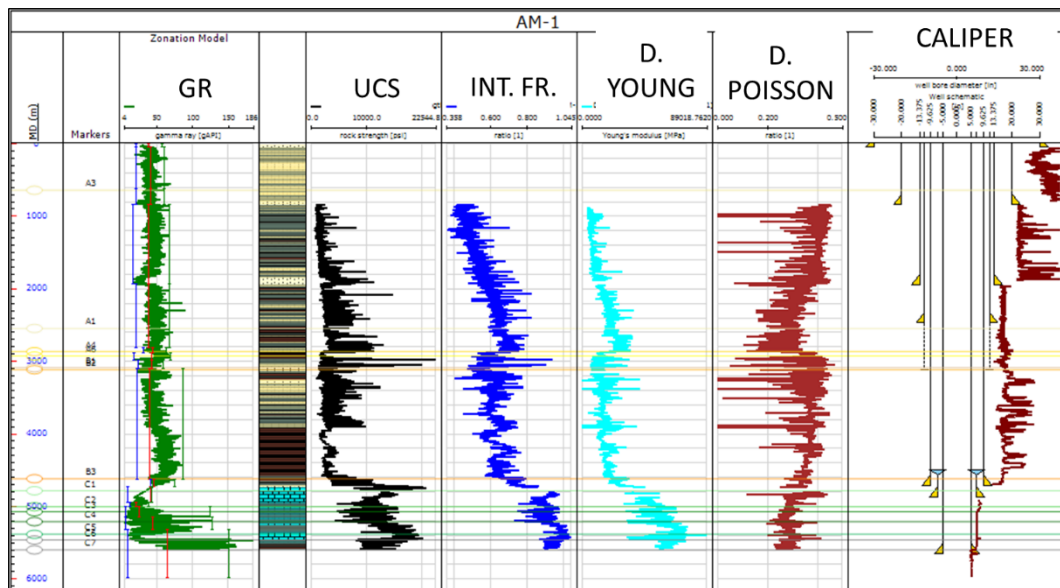


Figure 3.36. Rock properties curves calculated from logs, AM-1.

Principal Horizontal Stresses

Once the overburden, pore pressure, fracture gradient and rock properties were determined, the best model that calibrates well with all the data available and the drilling experience while using reasonable values for all parameters constituting the geomechanical model has to be found. This is a trial and error approach in order to determine the present in-situ stress state and magnitude. The different stress regimes were described in the Figure 2. 8 added in Chapter 2. According to the company, the AM1 field seems to be in a normal stress regime where $S_v > S_{Hmax} > S_{Hmin}$. Thus, in the first trial, the given information will be assumed the given information. Nevertheless, it is important to observe that according to the geological information presented at the beginning of this chapter, the area where all the wells are drilled is limited by four reverse faults (Figure 3. 2). But it is also important to mention that these faults are being interpreted in the Mesozoic (reservoir) and not in the Tertiary. In other words, it is difficult to assume whether this is an indication of a reverse regime or not. Nonetheless, a sensitivity analysis of the three regimes will be performed in case the results assuming a normal regime are not consistent with the data.

The magnitudes of the minimum and maximum horizontal stresses have to be calculated next. JewelSuite™ has three methods to calculate the horizontal stresses:

- Effective Stress Method
- Stress Contrast Method
- S_{Hmax} . Equilibrium Ratio Method

In this case study, the first one was used to calculate the principal horizontal stresses. In the Effective Stress Method, the maximum and minimum horizontal stresses can be calculated from the overburden stress, pore pressure and S_{Hmin} and S_{Hmax} effective stress calibration points. These points can be LOT's, FIT's or drilling events. The effective stress ratio points are dimensionless and can be fitted with a trend line as shown in Figure 3.

Proposed Approach and Experimental Method

37. In the last track of this figure, one can see that the magnitude calculated for the minimum horizontal stress is calibrated with LOTs.

The equations used in this method are:

$$ESR_{min} = \frac{(Sh_{min} - Pp)}{(Sv - Pp)}$$

Equation 3. 1

$$ESR_{max} = \frac{(Sh_{max} - Pp)}{(Sv - Pp)}$$

Equation 3. 2

Different scenarios were calculated in order to find the model that fitted better, the data that remained constant in each scenario were the following:

UCS Shale:	Hosrud vp
Failure Criteria:	Modified Lade
Biot:	Shale: 0.85, Sandstone: 0.7, Limestone: 0.7
Friction:	0.35 (shale)
Bedding cohesion:	725 psi
Bedding friction:	0.34

Additionally, in each scenario, sensibilities using bedding planes just in shale and without bedding planes were performed.

Normal regime

- Scenario 1 - $Sv > SH_{max} > Sh_{min}$

Strike slip

- Scenario 1 - $SH_{max} > Sv > Sh_{min}$
- Scenario 2 - $SH_{max} > Sv \sim Sh_{min}$
- Scenario 3 - $SH_{max} \sim Sv > Sh_{min}$

Thrust faulting

- Scenario 1 - $SH_{max} > Sh_{min} > Sv$
- Scenario 2 - $SH_{max} > Sh_{min} \sim Sv$
- Scenario 3 - $SH_{max} \sim Sh_{min} > Sv$

After several trials, the scenario that fitted the best was the one using a strike slip regime and weak bedding planes. Figure 3. 37 shows the magnitude of Sh_{min} and SH_{max} , the first two calibration points were taken from this well (AM-1) and the third calibration point around 3000m was taken from the well AM-11, in terms of true vertical depth, just for comparison.

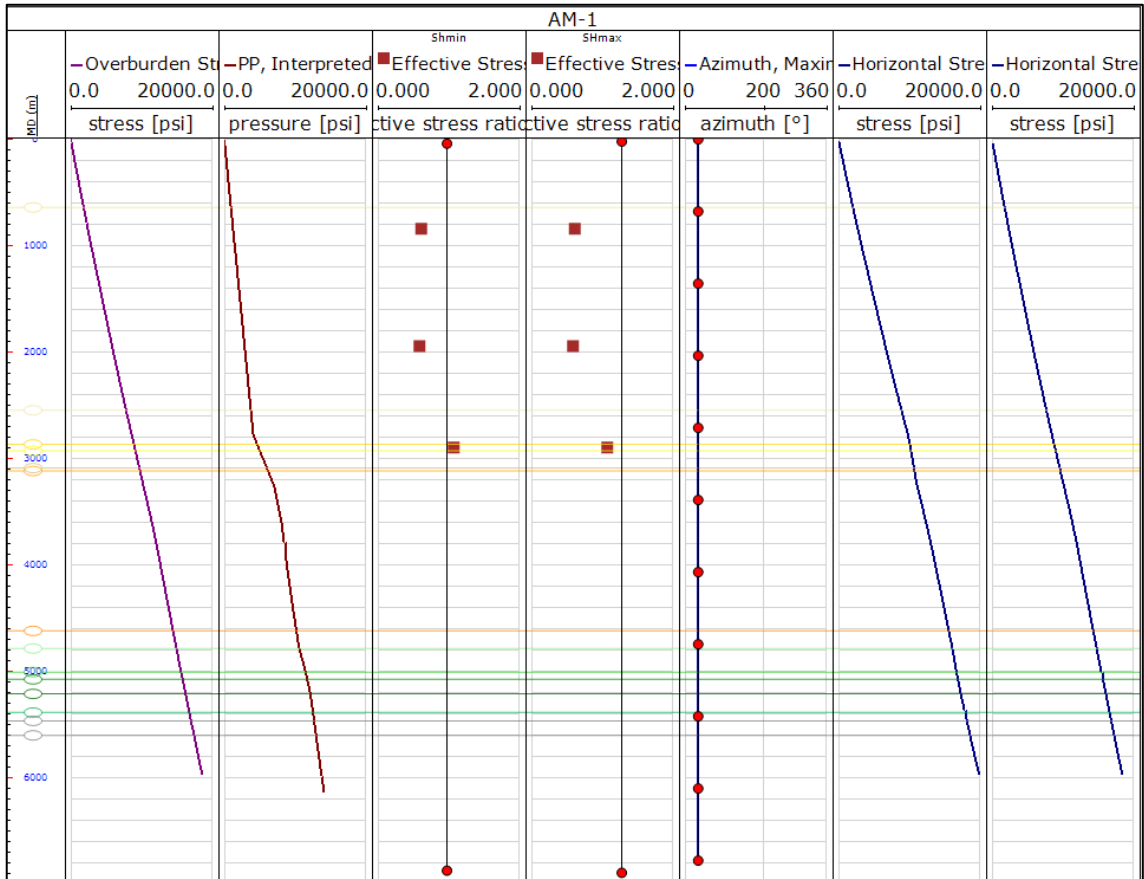


Figure 3. 37. Horizontal stress definition using the effective stress method, AM-1.

This model was calibrated using the failure criteria “Modified Lade” applied to all types of rocks. Using different failure criteria depending on stratigraphy and lithology is not a recommended approach. The predicted failure seems consistent with the drilling events in the analyzed section.

Proposed Approach and Experimental Method

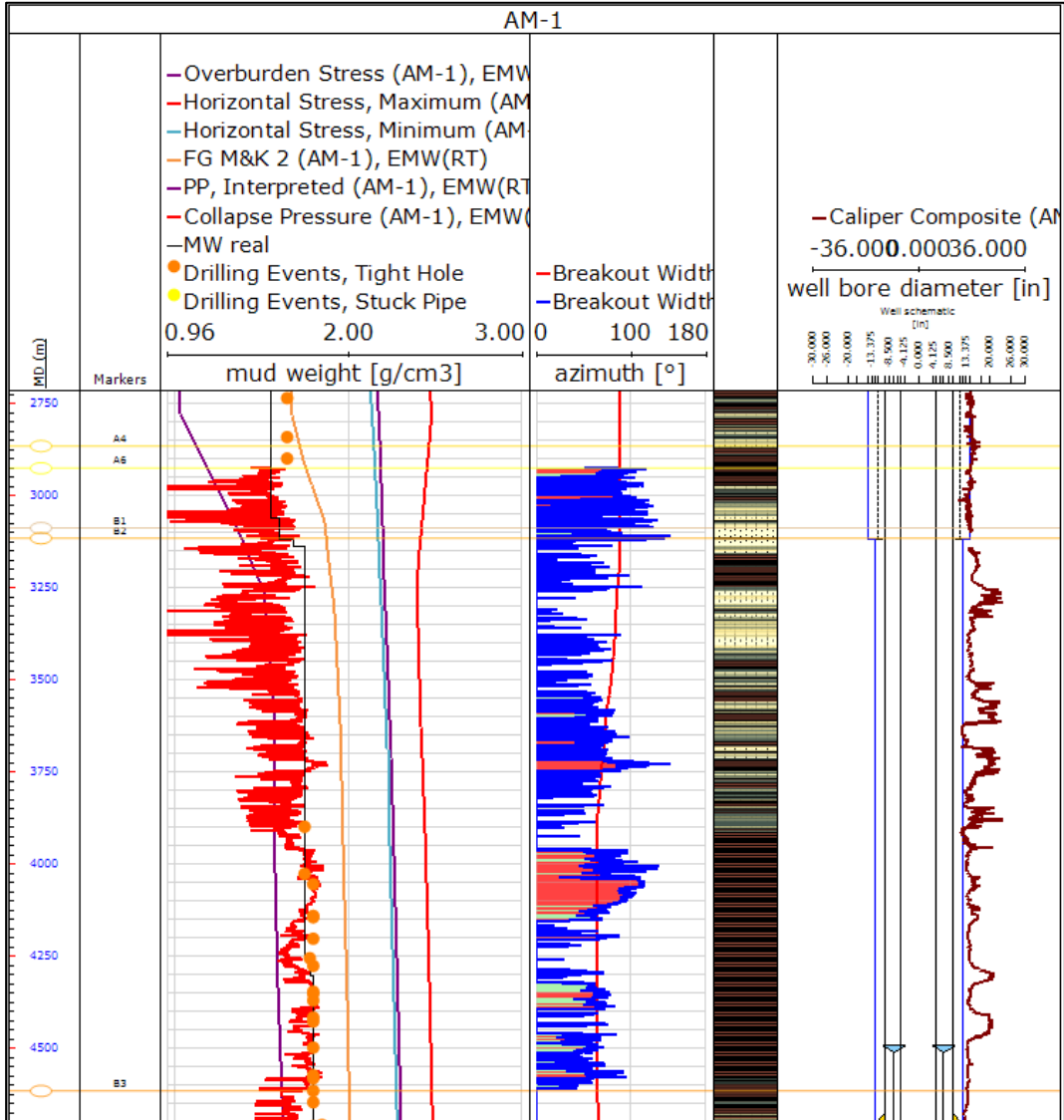


Figure 3.38. Collapse pressure calculated and calibrated with drilling events and caliper log, AM-1.

In Figure 3.38, we can see in the first track, the Collapse Pressure (red curve) together with the Interpreted Pore Pressure (purple curve), Minimum Horizontal Stress (blue curve), the actual Mud Weight used during the drilling operations (black line) and the drilling events used to calibrate the collapse pressure, tight hole (orange circles) and stuck pipe (yellow circles). In the second track, the calculated breakout width generated from the defined failure criteria and the breakout limit set as default and common practice: 90° when the well is vertical and 30° when deviated to horizontal. The last track shows the well schematics, borehole size and caliper log.

The geomechanical model at this moment seems to be consistent and calibrated. It is interesting to observe that even though in the exploratory well AM-1, there were no cavings reported, the caliper log and the drilling events give an indication of instability problems in the same formation B2. In this formation, one can notice that the mud weight window is very narrow and it is not possible to drill the section without facing problems;

the mud weight used in this section was 1.75 – 1.80 g/cc, in static conditions. Adding the friction losses the ECD can be + 0.05 g/cc or more over the static mud weight.

Well AM-11

The same procedure was applied to AM-11 but this time, the cavings issue will be analyzed and compare during the wellbore stability step.

Not to repeat the whole process, for this well we will only show the final data and curves corresponding to the zonation model, depth stretching, overburden, normal compaction trend lines, pore pressure, fracture gradient, principal horizontal stresses and rock properties. Only if there is a completely different step or any used equations or methods change for this well analysis, then we will be mention it.

The complete set of logs of the well AM-11 (Figure 3. 39) is shown from the tracks left to right as follows: gamma ray, shallow and deep resistivity, density, porosity, compressional sonic, shear sonic, well schematics, bit size and caliper. All of them are actual logs taken from this well except the upper part of the shear sonic log.

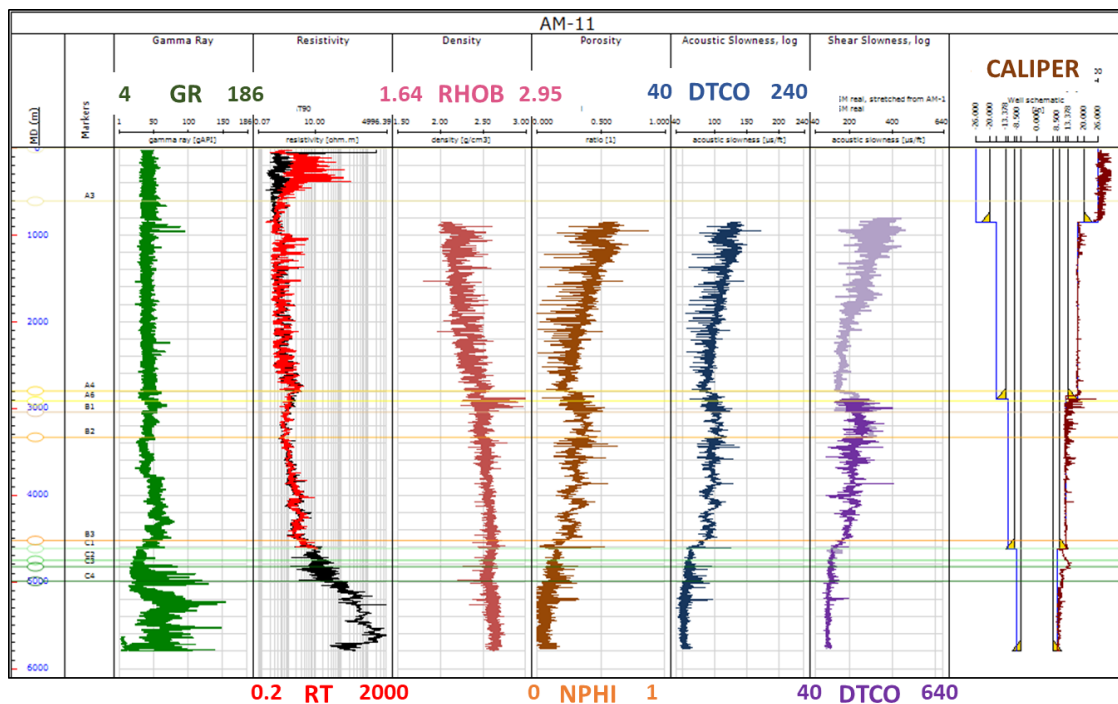


Figure 3. 39. Logs used for geomechanical analysis, AM-11.

The higher value of the overburden stress at the end of the well AM-11 is 2.34 g/cc, slightly lower than AM-1 due to its depth. For the pore pressure calculation, the exact same trend lines used in AM-1 were imported and applied to AM-11, the results of using Eaton’s method with NCT lines were very similar and there was no need to move the trend lines at all, which shows consistency in the data. In Figure 3. 40 and Figure 3. 41, the comparison between using one and two trend lines as in AM-1 is presented.

Proposed Approach and Experimental Method

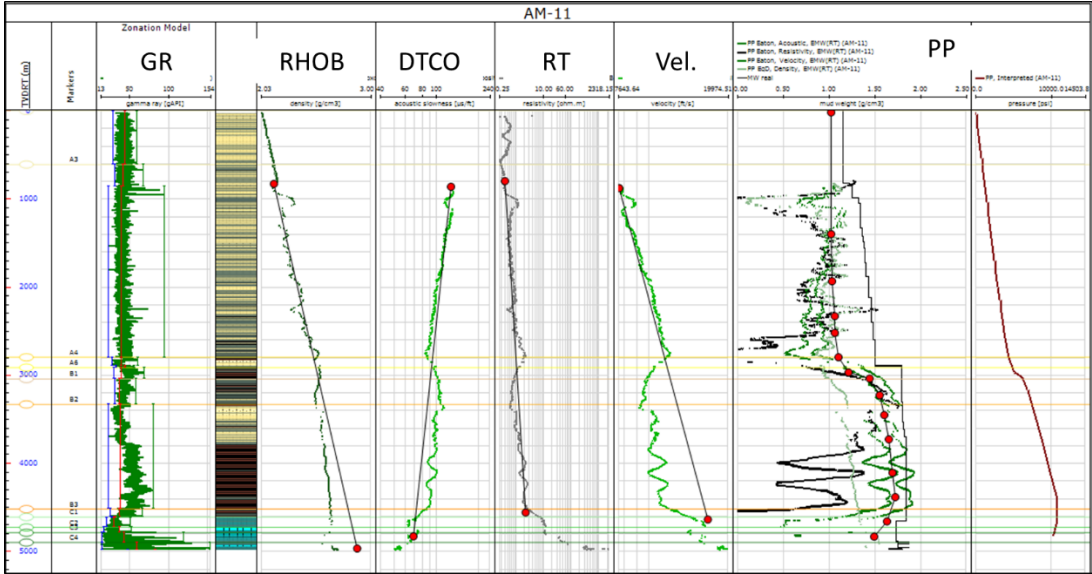


Figure 3. 40. AM-11, pore pressure calculated using the same trend line as in AM-1 (one trend line).

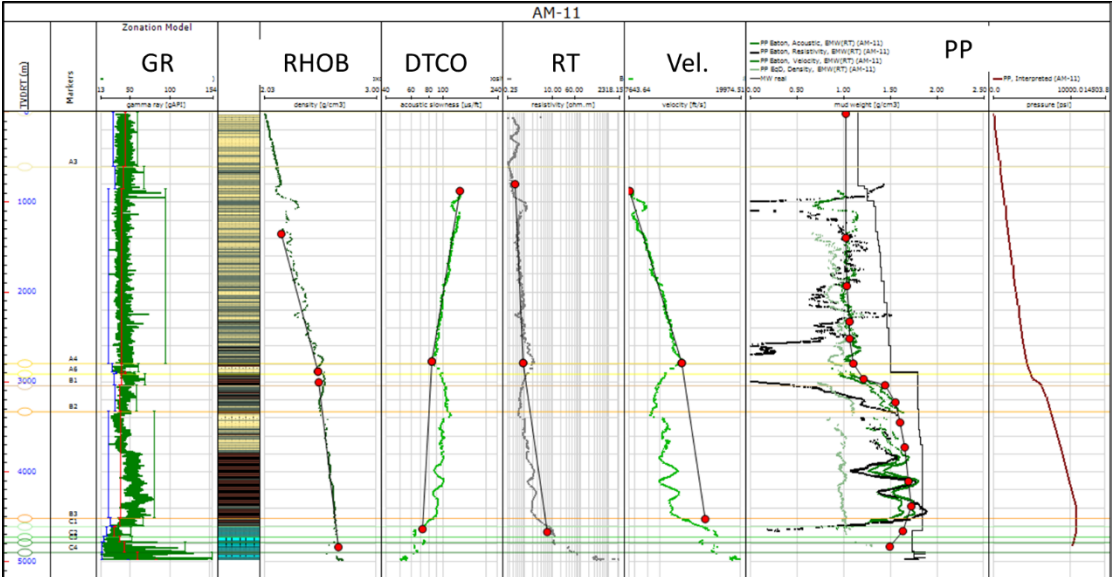


Figure 3. 41. AM-11, pore pressure calculated using the same trend lines as in AM-1 (two different slopes).

Regarding the fracture gradient calibration, there is a LOT taken at 2895m that was reported with a maximum equivalent density of 2.25 g/cc with a decrease down to 2.07 g/cc; they mentioned they took the last value to calibrate the minimum horizontal stress, Table 3. 6. In this analysis, both values are being plotted for comparison.

MD [m]	TVDSS [m]	MW [g/cc]	LOT [g/cc]	LOT [psi]
857	848	1.30	1.61	1962
2895	2885	1.79	2.25 / 2.07	9263 / 8522

Table 3. 6. LOTs taken in the well AM-11 during drilling operations.

The constants used in equations for AM-1 to calculate the fracture gradient do not seem to be fitting in this case. Instead of 0.55, this time, using 0.65 seemed to be a better fit. In any case, the second LOT is still very high for the profile as shown in Figure 3. 42. Both values, the first reported, 2.25 g/cc (purple dot) and the second one, after the “decrease”, 2.07 g/cc (light blue dot) are being plotted for comparison.

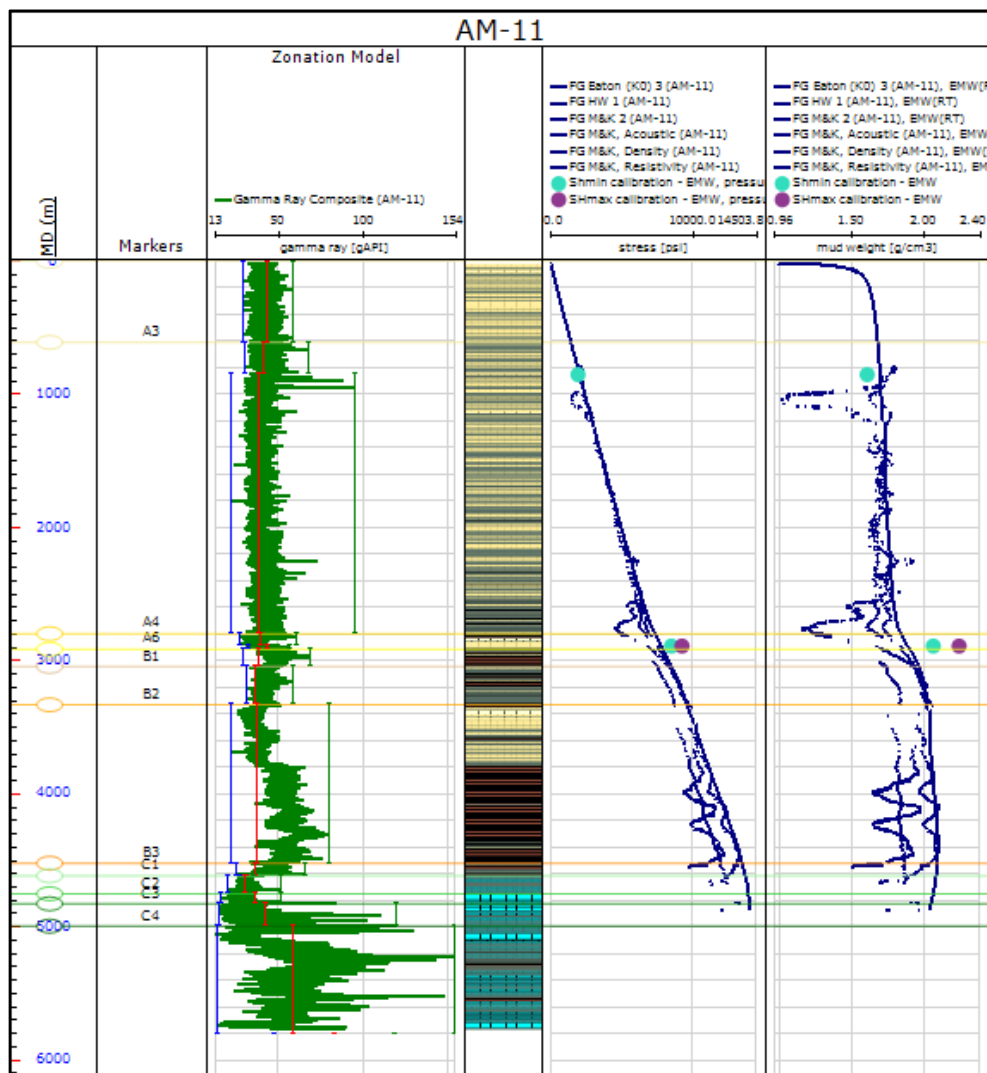


Figure 3. 42. Fracture gradient calculation, AM-11.

The results of the calculated breakout using the same equations and methods as in AM-1 show a good fit and consistent behaviour. The predicted failure can be observed in Figure 3. 43. The mud weight density used in the problematic section of this well was 1.79 g/cc – 1.84 g/cc, 0.04 g/cc higher than in AM-1.

Proposed Approach and Experimental Method

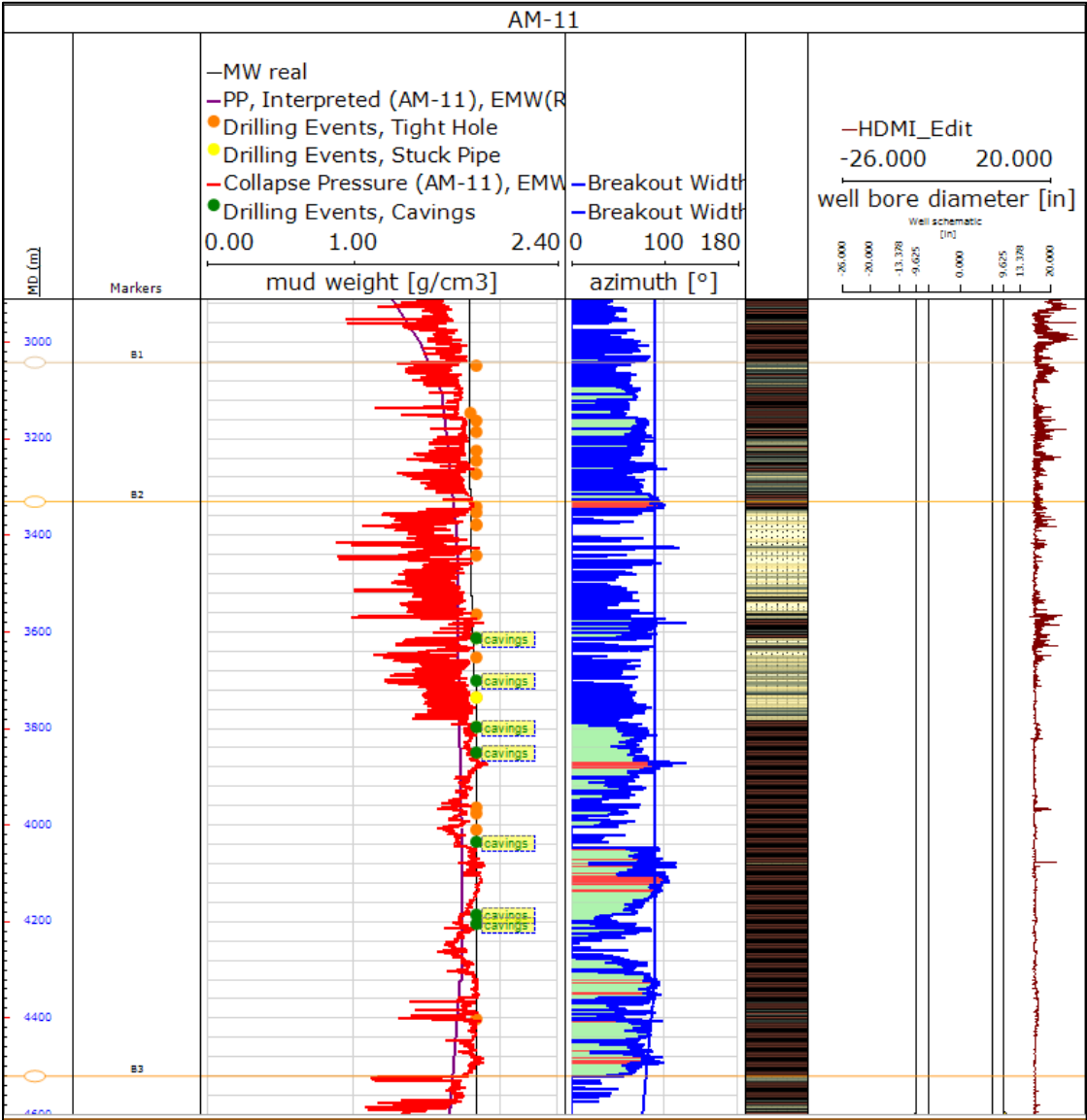


Figure 3.43. AM-11 calculated breakout width using same methods as in well AM-1.

Taking into consideration the theory of having anisotropic failure, weak bedding planes and micro-fractured shale (micro-fractures were observed in micro-CT scan), the model had to be calculated using the advanced mode that includes not only the rock properties but bedding planes as well.

From the seismic line in depth (Figure 3.44) crossing along the well AM-11, bedding angle around 25° above the fault and 5° after the fault, with bedding direction NW-SE, around 170° dip azimuth, can be determined. This information was used for the input in the advanced mode calculations.

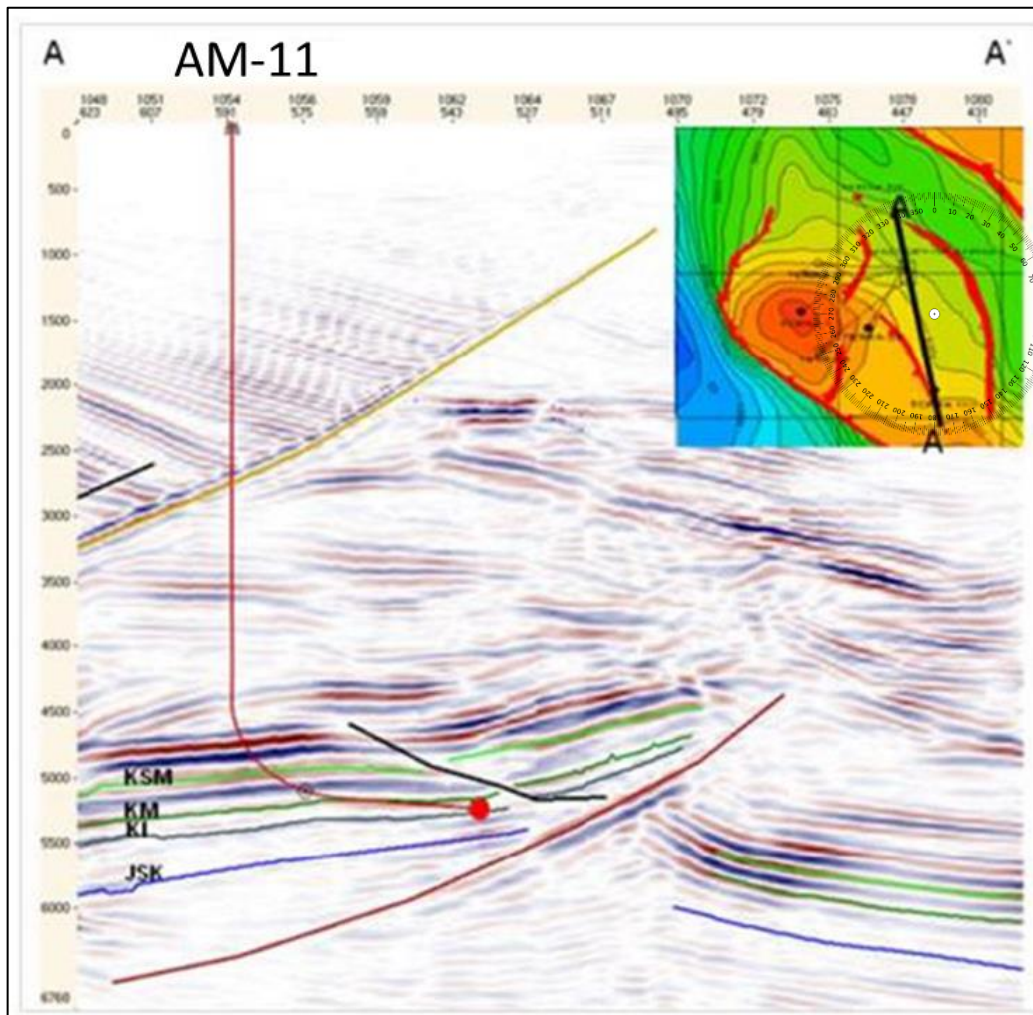


Figure 3. 44. Seismic line in depth across well AM-11. Company courtesy.

This information, Table 3. 7, was applied to the analyzed area (shale formation) to calculate and calibrate the model for AM-11.

Use	Top	Base	O/W ...	Top MD [m]	Top TVDSS [m]	Base MD [m]	Base TVDSS [m]	Bedding Dip [°]	Bedding Dip A...	Bedding Cohe...	Sliding Friction ...
<input type="checkbox"/>	AM-11-Top	A1_MS 2	<input type="checkbox"/>	0.00	-9.00	0.00	-9.00	20.0	170	1450	0.380
<input type="checkbox"/>	A1_MS 2	A3_MS 2	<input type="checkbox"/>	0.00	-9.00	607.91	598.90	23.0	170	1450	0.380
<input type="checkbox"/>	A3_MS 2	A4_MS 2	<input type="checkbox"/>	607.91	598.90	2795.70	2786.17	25.0	170	1450	0.380
<input type="checkbox"/>	A4_MS 2	A6_MS 2	<input type="checkbox"/>	2795.70	2786.17	2912.24	2902.66	25.0	170	725	0.380
<input checked="" type="checkbox"/>	A6_MS 2	B1_MS 2	<input type="checkbox"/>	2912.24	2902.66	3041.66	3032.08	5.0	350	725	0.340
<input checked="" type="checkbox"/>	B1_MS 2	B2_MS 2	<input type="checkbox"/>	3041.66	3032.08	3330.22	3320.64	5.0	170	725	0.340
<input checked="" type="checkbox"/>	B2_MS 2	B3_MS 2	<input type="checkbox"/>	3330.22	3320.64	4519.81	4508.24	5.0	170	725	0.340
<input checked="" type="checkbox"/>	B3_MS 2	C1_MS 2	<input type="checkbox"/>	4519.81	4508.24	4614.31	4598.39	5.0	170	725	0.340
<input type="checkbox"/>	C1_MS 2	C2_MS 1	<input type="checkbox"/>	4614.31	4598.39	4748.73	4716.73	8.0	350	1450	0.300
<input type="checkbox"/>	C2_MS 1	C3_MS 2	<input type="checkbox"/>	4748.73	4716.73	4823.65	4776.10	8.0	350	1450	0.300
<input type="checkbox"/>	C3_MS 2	C4_MS 2	<input type="checkbox"/>	4823.65	4776.10	4991.59	4887.21	8.0	350	1450	0.300
<input type="checkbox"/>	C4_MS 2	AM-11-Base	<input type="checkbox"/>	4991.59	4887.21	6048.24	4967.29	8.0	350	1450	0.300
<input checked="" type="checkbox"/>			<input checked="" type="checkbox"/>								

Table 3. 7. Bedding planes and rock properties used in the Advance Mode of JewelSuite™, AM-11.

As mentioned before, the model calibrated better with the strike slip regime and seemed to be more consistent using bedding planes than without using this said advanced mode. The results show a better match on the calculated breakout width and a better fit with

the drilling events. After this step, the trajectory was analyzed and consequent findings are presented in the validation of the model.

3.5.4 Validation of the Geomechanical Model

In order to verify that the predicted failure is consistent with the drilling events, the depth based CMW of AM-1 and AM11 are displayed below.

Well AM-1

It is important to mention that there were not cavings reported during the drilling operations of well AM-1. Additionally, from our pool of wells, it is the only one that has a different inclination and azimuth in this section. Therefore, well AM-1 was used to verify the model.

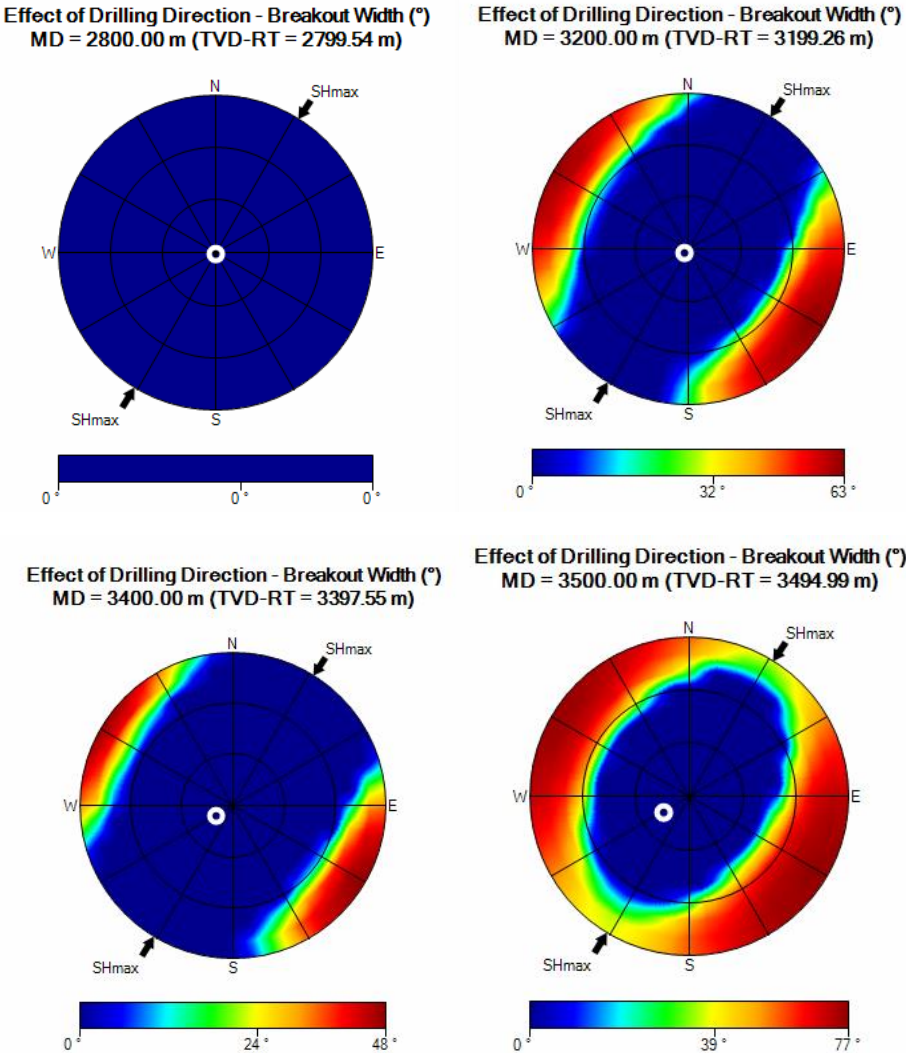


Figure 3. 45. Depth based CMW at 2800m, 3200m, 3400m and 3500m displaying the predicted failure, AM-1.

Based on the reported drilling events, there were not major problems in the area from 2800m to 3700m, so the depth based analysis (Figure 3. 45) seems to be consistent with the data.

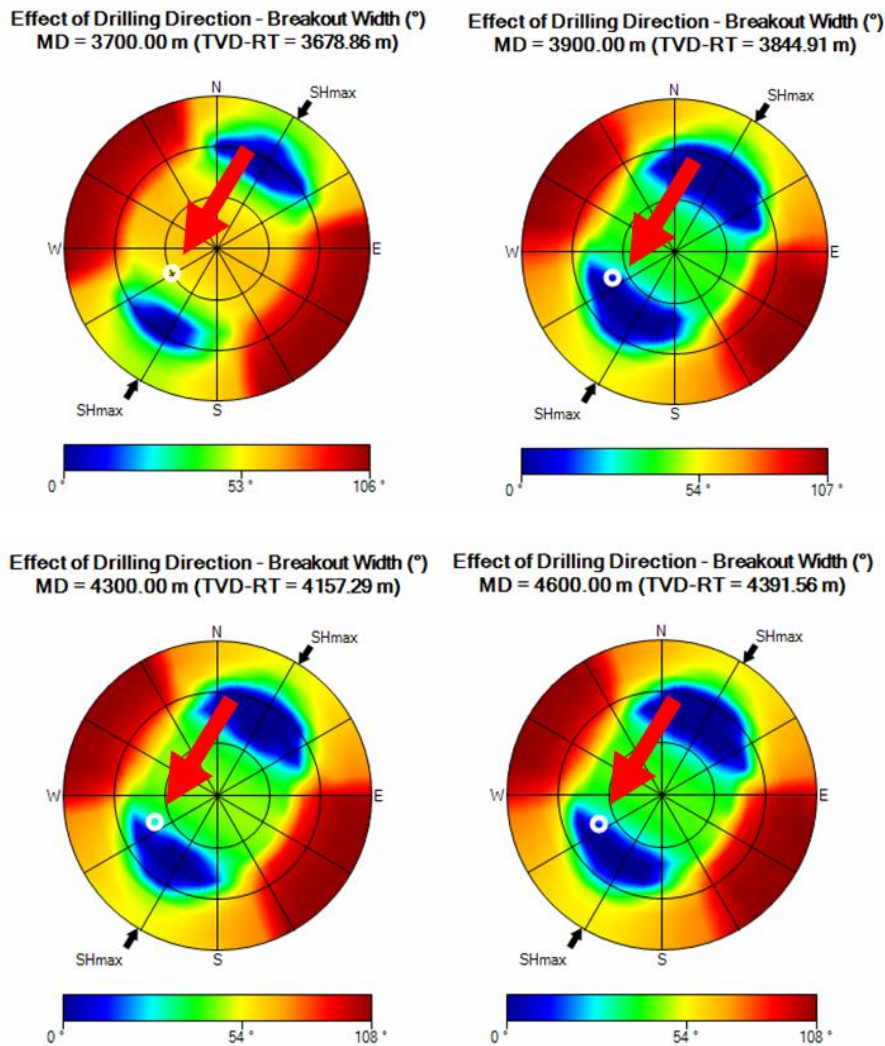


Figure 3. 46. Depth based CMW at 3700m, 3900m, 4300m and 4600m, displaying the predicted failure, AM-1.

On the other hand, from 3700m to 4600m, there were several tight-hole events. According to Figure 3. 46, the model predicts failure in this area but considering the trajectory of the well (white dot pointed by red arrow), we would not expect to have breakouts, which is consistent with the data. The model was calibrated with a bedding angle of $\sim 5^\circ$ and a bedding dip azimuth of $\sim 170^\circ$. We observed that when drilling a vertical well the breakout width ranges from $\sim 20^\circ$ to $\sim 50^\circ$ and a well, with an inclination over $\sim 30^\circ$ in direction of the S_{Hmax} would be a better option to avoid the breakouts.

Well AM-11

Regarding AM-11, cavings and tight-hole events were reported in this section, starting at 3000m. The major drilling problems were in the section from 3000m to 4400m. Figure 3. 47 shows that the predicted failure is consistent with the data calculating breakout width of $\sim 70^\circ$ in the upper part, and $\sim 40^\circ$ in the lower part of this section.

Proposed Approach and Experimental Method

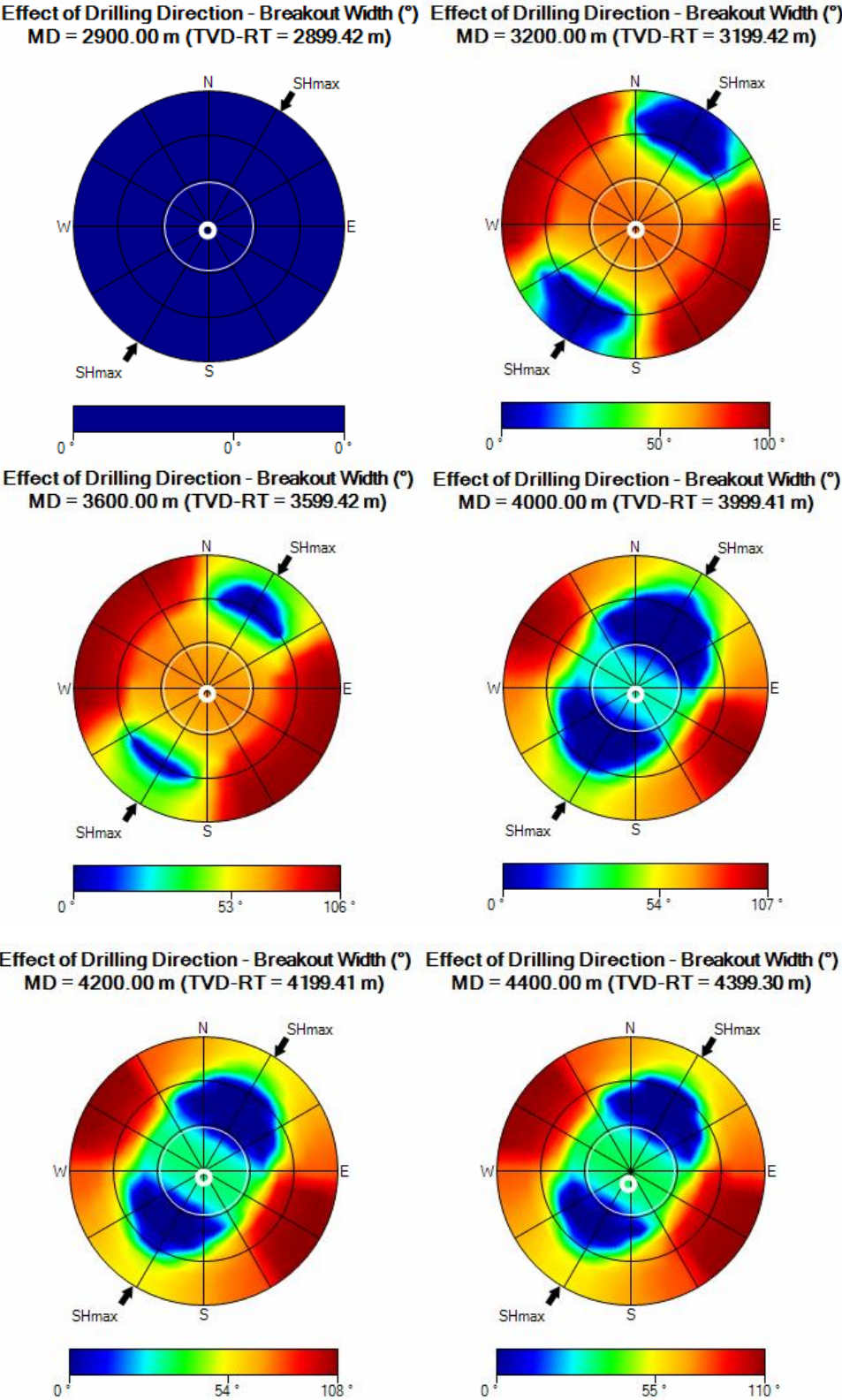


Figure 3. 47. Depth based CMW at 2900m, 3200m, 3600m, 4000m, 4200m and 4400m displaying the predicted failure, AM-11.

3.6 Shale Evaluation

Having the shale samples of well S-6081 (formation A4) and in order to analyze the micro-fractures and pore plugging effects. The experimental part was introduced in the methodology. During the study of this field, the following questions raised:

- a) What is the overpressure mechanism in this area?
- b) Is this shale formation a source rock?
- c) If the shale formation were a source rock, would it be possible that the hydrocarbon generation played a role in the overpressure mechanism and micro-fractures?

To have a better understanding of the cause of the instability problem, it was decided to run TC, S, TOC and pyrolysis measurements as well as taking an image of the samples in high resolution using the micro-CT scanner.

3.6.1 Cleaning Methods

In collaboration with the Chair of Petroleum Geology at the Department Applied Geosciences and Geophysics and the Chair of Reservoir at DPE, it was proposed to evaluate the shale samples.

First, the conditions under which the samples have been collected had to be considered. Due to the nature of the shale rocks of being reactive to some fluids and having the effect of cation exchange capacity (CEC), it is a common practice in the study area to use an oil-based mud system to stabilize the shale formations. This is the first encountered challenge when it came to evaluating the shale, because the oil-base mud is made, in this case, with diesel. The chemical composition of diesel is about 75% saturated hydrocarbons (primarily paraffin including *n*, iso, and cycloparaffin), and 25% aromatic hydrocarbons (including naphthalene and alkylbenzene; Diffen, 2019). These hydrocarbons will affect the measurement of the TC and TOC, thus the determination of the kerogen type. For this reason, it is important to clean the samples before analyzing them.

There were two options to clean them, the Dionex and the Soxhlet methods already explained in Chapter 2. The Dionex which operates at high pressure and temperature is the fastest way to clean the samples but the disadvantage, for this methodology, is that the containers where the samples are placed are about 5cm high x 2 cm diameter. This is a disadvantage because besides measuring the parameters mentioned before, it is also required to build a disk for the HPHT filter test (explanation in point 3.5) after the cleaning in order to compare the results obtained with clean and unclean samples.

On the other hand, the second method, the Soxhlet extractor, allows placing bigger pieces to be cleaned but the required time for this process is at least 24 hours (more than 72 cycles) per sample. Additional to this, depending on the size of the boiling flask and extractor chamber, the quantity of solvents becomes expensive.

To compare the results of the rock evaluation, it was decided to clean the samples with both methods.

Proposed Approach and Experimental Method

The samples obtained from well S-6081, field AM2, correspond to cavings from the Miocene at 2700m and 3400 m and cuttings from the Eocene at 3900m. Thus, three samples were analyzed in this study.

The procedure to clean the samples with each method is explained as follows,

Dionex procedure:

To assess the impact of the sample size on the cleaning process, three different sample sizes of the cavings (2700m and 3400m depths) were cleaned and measured, Figure 3. 48.

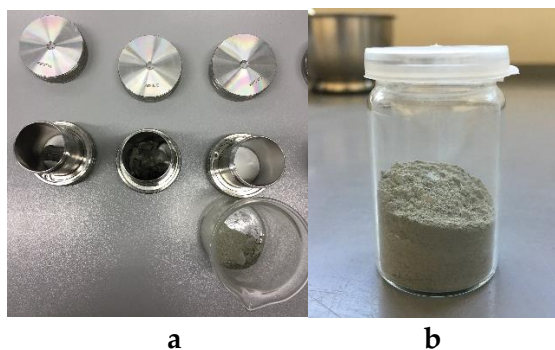


Figure 3. 48. Samples measured in Dionex. a) Left to right: complete small caving, crashed to little pieces, milled to powder, well S-6081, 2700m depth. b) Powdered sample, well S-6081, 2700m depth.

The samples were placed in the Dionex and cleaned with the following parameters:

Soxhlet extractor procedure:

The Soxhlet extractor used in this methodology is comprised by a 4 litres flask, 6 cm diameter extractor chamber and 50cm length condenser. The whole system is 1.50 m height including the electrical heater. It is required to be placed in a fume hood to extract the vapours of the solvents and to have a continuous cold-water source. The latter was set up using a refrigerated circulator to maximize the efficiency of the condenser and avoid solvent losses during the whole process, Figure 3. 49. The water was circulated with 10°C in the condenser.

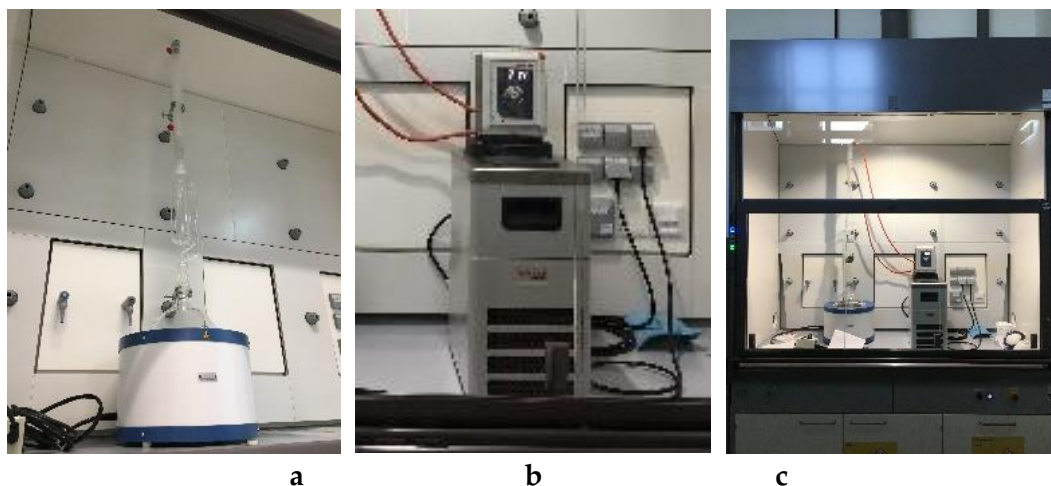


Figure 3. 49. Left to right: a) Soxhlet extractor set up, b) refrigerated circulator and c) whole system in the fume hood. DPE Laboratories.

The cleaning procedure followed the recommendations mentioned on the paper: *Impact of Different Cleaning Methods on Petrophysical Measurements* (Gupta et al., 2017). The azeotrope mixture of solvents used to clean the cavings were Methanol (88% vol.) and Toluene (12% vol.), according to the azeotrope data of this mixture, the temperature of the boiling point is 63.5°C, then the temperature in the Soxhlet was set between 65°C and 70°C same as in the paper just mentioned.

The volume of solvent used in this case was 1 litre of the total mixture. Each sample was cleaned for three days during working hours for a total of 24 hours cleaning; with this set up (Soxhlet size, volume of solvents and temperature), it was observed 3 to 4 cycles per hour. Giving at the end something between 72 and 96 cycles in total, which was in the range of the requirement to obtained good results. Because the samples were the cavings (2 - 4 cm size), they were placed in the extractor chamber without a thimble or filter paper, Figure 3. 50 , when cleaning the cuttings, the thimble is required.



Figure 3. 50. Cavings in the extractor chamber.

3.6.2 TOC and SRA Evaluation and Cleaning Methods Comparison

As mentioned and described in Chapter 2, the total carbon (TC), total sulphur (S) and total organic carbon (TOC) contents were analyzed using an ELTRA Elemental Analyzer for all samples at the Chair of Petroleum Geology. The analyzed samples were cleaned as follows:

- The cavings collected at 2700m were cleaned just in one size, the complete caving, with both methods, Dionex and Soxhlet extractor.
- The cavings collected at 3400m were cleaned with the Dionex (3 particle sizes, Figure 3. 48) and Soxhlet extractor (complete cavings, Figure 3. 50).

All the samples mentioned before were crushed to powder, weighted and decarbonized with concentrated phosphoric acid for TOC measurements, Figure 3. 51. The results will be discussed in Chapter 5 and given in weight percent (wt.%). The total inorganic carbon (TIC) was determined with the formula: $TIC=TC-TOC$ and further used to calculate calcite equivalent percentages with the formula: $Calcite\ equivalent=TIC*8.333$.



Figure 3. 51. Samples ready to be analyzed by the ELTRA Elemental Analyzer.

The pyrolysis measurements were performed using a “Rock-Eval 6” instrument, Figure 2. 4. The analyzed samples were the same, described before, analyzed with the ELTRA Elemental Analyzer.

The values obtained from S1 and S2 peaks (mg HC/g rock) were used to calculate the petroleum potential ($S1+S2$ [mg HC/g rock]), the production index ($PI=S1/(S1+S2)$), and the hydrogen index ($HI=S2/TOC*100$ [mg HC/g TOC]).

T_{max} was measured as a maturity indicator. The amount of hydrocarbons that can be generated below 1 m² of surface area was calculated using the Source Potential Index ($SPI=thickness*(S1+S2)*bulk\ density/1000$; Demaison and Huizinga, 1994).

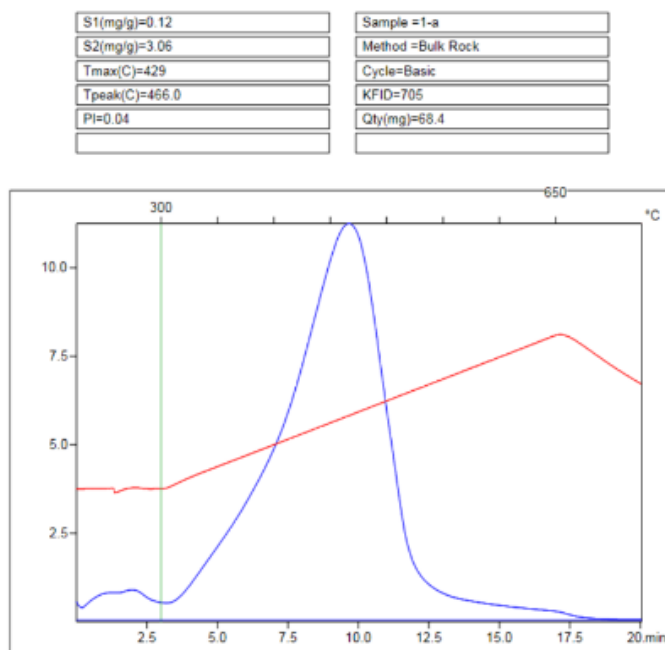


Figure 3. 52. Example of the results obtained from the Rock Eval analyzer.

The blue graph is the measured curve in time. The height is an indicator for intensity. The green line indicates the reached temperature (300°C) when the measurement of S2 starts. The red line is the calibration of the machine.

3.6.3 CT Scanner Images

One of the assumptions that arose while analyzing the probable causes of the cavings while drilling these formations was that the shale could be micro-fractured. If the shale, in fact, has this condition, then the permeability would increase leading to allowing the drilling fluid to invade and weaken the formation. In order to investigate this theory, it was proposed to scan the cavings looking for an indication of micro-fractures.

There are two CT scanners available at the DPE Laboratories, the medical and the micro CT scanners. When we talk about micro-fractures, as it was mentioned in Chapter 2, we are referring to sizes that ranges from 1 to 6 μm . The scanner used in this analysis was the micro-CT scanner because the resolution of the medical one is not as high as required to observe these features.

The resolution of the micro-CT scanner is expressed in terms of voxels. A voxel is a combination of volume and pixel and represents a value on a regular grid in three-dimensional space (3D ProScan 2016). The shape and size of the sample are factors that affect the resolution of the images. For this analysis, one of the cavings was carefully grinded to a cylindrical shape, which is the one that gives the best resolution. The sample that was scan, Figure 3. 53, was 25mm height x 10mm diameter. With this sample, we obtained an image of 6.8 voxels, a resolution sufficient to observe micro-fracture features if any.

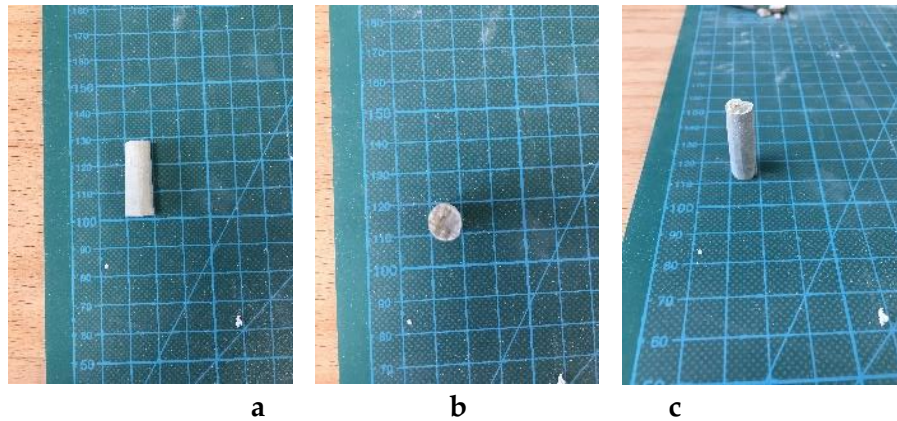


Figure 3. 53. Sample preparation for the micro-CT scanner. Showing a) the height of sample (30mm), b) the diameter of the sample (10mm) and c) the complete sample.

3.7 Pore Plugging Analysis

3.7.1 Fluid invasion

As mentioned in Chapters 1 and 2, it was observed from a thorough review of the resistivity logs that the wells analyzed in this study seem to present a fluid invasion, especially in the shale formation where the cavings were reported and the caliper log is out of gauge, Figure 3. 55. Fortunately, most of the wells have both curves, deep and shallow resistivity so a review and comparison could be performed.

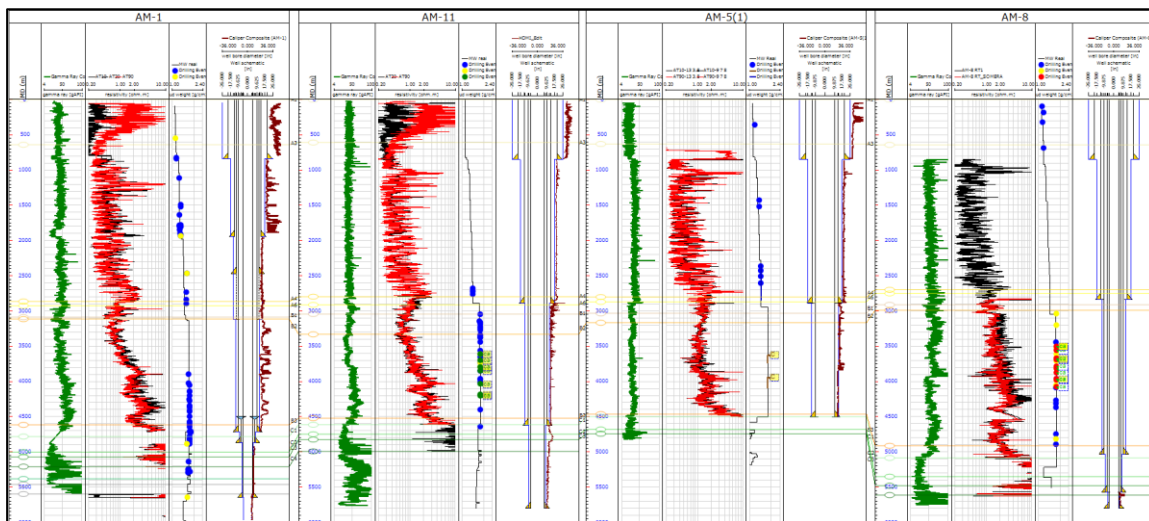


Figure 3.54. Overview of the gamma ray and resistivity logs (deep and shallow curves) together with the drilling events, well schematics and caliper logs, wells AM-1, AM-11, AM-5 and AM-8.

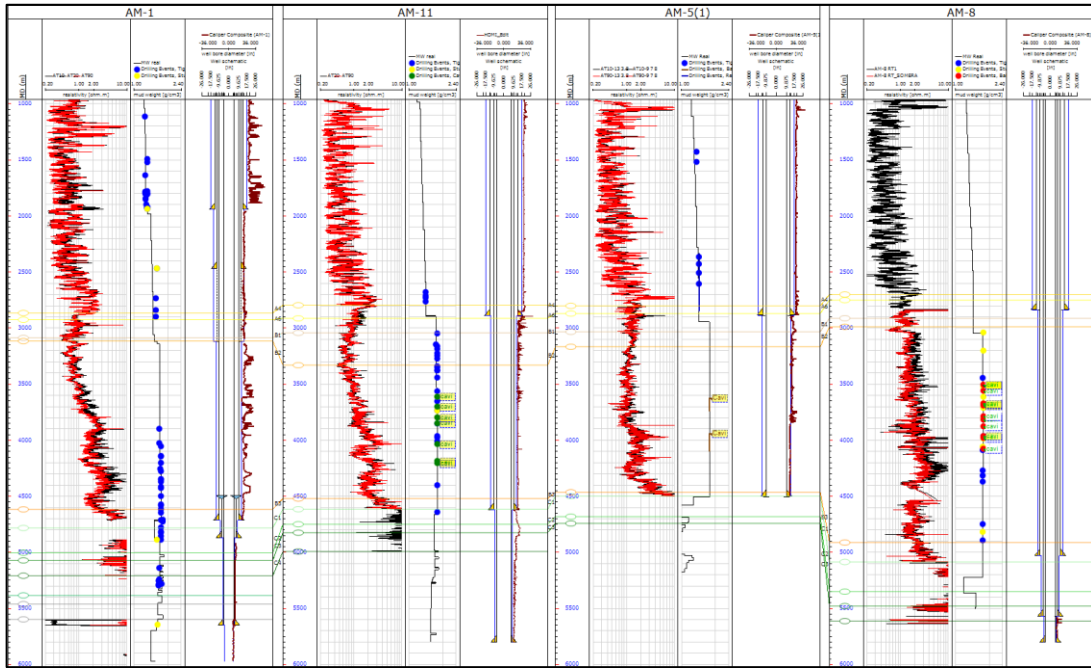


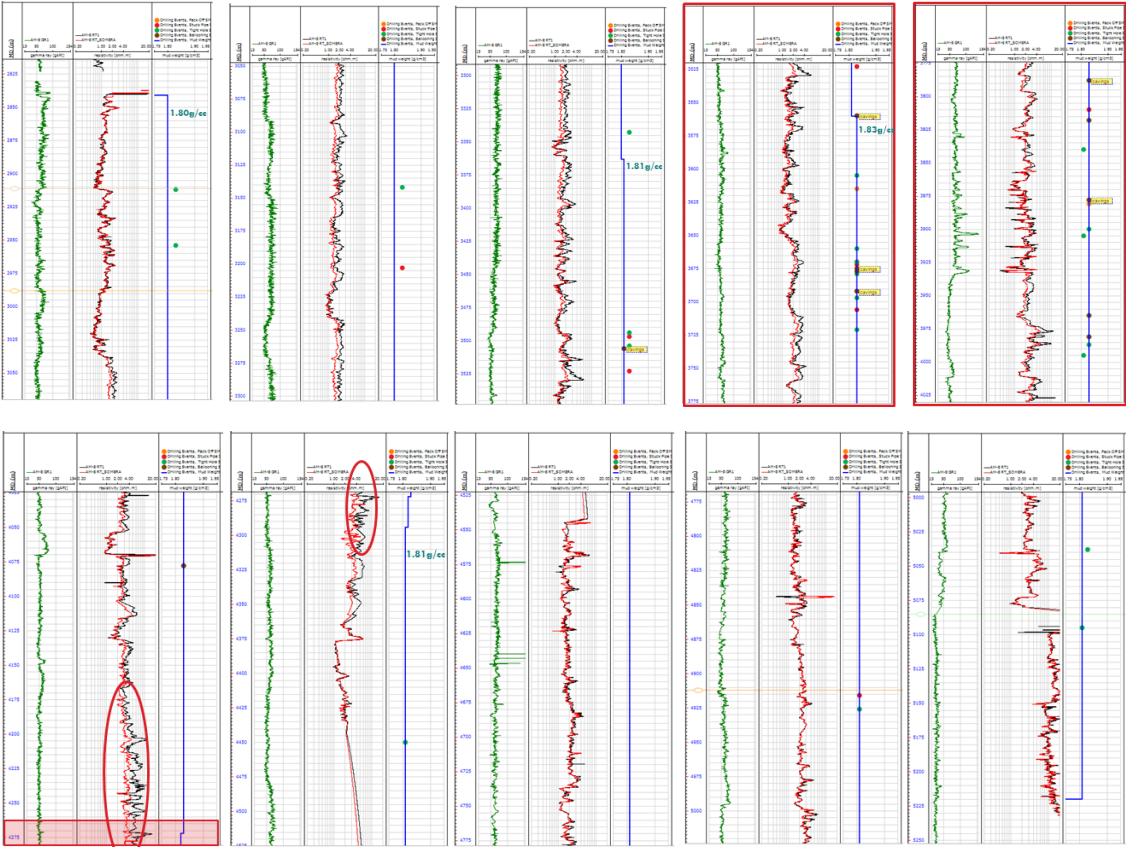
Figure 3.55. Closer view of the resistivity logs (deep and shallow curves), drilling events, well schematics and caliper logs, wells AM-1, AM-11, AM-5 and AM-8.

The exploratory well, AM-1, interestingly did not present reported cavings during the drilling operations. Nevertheless, the caliper and resistivity log seem to show an enlargement in the same problematic formation as well as a possible fluid invasion respectively.

Wells AM-11 and AM-5, in a lesser magnitude also show some indications of filtration. Yet, AM-11 presents a higher separation of the curves in an upper layer.

The well that had the worst problems (higher volume and bigger pieces of cavings) during drilling was AM-8, which at first glance presents the higher curves separation. In the following pages, a closer look to these events will be presented.

Proposed Approach and Experimental Method



33 hours break failure

Figure 3. 56. Gamma Ray and Resistivity logs compared to the mud weight and drilling events, probable invaded formations shown in red.

As we can see in Figure 3. 56, there is an indication of high level of filtrate into the formation during the drilling operations of AM-8, specifically in the unit B2. In this well it can be observed that most probably, the fluid invaded the formation from 3040- 4370m, reaching the higher values from 4200-4330m (marked in red). The red circles show the higher separation of the curves, it is important to mention that at this depth, the break had a failure and the drilling operations had to be suspended for a period of 33 hours while the crew fixed the problem. This remark will be discussed when the results of the pore plugging tests are described in Chapter 4.

If the fluid filtration occurred in these formations and affected the wellbore integrity and its strength, the common thought that comes to mind is that lost circulation material is needed to be added to the mud in order to minimize or avoid this problem. The company provided the fluid program and after a review of it, it was noticed that they were actually using LCM (lost circulation material) during the drilling operations of these formations. Thus, it was speculated if the LCM used in these wells was the right one or not. When it comes to LCM selection, as it was explained in Chapter 2, there are several factors to be considered, especially in non-conventional formations such as anisotropic micro-fractured shales could be. It becomes very tricky because normally the size particle of the LCM is selected depending on the porosity, permeability, pore size distribution of the rock, but in this case, as we talk about shale, all these characteristics are completely

different from a conventional formation such as sandstones. In the previous point, Shale Evaluation, it was mentioned that during the scanning of a small sample of the cavings, it was found 2-3 micro-fractures proving that this shale is in fact micro-fractured and it would probably not have too low permeability due to this characteristic. Then, if the selection of the LCM cannot be assessed by analyzing the pore distribution, it was thought if it could be determined by analyzing the micro-fractures in the shale.

In order to prove or reject this assumption, it was proposed to develop a different set up of the HP/HT filter press and run this test to investigate the behaviour of the actual rock with the drilling fluid.

3.7.2 Proposed PPT Set Up

The HP/HT filter press used to evaluate lost circulation materials in the drilling muds, as mentioned in Chapter 2, is a conventional apparatus from the Oil and Gas industry. Nevertheless, there is always room to do things differently and thinking out of the box. In the previous point was explained why the LCM selection for this particular problem could be a difficult task to perform. For this reason, it was thought about a possible method that could help to have a better understanding of the interaction of these types of formations with the drilling fluid at bottom hole conditions.

At the beginning of this Chapter, it was mentioned that in order to apply the methodology proposed in this master thesis, it was necessary to have the samples of the cavings at least 2 to 3 cm's size available for testing. The idea behind this requirement is to use the shale sample instead of the ceramic disks that conventionally are used for these kinds of tests. Since the filter press can be run at 260°C and 1800 psig and the drilling mud at borehole conditions can be simulated, then, why not trying with the real rock formation and observe what is their interaction. Thus, the proposed set up for the pore plugging test in this thesis. Even though, there were three limitations that could have possible happened: 1) no filtrate at all due to the low permeable formation characteristic, 2) not to achieve an effective seal in the build disk and, 3) epoxy not suitable for tests, the tests were performed and the results will be discussed in Chapter 4.

The setup of the test cell itself would not change and similar procedure as the one used with the ceramic disks will be followed.

Chapter 4 Shale Disks

4.1 Building the Shale Disks

The cavings from the field analyzed in this research, field AM1, were not available anymore because the company normally just storage the cuttings collected and described by the mud loggers (very often just in the reservoir). Cavings are usually collected by the drilling crew, they just take photos showing shape and size to send them to the geomechanics specialists who determine the type of failure and possible solution. It is not common to storage or analyze them in composition or properties.

70 km's from AM1, there is another field, AM2, which also presents the cavings with the same shape and size as in AM1. Fortunately, at the moment of this research, there was a well, S-6081, having exactly the same problems and circulating out the cavings.



Figure 4. 1. Cavings collected at the drilling site, well S-6081. a) Showing one sample just taken from the shale shaker, b) All samples collected from the shale shaker.



Figure 4. 2. Cavings cleaned with a fabric and sorted by size, well S-6081.

The cavings were collected on the drilling rig site, Figure 4. 1, where well S-6081 was being drilled at a depth of 2700m (md). The drilling mud used at that moment, OBM, was also collected and shipped to Austria.

Shale Disks

The shale samples were cleaned, piece by piece, using a strip of dry fabric and sorted by size, Figure 4. 2. The biggest pieces were approximately 4 cm x 2 cm x 2 cm. It is very important to mention that the samples have to be properly cleaned and preserved to achieve as best results as we can. On a side note, never use water to clean these samples. Shale rocks are mudstones and they will disintegrate in contact with water, unless the water has additives to avoid the hydration of the rock.

Shale sampling procedure:

1. Standing at the shale shakers wearing PPE including gloves for high temperature substances, when the cavings are coming out, choose the biggest cavings you can see.
2. Place them in a container with a bottom mesh.
3. Once in the camping truck, wait until the cavings are not too hot anymore and using a piece of dry fabric (never wet), clean 15-20 cavings depending on the size.
4. Use two or three plastic bags that can be sealed to have them preserved.
5. When storage or transporting, handle the bags carefully and out of any humidity.

Once the samples arrived at DPE, the challenge was to build a disk out of cavings, similar to the conventional ceramic disks (Figure 4. 3) with the following specifications:

- 6cm (diameter) x 6mm (thickness).
- Resistant to high pressure and temperature.
- Using an impermeable material (adhesive) that ensures the sealing in the transition rock/adhesive and adhesive/PPA.



Figure 4. 3. Conventional ceramic disk used in the HP/HT filter press.

Since the medium used to keep the pieces together had to be impermeable to ensure that the mud filtrate would only pass through the shale sample and the results would not be affected, the material that came to mind was an epoxy/resin or something similar to that.

Then, the first solution was to build a block or cube of epoxy with several cavings immersed and drill a 6cm core from it. Afterwards, cut the core every 6mm to obtain several disks from this sample. The problem with this idea was that according to specialists from the Subsurface Engineering Department, to cut epoxy with their equipment was not viable because cutting through this kind of material could be very tricky. If the resin is not cut slowly enough it will crack or get damage, if additionally to this, we add another material, such as shale, which can also be very tricky to be cut because of its lamination and brittleness, the whole combination would make it very difficult to obtain clean cut disks as required. Besides this advice, it was agreed to try

this method in a small sample with the assistance of the Petroleum Geology Department. The sample was prepared in a cylindrical shape instead of a block to reduce the cutting process and when it was tried to be cut, it was not possible to do it. Firstly, the cut of the epoxy was not possible to be as smooth and clean as desired and became more difficult when encountering the shale. Secondly, a point that was not considered was that this cutting process is performed under water, which as we mentioned in the sampling procedure, the shale should not be in contact with water unless it has the proper additives. The result of this method was not satisfactory.

Cutting a sample prepared with the epoxy and the shale is a difficult task to perform, thus, a second solution was presented. This time, it was thought to flatten the shale samples until obtaining a 6mm flat sample from them, to make a form with the exact size of the ceramic disk and to place just one sample big enough in the middle of the disk. A especially made form for handling epoxy with a diameter of 6cm was ordered. Even though the ceramic disk has a slightly higher diameter for one or two millimetres, it was recognized that the rubber seals from the HP/HT filter press would allow a smaller disk without compromising the complete seal in the system. The form was 5cm high, this could have been cut to 6mm in height but at the end it was decided not to cut it but to mark the 6mm height in the form to use it as a benchmark. When deciding how to flatten the shale sample, two options were thought, 1) to grind them until reaching the desire thickness with a rotary tool using diamond grinding slice-cutting discs, or 2) to cut them with a Dremel® using a diamond edge blade. The problem with the first option was having the concern about affecting the permeability by grinding or kind of polishing the sample accidentally. Thus, it was decided to use the Dremel® and diamond blade. Another challenge was to have the shale sample unsealed by the epoxy when preparing the disk, it was observed that the upper surface of the shale could remain exposed above the epoxy level but the bottom one in any case had to be covered by the epoxy. To solve this issue, the bottom surface was protected using a thick masking tape and cut with a cutter when the epoxy was cured. The disk was build and let cured for a minimum of 3 days to ensure the integrity of the epoxy.

Epoxy evaluation

Two different epoxy systems were evaluated in order to compare their properties and limitations: Epoxy 1 and Epoxy 2. As it was mentioned before, the adhesive material had to withstand high pressure and temperature similar to the borehole conditions and be impermeable to ensure the sealing capability in the transition rock/material and material/PPA. There are many epoxy systems on the market with different properties and most of the times, the temperature and strength limitations are not mentioned in the technical specifications, which made the selection process a little bit tricky. Both selected systems, The epoxies considered, are normally used as coating material and the mixing and application are similar, the percentage of the resin and hardener changes but both of them have a working time of 30 minutes after mixing.

The first one evaluated, E1, was suggested by the Petroleum Geology Department. They normally use this type of epoxy to encapsulate the rock samples to be examined in the microscope or to build thin sections.

The resin system as follows:

Shale Disks

- E1 100 pbw
- Hardener H1 20 pbw

According to the technical specifications and properties, it has good heat resistance as well as good resistance to atmospheric and chemical degradation (Vantico Ltd, 2000).

After placing the disk with the shale in the test cell and fill it with the oil-base mud, the test was run applying 500 psi and 65°C. Almost instantaneously, there was a cracking sound and mud leaking was observed. The test was ended to inspect the disk; the disk had a crack that also broke part of the shale sample allowing the mud to pass through it.

The second epoxy system evaluated, E2, has being used in an ongoing research to improve properties in the cement. According to specifications, it helps to minimize cracking in underpayments and toppings (Ardex L.P., 2012).

The resin system as follows:

- Resin E2 60 pbw
- Hardener H2 40 pbw

It was tested using the same conditions as before, 500 psi and 65°C. After pre-heat the test cell, placing the disk, filling with mud and closing the cell, the HTHP filter press was turned on and monitored. This time there was no mud leaking like it happened with the previous epoxy. As it was uncertain how long would it take to start filtrating or even if it would have been possible to observe any filtration at all, after 30 minutes of monitoring it was decided to let it run for 24 hours. The next day, after 22 hours of testing it was observed 1 ml of filtrate. The disk was retrieved from the cell for evaluation. It was observed that it was slightly deformed, but the filtrate indeed passed through the shale rock and not through the epoxy, edges or interface between the epoxy and the shale rock. This test was considered successful and the E2 was selected for this methodology.

Disk building procedure:

1. Choose the bigger samples with an already flat surface if they have one.
2. Wearing glasses, dust mask and gloves, select the proper cutting blade for the Dremel®.
3. Mark with a pen the parts to be cut to obtain a flatten piece of rock a little bit higher than 6mm (up to 8-9mm should be recommended)
4. Using the Dremel®.with the cutting blade and tweezers to hold the sample, very carefully and slowly cut the marked areas in the shale caving.
5. Once you have the flatten shale, use a thick masking tape to cover the flattest part of the sample.
6. Mark the height of the ceramic disk (approximately 6mm) in the form.
7. Prepare 30-40 ml of epoxy (resin + hardener) according to the required volume of each and stir very slowly for 3-5 mins.
8. Place the shale sample (with the covered surface on the bottom) in the middle of the form.
9. Very carefully, pour the epoxy little by little in the surrounding areas of the sample without dropping any of the epoxy on the upper part of the sample, until reaching the mark.
10. Let it dry for at least 2 or 3 days.

11. Remove the sample from the form and using a cutter uncover the epoxy and masking tape from the bottom surface. Cut an area slightly smaller than the area of the sample to ensure the sealing.



Figure 4. 4. Building procedure of the shale and epoxy disk to be tested.

4.2 Performing PPT with Shale Samples

The next step in the proposed methodology was to test the built disk in the previous point in the Fann High-Pressure, High-Temperature Filter Press. As mentioned in Chapters 1 and 2, this apparatus simulates borehole conditions up to 500 °F (260 °C), 1800 psig in the cell and 750 psig in the back-pressure receiver when the filtration properties of drilling muds want to be evaluated.

Once the first disk was built, measured and ready to be tested, the following was to set up the filter press and the drilling fluid.

The company provided the drilling fluid used in this experiment; the commercial names of the additives cannot be mentioned but the generic names will be added. The cavings in this field, AM2, are present in formation A4, at shallower depth than in field AM1. This section, corresponds to the 12 ¼" bit size, and is being drilled with an oil-base mud (OBM) from a service company with the characteristics listed in the following Table 4. 1.

Shale Disks

Fluid type	Dens. [g/cc]	Visc. [seg]	Filt. [ml]	O/W ratio	Solids %	PV [cP]	YP [lb/100 ft ²]	Gel-0 [lb/100 ft ²]	Gel-10 [lb/100 ft ²]	Salin. [ppm x1000]	Emuls. [Volts]
OBM	1.42	55-75	< 2	80/20	17-21	21-24	15-24	7-12	14-23	200-220	700s

Table 4. 1. Properties of the fluid used in the PPT. Company courtesy.

The materials and additives used in the mixture as follows:

- Barite
- Organophilic clay
- Calcium hydroxide
- Primary emulsifier
- Secondary emulsifier
- Asphalt
- Gilsonite
- Calcium chloride
- Calcium carbonate (25 kg/m³)

During the first test of the shale sample, it was expected to have a long testing period due to the low permeability characteristically of shale rocks but the exact time was completely unknown, it could have been hours, days or even weeks.

The setup of the filter press was the same as mentioned before, only that this time instead of placing the ceramic disk, the disk build with the shale sample and the epoxy was used.

The applied pressure in the cell was calculated from the differential of the pore pressure and hydrostatic pressure at bottom hole conditions, resulting in 700psi but it was decided to try first at a lower pressure of 500psi. The temperature for the set up was obtained from the geothermal gradient, resulting in 65-70°C.

The drilling fluid was stirred in order to have a completely homogeneous mixture in the cell.

Having the bottom hole conditions, the drilling fluid and the shale sample prepared, the test was started. It is important to mention that due to the uncertainty of the testing time, all the precautionary measures were taken into account, especially when using a high pressure device. The filter press was located in a closed room in the laboratory where people were not allowed to enter during the test. Since it was the first time testing an actual rock (with very low permeability) in this device, every safety precaution was taken during the testing procedure

HPHT Filter press test using disks made of epoxy and shale rock:

1. Pre-heat the HPHT filter press to the desired temperature.
2. Place the epoxy/shale disk in the cell with the flattest part facing the bottom of the cell where the filtrate will be collected.
3. Stir the oil-base mud for 5 minutes or until is completely homogeneous.
4. Fill the cell 2-3 cm below the mark.
5. Close and place it in the chamber.
6. Connect the valves and set up the desired pressure.



Figure 4. 5. HPHT Filter press test using disks made of epoxy and shale rock, and oil-base mud sample.

Using the same procedure, Figure 4. 5, three more disks were created using different conditions, at the end four samples were tested:

- a) Two disks using an unclean sample
- b) One disk using a clean sample (cleaned with the soxhlet)
- c) One disk using more than one sample in the same disk

After the first time running the test, it was observed that at least 22 hours were necessary to obtain 1ml of filtrate. For this reason, the following tests were designed with longer testing periods to have enough information to compare and analyze. Results and observations will be discussed in Chapter 5.

Chapter 5 Results and Discussion

5.1 Results and Discussion

This thesis was proposed to investigate the causes of borehole instabilities in shale formations experienced in the AM1 Field (onshore Mexico). The approach includes experimental work using cavings recovered from affected wellbores in the area. Most of the time, the cavings are just analyzed for their shape to determine the type of failure. In this work, the main objective was to propose and develop analyses that can be run using the cavings, in order to have a better insight of what could be happening, thus propose a solution. Besides the geomechanical analysis, the study of the causes of the overpressure in this formation and the interaction between the drilling fluid and the shale itself, the shale composition was analyzed and a different setup of the HPHT filter press was developed. The results of every analysis mentioned and performed will be discussed in this Chapter.

Regarding the geomechanical analysis, the sensitivity of the stress regime showed that the strike-slip model appeared to calibrate well with the drilling experience including reasonable values for all parameters constituting the geomechanical model (biot coefficient, internal friction, cohesion, UCS, failure criteria, etc.). One of the scenarios using thrust faulting regime seemed to have a good calibration too, but considering regional tectonic aspects, the strike-slip model was a better fit.

According to the results of the wellbore stability analysis, the mud weight window to drill the shale formation is very narrow. In order to reduce the cavings and instability problems in well AM-11, the section should have been drilled with higher mud weight between ~ 1.88 g/cc and ~ 1.91 g/cc.

Additionally, the analysis showed that drilling a well with an inclination between $\sim 30^\circ$ and $\sim 60^\circ$ and an azimuth in the direction of $S_{Hmax} \sim 32^\circ \pm 60^\circ$ or $\sim 212^\circ \pm 60^\circ$ in this section, would likely reduce the risk of having cavings or drilling events related to wellbore instability such as tight hole, stuck pipe, etc. Following the recommendations mentioned before, a specific assessment in future wells will be necessary in order to determine the mud weight required in the analyzed formations.

The geomechanical analysis seems to match with the field development (Figure 3. 2) and drilling plan of the existing wells. The wells that reported cavings and had wellbore instability problems during the drilling activities in this formation (AM-21, AM-11, AM-25, AM-4 and AM-8) were drilled vertically, with the exception of AM-8, which KOP started at ~ 3037 m in direction of S_{hmin} , which is the opposite direction from the recommended in this analysis (Figure B. 5). Interestingly, the latter was the well that had the highest volume of cavings according to the company specialists, which complies with the results of this geomechanical analysis.

Results and Discussion

Concerning the recommended mud weight in this analysis, wells AM-1, AM-11, AM-5 and AM-8, were drilled with a mud weight between 1.75 g/cc and 1.84 g/cc. According to the present work, a higher mud weight between ~1.88 g/cc and ~1.91 g/cc is required in this problematic area. There were not partial or total losses reported in this formation but according to this analysis, the calculated mud weight window is very narrow and the ECD, when using a higher static mud weight might, reach the fracture gradient. Therefore, in order to minimize the risk of fracturing the formation, the following comments should be considered in future wells design: 1) The upper limit has a certain degree of uncertainty due to the LOTs and FITs reported in this field. Most of them are FITs where the operator determines the FIT “test-to” value, and the leak-off point is not reached. Sometimes, operators prefer to perform FITs in order to avoid the risk of decreasing the future pressure-containment capability. Therefore, an evaluation of the risks versus the benefits of performing LOTs should be carried out. 2) Adding a casing +/- 100m below the B2 top formation would allow to increase the mud density and minimize the risk of having losses or fracturing the formation in this section. However, the latter, is a recommendation based only on the geomechanical point of view and further economic impact assessment should be performed.

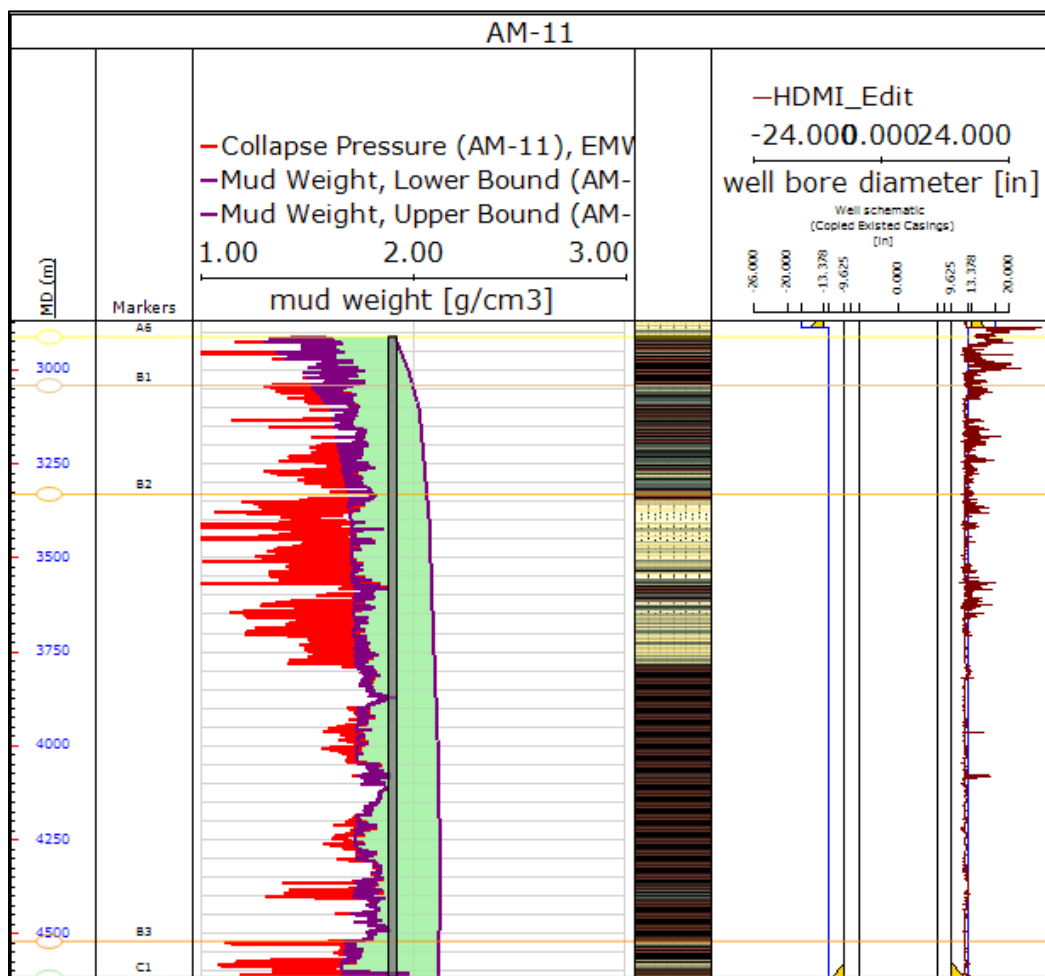


Figure 5. 1. Results of the wellbore instability analysis of well AM-11.

The results of the shale characterization, the measured values of TC, TOC, S and Rock Eval of the cavings and samples of cuttings, mentioned in Table 5. 1, define which size of the samples and which cleaning method are the most effective when the samples are recovered and contaminated with oil-based mud.

#	Sample depth	Sample size	Cleaning method	Comments
1	2700	Complete caving	Dionex	Cleaning method evaluation
2	2700	Complete caving	Soxhlet extractor	
3	3400	Complete caving	Soxhlet extractor	Cleaning method evaluation
4	3400	Complete caving	Dionex	Sample size evaluation
5	3400	Small pieces	Dionex	
6	3400	Powder	Dionex	

Table 5. 1. Samples used for the analysis of the shale evaluation at different depth in the formations where the cavings and instability problems were present.

Comparing the cleaning methods Soxhlet extractor vs Dionex:

Comparing the results obtained from samples 1 to 4 (Figure 5. 3 and Figure 5. 4), we can observe that between Dionex and Soxhlet, the cleaning method that seems to give a better results is the Dionex. This is evaluated by the shape of the curve, the first peak is the measurement of S1 and the second peak, of S2. The sample is contaminated when there is a double peak in the plot as shown in Figure 5. 2. This plot is the result of the shale with no cleaning process. Even though the Dionex gave better results, it was also noticed that it has a limitation when the samples are heavily contaminated with mud. If it is the case, the samples should be cleaned with the Soxhlet extractor.

Results and Discussion

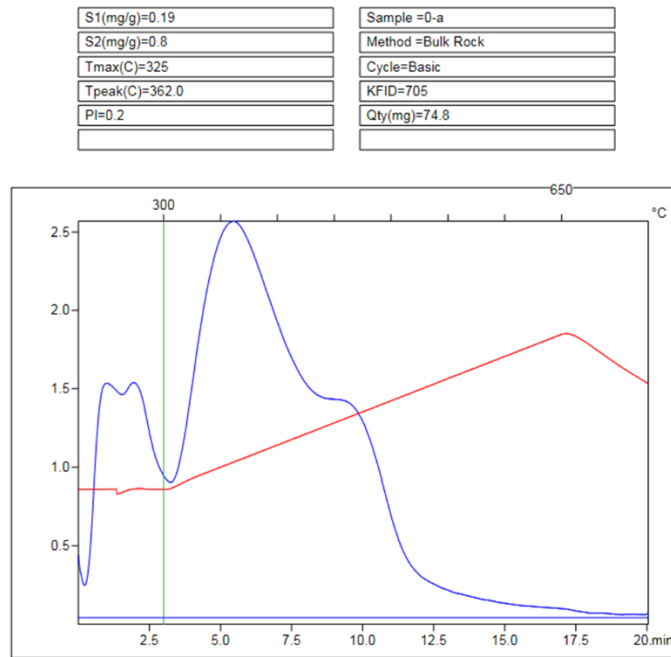


Figure 5. 2. Rock Eval results of the contaminated shale sample with oil-based mud (no cleaning process).

Sample 2700m

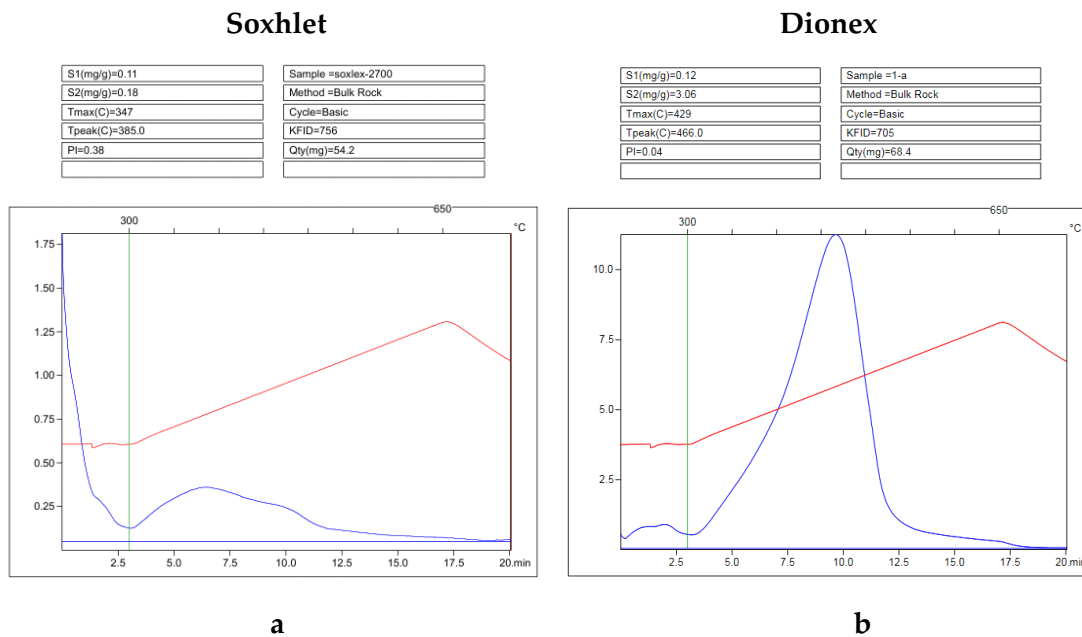


Figure 5. 3. Rock Eval results comparison of samples 1 and 2 cleaned with two methods, Soxhlet and Dionex. a) Shale sample from 2700m cleaned with Soxhlet method, b) shale sample from 2700m cleaned with Dionex method. Values shown in Table 5. 2.

Sample 3400m

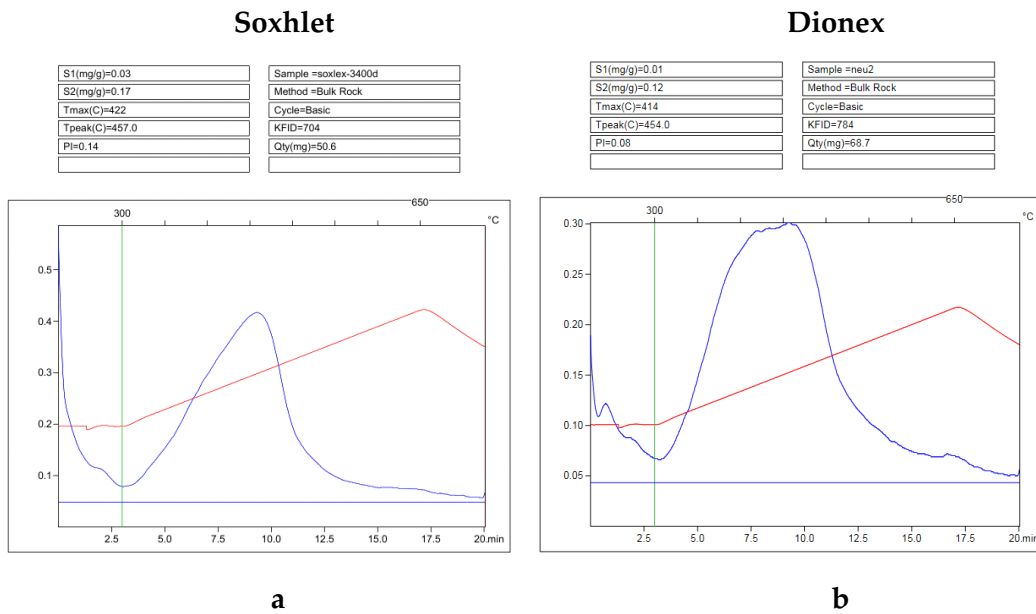


Figure 5. 4. Rock Eval results comparison of samples 1 and 2 cleaned with two methods, Soxhlet and Dionex. a) Shale sample from 3400m cleaned with Soxhlet method, b) shale sample from 3400m cleaned with Dionex method. Values shown in Table 5. 2.

Comparing the size of the samples:

The results of the complete caving, small pieces and powder cleaned with the Dionex method (samples 4, 5 and 6) were compared (Figure 5. 5). According to colleagues from the Petroleum Geology department, the caving sample should give more accurate results in this case. The reason is that the organic matter of the rock is not removed because the solvent passes through the matrix, removing just the oil-based mud.

Sample 3400 m

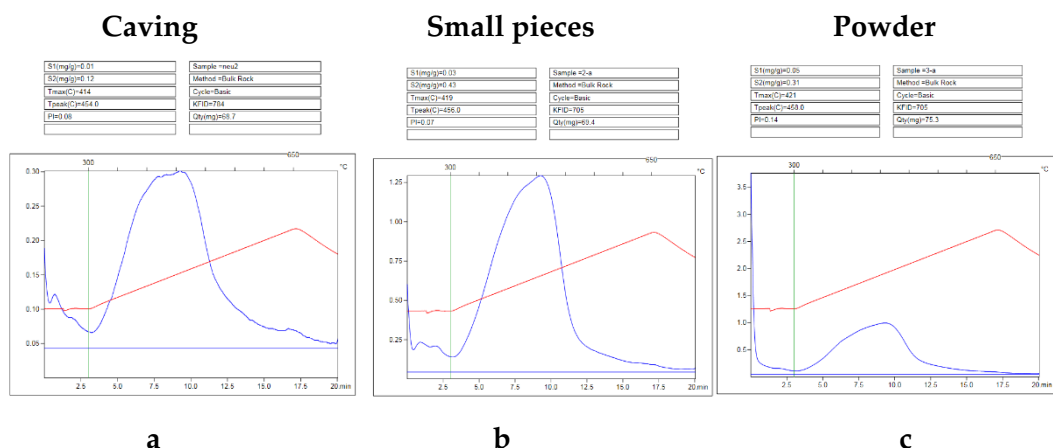


Figure 5. 5. Rock Eval results comparison of samples 4, 5 and 6 cleaned with the Dionex method. a) Complete caving from 3400m, b) sample crushed to small pieces from 3400m and c) sample milled to powder from 3400m. Values shown in Table 5. 2.

Results and Discussion

At the end, this analysis provides the type of kerogen that the shale rock contains. These are two important pieces of information to determine: what was the depositional environment and what kind of hydrocarbons were generated. In this case study, we can observe (Table 5. 2) that the samples contained kerogen type III and IV, which indicates terrestrial organic matter and proximity to the shore. Kerogen type IV corresponds to non-hydrocarbon generation and Kerogen type III corresponds to generation of gas. The low maturity of the samples (below 430°C T_{max}) rules out the hydrocarbon generation as the cause of the overpressure and micro-fracturing. Some values are different from the others, this might be due to the uncertainty in the depth interval. The cavings fall down to the bottom hole from upper layers and having control of the depth in this case, is not a straightforward activity.

#	Sample depth	Sample size	Cleaning method	Comments	S1(mg/g)	S2(mg/g)	Tmax(C)	TCC	SS	TOC	TIC	calcite equ.	SPI	SBPI
11	22700	Complete caving	Dionex	Cleaning method evaluation	0,120	3,060	429	2,566	2,9	2,44	0,12	1,0	7,6	
22	22700	Complete caving	Soxhlet extractor		0,110	0,180	347	2,566	2,9	2,44	0,12	1,0	0,7	
3	3400	Complete caving	Soxhlet extractor	Cleaning method evaluation	0,030	0,170	422	0,833	0,49	0,53	0,30	2,5	0,5	
4	3400	Complete caving	Dionex	Sample size evaluation	0,010	0,120	414	0,833	0,49	0,53	0,30	2,5	0,3	
5	3400	Small pieces	Dionex		0,030	0,430	419	0,833	0,49	0,53	0,30	2,5	1,1	
6	3400	Powder	Dionex		0,050	0,031	421	0,833	0,49	0,53	0,30	2,5	0,2	

	S1(mg/g)	S2(mg/g)	Tmax(C)	Sample depth	Sample size	TOC	Cleaning method	calcite equ.	Comments	HI	S1(mg/g)	S2(mg/g)	Tmax(C)	TC	S	TOC	TIC	calcite equ.	
Cleaning method evaluation	0,120	3,060	429	22700	Complete caving	2,44	Dionex	1,0	Cleaning method evaluation	7,6	125,4	0,120	3,060	429	2,56	2,9	2,44	0,12	1,0
	0,110	0,180	347	22700	Complete caving	2,44	Soxhlet extractor	1,0		0,7	7,4	0,110	0,180	347	2,56	2,9	2,44	0,12	1,0
Cleaning method evaluation	0,030	0,170	422	3400	Complete caving	0,53	Soxhlet extractor	2,5	Cleaning method evaluation	0,5	32,1	0,030	0,170	422	0,83	0,49	0,53	0,30	2,5
Sample size evaluation	0,010	0,120	414	3400	Complete caving	0,53	Dionex	2,5	Sample size evaluation	0,3	22,6	0,010	0,120	414	0,83	0,49	0,53	0,30	2,5
	0,030	0,430	419	3400	Small pieces	0,53	Dionex	2,5		81,1	0,030	0,430	419	0,83	0,49	0,53	0,30	2,5	
	0,050	0,031	421	3400	Powder	0,53	Dionex	2,5		5,8	0,050	0,031	421	0,83	0,49	0,53	0,30	2,5	

Table 5. 2. Calculations of the TIC, calcite equivalent, SPI, HI and PI.

One of the cavings was used to prepare a small and cylindrical shale sample for image scanning (Figure 3. 53). The size of the sample was 30mm in height and 10mm in diameter. Once the sample was scanned, the images obtained were visualized using the software Fiji, an open-source image-processing package. The features that seemed to be micro-fractures were easier to visualize using the image sequence and moving up and down through the sample. As a single image, it is difficult to see the complete micro-fracture.

From a sequence of 688 images, five features appear to be micro-fractures (Figure 5. 7 to Figure 5. 13). The width of these micro-fractures was measured in several points along it, in order to make a distribution of values. The following results were obtained from the histogram (Figure 5. 6): mean = 111µm, average = 145 µm and standard deviation = 94µm. It is important to mention that there were some micro-fractures in white color and others in black. The change in colors indicates that there is a variation in the density (white: cemented, black: open). It was concluded that there were cemented and opened

micro-fractures. This analysis, in addition to the successful pore plugging test that was run using the shale, suggests that the shale in this area is indeed micro-fractured and the permeability might be higher than for other shales at these depths. It should be pointed out there is uncertainty whether the open micro-fractures (black) encountered in the sample are in-situ in the rock or were induced during drilling or the lab-preparation process. However, the cemented micro-fractures (white) suggest a diagenetic process, which would exclude drilling-induced damage.

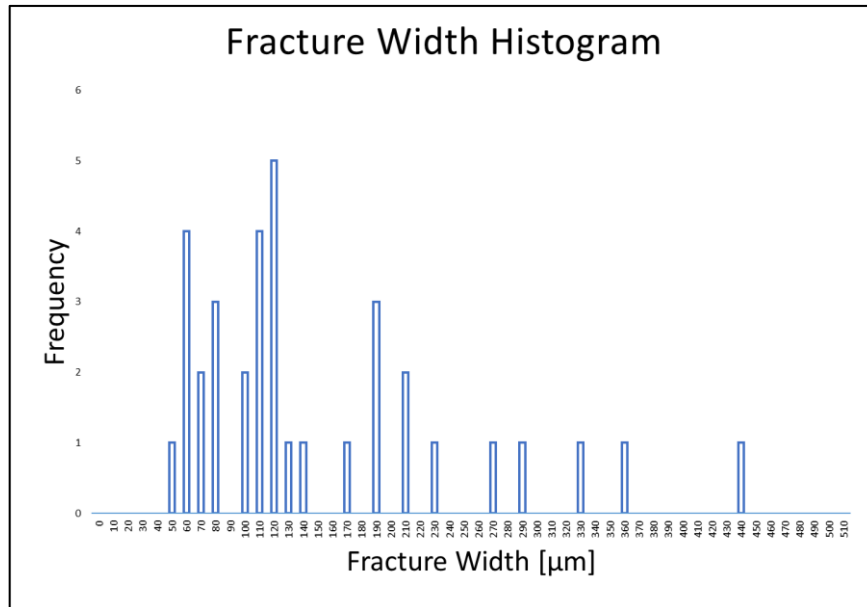


Figure 5. 6. Histogram of the fracture width measured in the images from the micro-CT scanner from all the micro-fractures found.

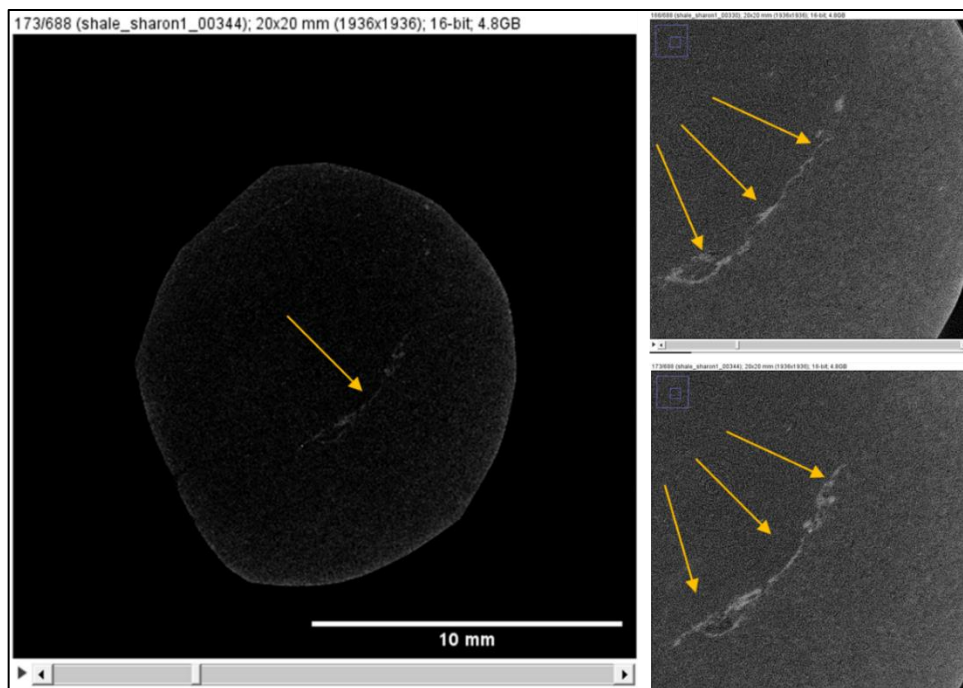


Figure 5. 7. Images 166 (top right) and 173 (bottom right) from micro-CT scanner displaying the micro-fracture. Measured width: 207μm, 237 μm, 352 μm, 223 μm, 132 μm.

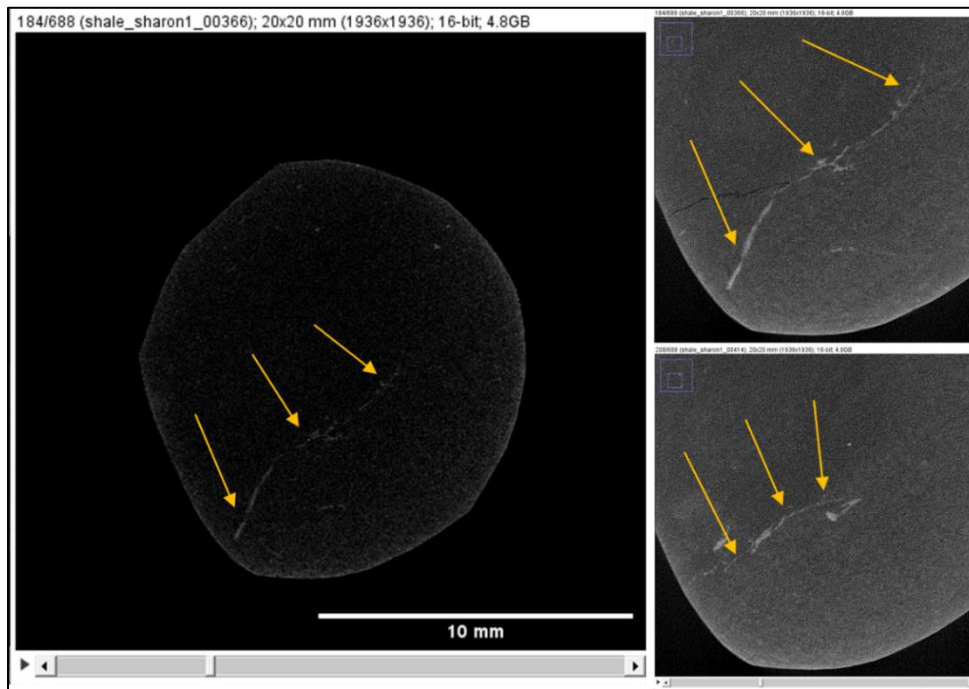


Figure 5. 8. Images 184 (top right) and 208 (bottom right) from micro-CT scanner displaying two micro-fractures with different color and direction. Measured width white: 185 μ m, 117 μ m, 167 μ m, 120 μ m, 92 μ m.

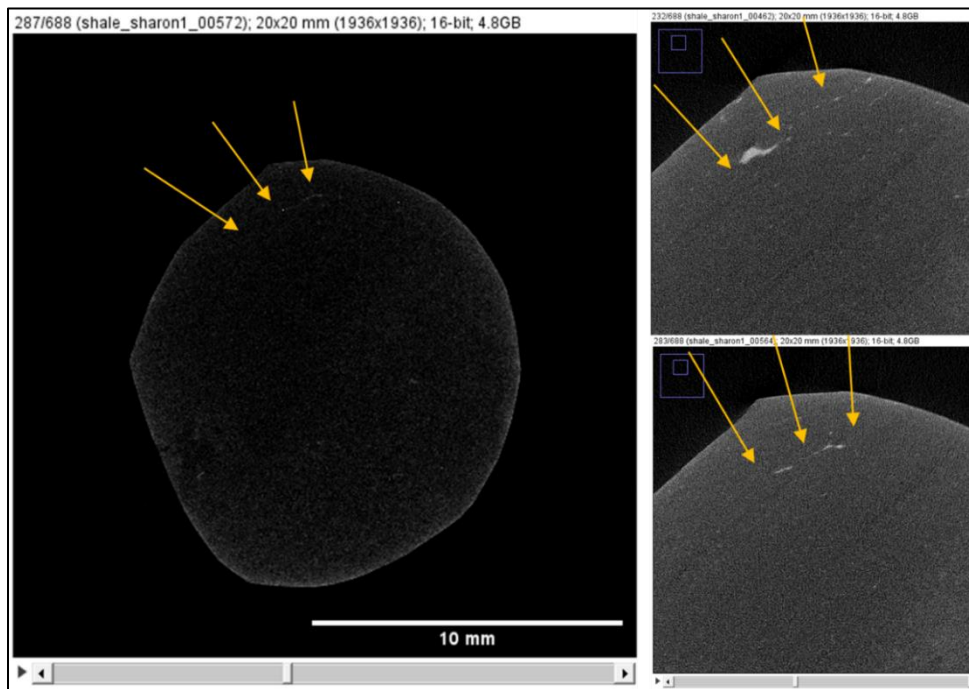


Figure 5. 9. Images 232 (top right), 283 (bottom right) and 287 (left), from micro-CT scanner displaying a white micro-fracture. Measured width: 50 μ m, 55 μ m, 57 μ m, 62 μ m.

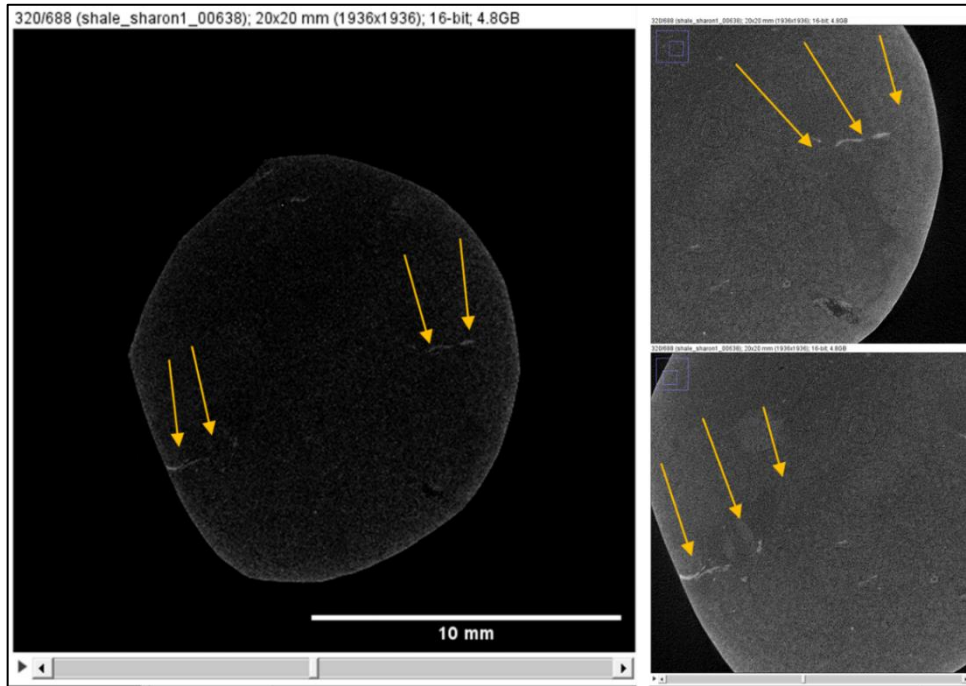


Figure 5. 10. Image 320 from micro-CT scanner displaying three micro-fractures, two white (both with the same direction) and one black with different direction. Measured width white: 126 μ m, 111 μ m, 103 μ m.

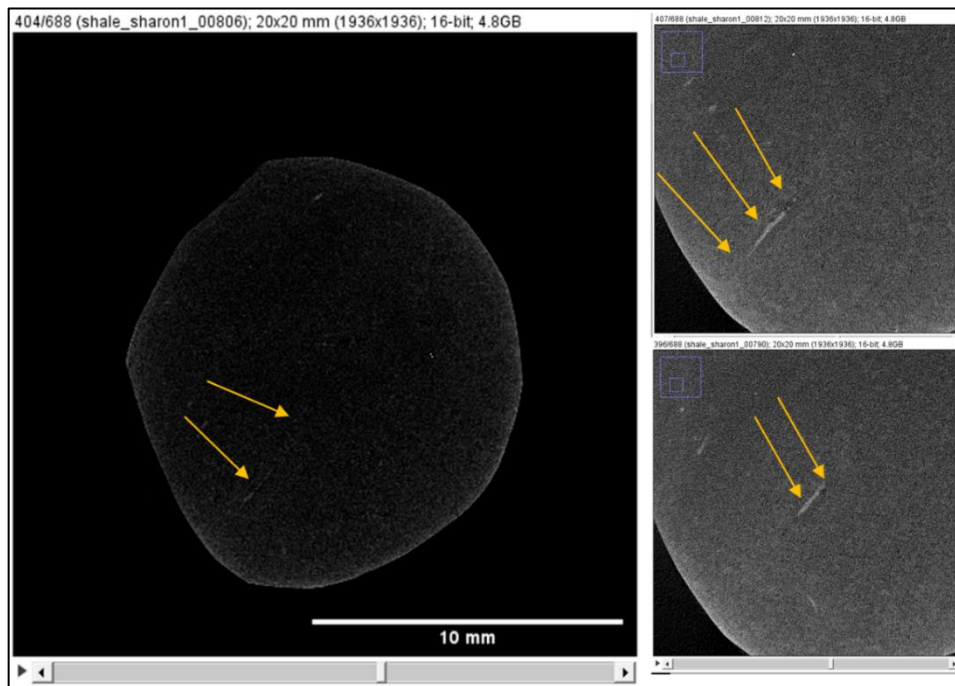


Figure 5. 11. Images 407 (top right), 396 (bottom right) and 404 (left), from micro-CT scanner displaying a white micro-fracture. Measured width: 103 μ m, 74 μ m.

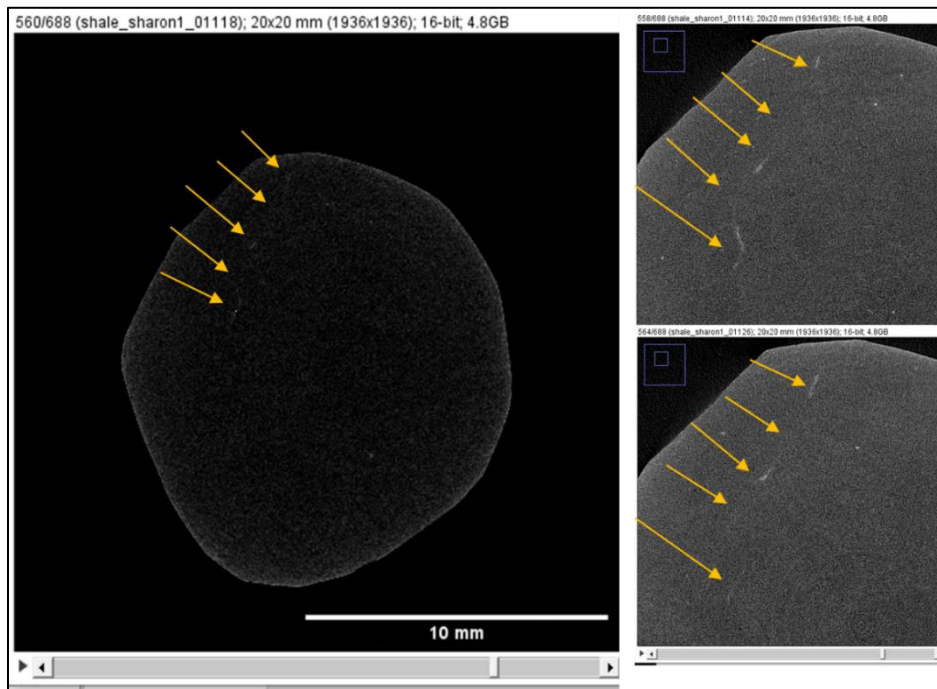


Figure 5. 12. Images 558 (top right), 564 (bottom right) and 560 (left) from micro-CT scanner displaying a white micro-fracture. Measured width: $62\mu\text{m}$, $103\mu\text{m}$, $74\mu\text{m}$, $92\mu\text{m}$, $52\mu\text{m}$.

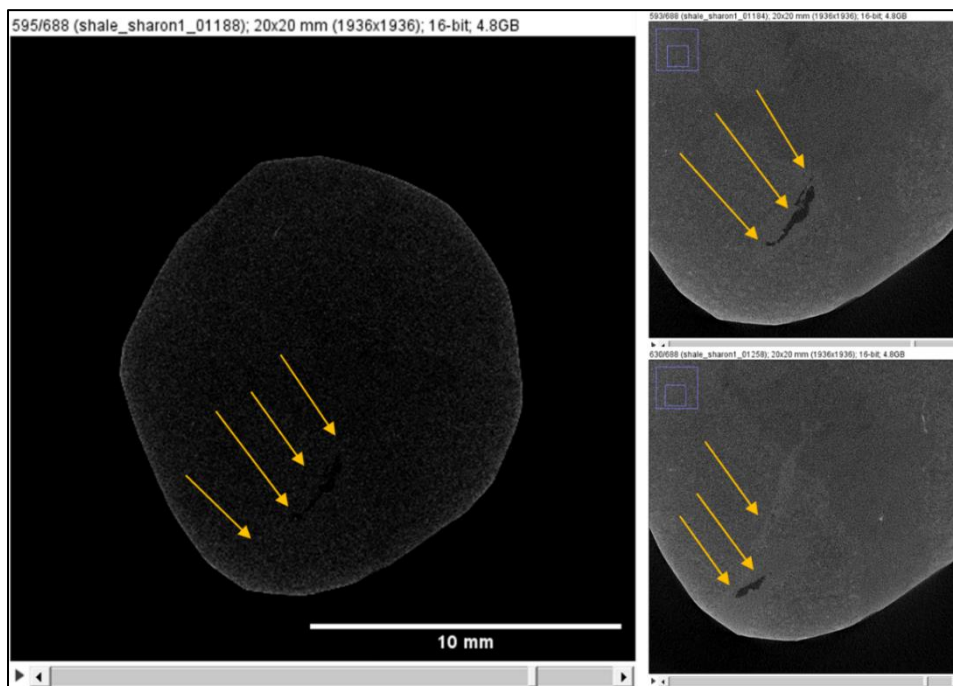


Figure 5. 13 Images 593 (top right), 630 (bottom right) and 595 (left) from micro-CT scanner displaying a possible black micro-fracture or fossil. Measured width: $439\mu\text{m}$, $323\mu\text{m}$, $185\mu\text{m}$, $281\mu\text{m}$, $269\mu\text{m}$.

Regarding the HPHT filter press setup, four disks were built using epoxy and the shale rock from the cavings samples. At the beginning, there was an uncertainty about the time of the test, due to a possible low permeability of the shale samples.

The first disk was tested in the HPHT filter press at 11:00h and it was decided to test it for 24 hours at 65°C and 500psi. The pressure and temperature were monitored throughout the day. The filtration started at some point during the night because the next day, 0.9 millilitre of filtrate was observed. The test was stopped at 11:00h the next day, to evaluate the disk and the shale. The seal shale/epoxy, epoxy/rubber was hermetic, and it was confirmed that the mud had passed through the shale and not through the boundary between the epoxy and the shale. The filtrate had a light-yellow color. A slightly deformation of the disk was also observed: even though it didn't affect the results, it was decided to use a different epoxy in the next test to compare the performance of the different epoxy types (Figure 5. 14).

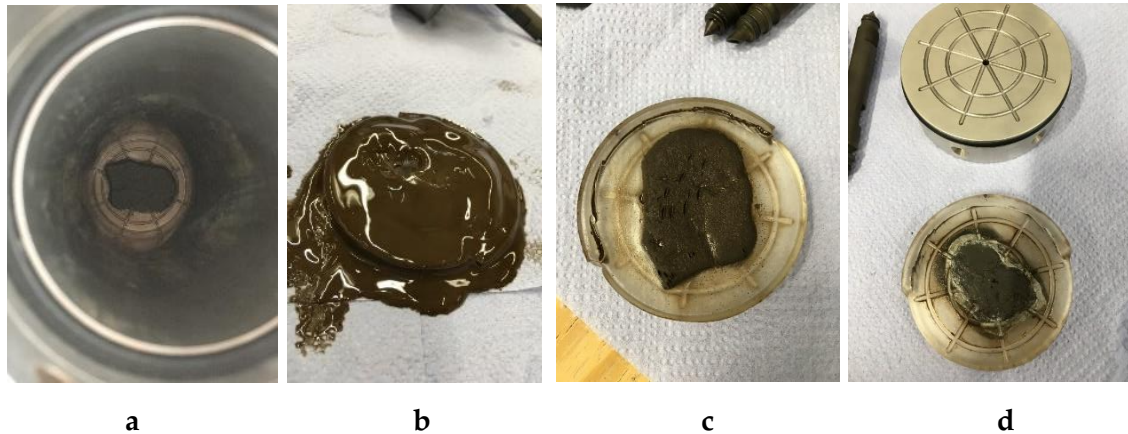


Figure 5. 14. Disk 1, shale from 2700md. a) disk placed in the HPHT filter press, b) filter cake after the test, c) shale after removing the filter cake and, d) bottom face of the disk.

Using a different epoxy, disk number 2 was built and tested under the same conditions. When the pressure was applied, a cracking sound was heard and the mud started to leak then the test was stopped to evaluate the disk. This time, the epoxy cracked affecting the shale as well. Therefore, this epoxy was ruled out for further use (Figure 5. 15).

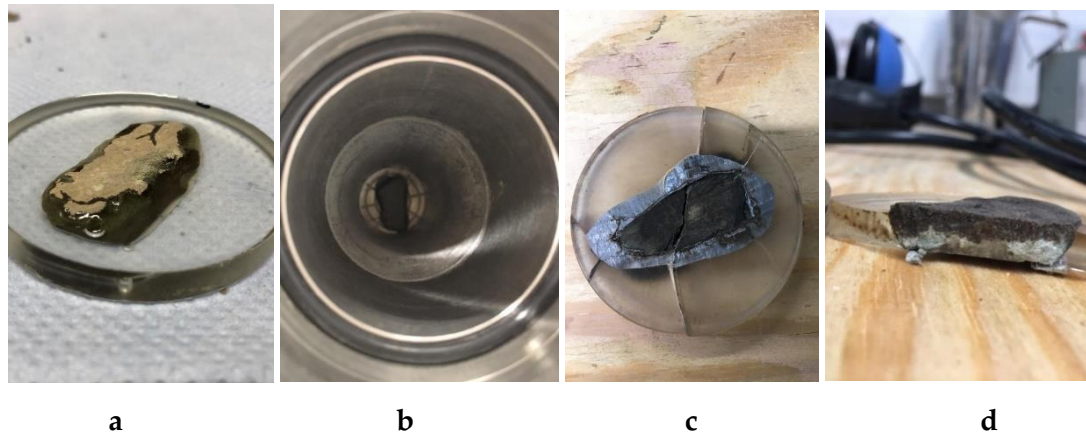


Figure 5. 15. Disk 2, shale from 2700md. a) shale disk, b) disk placed in the HPHT filter press, c) shale after test and, d) disk broken to be evaluated.

The third disk was tested for 24 hours obtaining a 0.6 milliliters filtrate, but this time the color of the filtrate was dark brown. It is believed the color changed because the clay mineral might have been washed out. In this test, the shale had different aspect and texture: it was observed that the lower face of the disk, which is in contact with the outlet, was sort of sandy. There were little sandy-looking particles in the space where the filtrate was collected. This was associated with the change in colors of the filtrate, but the reason is not certain. Not in the scope of this master thesis but for future work, we consider to analyze the filtrate in order to determine whether the clay mineral was washed out or what is the reason behind the changes in color and texture (Figure 5. 16).

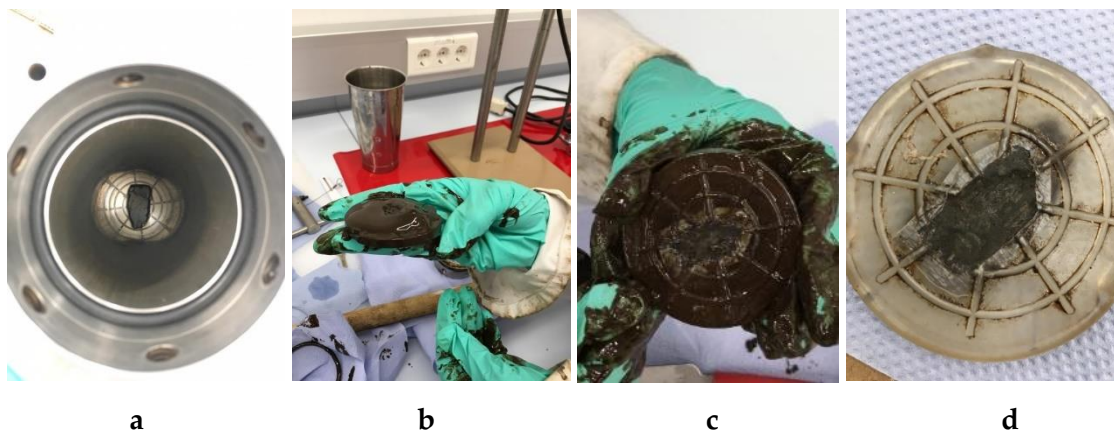


Figure 5. 16. Disk 3, shale from 3400md. a) disk placed in the HPHT filter press, b) filter cake after the test, c) bottom face of the disk after test and, d) bottom face scratched.

It was decided to test the last disk for 72 hours to compare the behavior of the shale over a longer period. The results were similar to the third disk but in this case, the filtrate collected was slightly higher. In this test, there was 1.1 milliliter of filtrate collected, the color was dark brown and the shale had the same texture as in disk number 3 (Figure 5. 17).

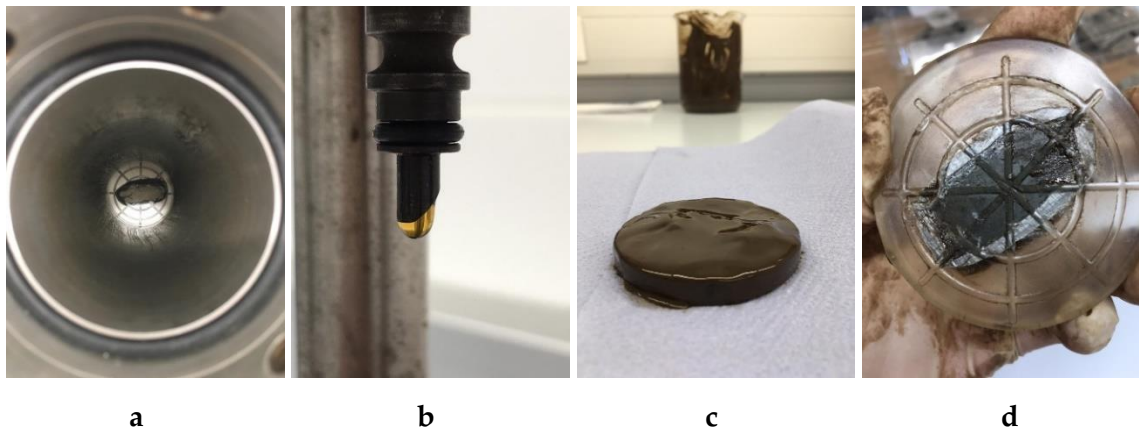


Figure 5.17. Disk 4, shale from 3400md. a) disk placed in the HPHT filter press, b) a drop of filtrate, c) filter cake after the test and, d) bottom face showing sandy texture.

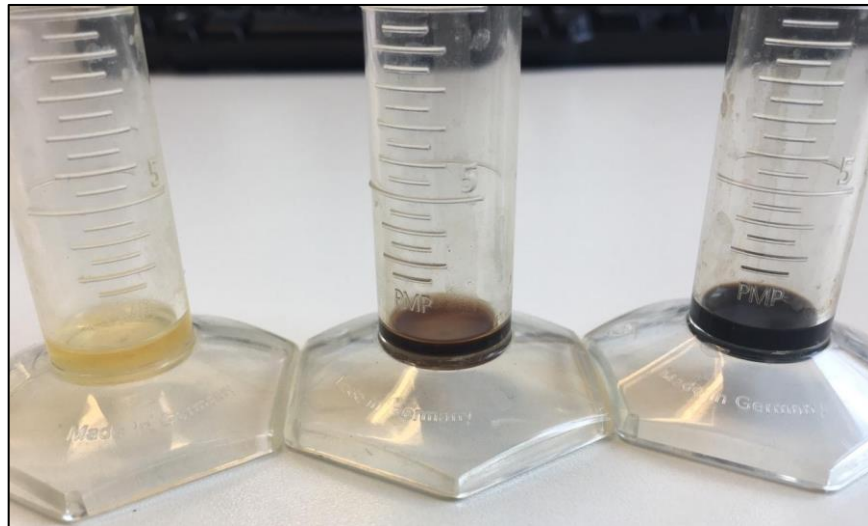


Figure 5.18. Filtrate obtained from the three disks, left to right: disk 1, disk 3 and disk 4.

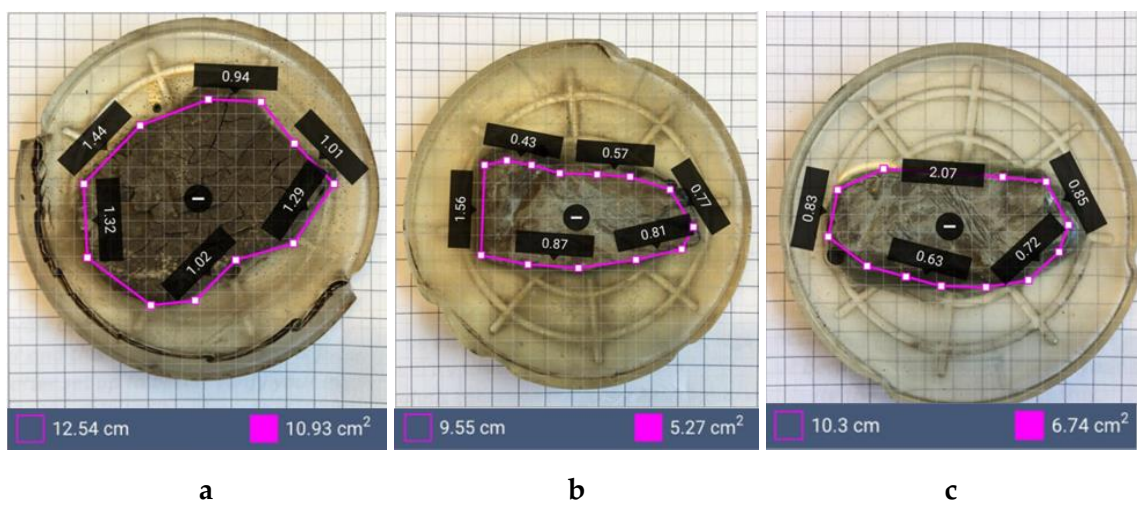


Figure 5.19. Area of the cavings measured with a commercial application. a) Area, disk 1: 10.93cm², b) area, disk 3: 5.27cm², c) Area, disk 4: 6.74cm².

Results and Discussion

Sample	Filtrate ml	Area cm2	Ratio	Factor API	Filtrate calculation ml
Disk 1	0,9	10,93	38,7	2	4,66
Disk 3	0,6	5,27	18,6	2	6,44
Disk 4	1,1	6,74	23,8	2	9,23
Complete disk		28,27			

Table 5. 3. Filtrate results based on the ratio epoxy/shale for all samples.

The areas of the cavings used in the tests were measured in order to obtain the ratio shale/epoxy of each disk, Figure 5. 19. Once these parameters were determined, the total filtrate in each test was calculated according to API of the HPHT filter press, Table 5. 3. Even though the ratio of the filter medium was considered in the calculations, the results cannot be compared with the values of a conventional test. The test time and monitoring conditions are different and there are no guidelines for this setup yet. Nevertheless, it gives us the general idea of the behaviour of the shale and the drilling fluid under bottom-hole conditions and an approximation of the filtrate in these formations.

Conclusions

The methodology proposed in this master thesis was applied to better understand the root causes of the wellbore instability in caprock shale as well as the interaction between the shale and drilling fluid, by developing an experimental setup of the HPHT (High Pressure High Temperature) filter press. The results of the laboratory tests, the geomechanical analysis and the shale characterization gave us a better comprehension of the behaviour of the shale under borehole conditions, the in-situ stress state of the area and the possible causes of the problem.

First, it was shown that the direction of the well trajectory does have an impact on the wellbore instability, due to the presence of weak bedding planes, micro-fractures and in-situ stress state. There are two suggested options to minimize the problem in this case: 1) increase the mud weight in small steps in that section (mud weight between ~ 1.88 g/cm³ and ~ 1.91 g/cm³) or 2) design trajectories with an inclination between $\sim 30^\circ$ and $\sim 60^\circ$ and an azimuth in the direction of $S_{Hmax} \sim 32^\circ \pm 60^\circ$ or $\sim 212^\circ \pm 60^\circ$ in this section.

Second, increasing the mud weight in that section will lead to a second problem. Based on the micro-CT scanning and the HPHT filter press tests, it was observed that the filtrate might increase too, due to the presence of micro-fractures and weak bedding planes. Therefore, the lost circulation material should be carefully designed, considering the fracture width obtained from the histogram presented in this analysis: mean = 111 μ m, average = 145 μ m and standard deviation = 94 μ m.

Finally, by using the experimental setup of the HPHT filter press test, it was observed that the bottom part of the shale presented a kind of a sandy texture after the test. The change in the texture might be related with the water content in the filtrate or a probable wash out of the clay mineral. Considering that 1-2 ml in 30 min is the maximum allowed filtrate in a conventional test, the total filtrate volume obtained in these experiments (3.1 ml, 9.66 ml and 9.23 ml) might give an indication of a possible cause of the weakening of the formation. However, this last point is uncertain due to the differences in borehole/surface conditions and further tests should be run in both shale and filtrate in order to investigate the cause of the sandy-looking evidence and total volume of the filtrate.

The objectives of this master thesis have been met. However, it is important to point out that this analysis was based on the information from four wells of the field. In order to give specific solutions to this problem, further tests and analysis should be done, with the information available from all the wells of the field.

Appendix A

Rig site indications (Bowes and Procter 1997):

Unconsolidated formations

- Increase in pump pressure.
- Fill on bottom.
- Overpull on connections.
- Shakers blinding.

Mobile Formations

- Overpull when moving up, takes weight when running in.
- Sticking occurs with BHA at mobile formation depth.
- Restricted circulation with BHA at mobile formation depth.

Fractured & Faulted Formations

- Hole fill on connections.
- Possible losses or gains.
- Fault damaged cavings at shakers.
- Sticking can be instantaneous.

Naturally Overpressured Shale Collapse

- Cavings (splintery) at shakers.
- Increased torque and drag.
- Gas levels, D exponent.
- Circulation restricted or impossible.
- Hole fill.
- An increase in ROP.
- Cuttings and cavings are not hydrated or mushy.

Induced Overpressured Shale Collapse

- Cuttings / cavings show no sign of hydration.
- Cavings (splintery) at shakers.
- Tight hole in casing rat hole.
- Increased torque and drag.
- Circulating restricted or impossible.
- Hole fill.

Reactive Formations

- Hydrated or mushy cavings.
- Shakers screens blind off, clay balls form.
- Increase in LGS, filter cake thickness, PV, YP, MBT.
- An increase or fluctuations in pump pressure.
- Generally occurs while POOH.
- Circulation is impossible or highly restricted.

Hole Cleaning

- Overpulls increasing while POOH from TD in deviated hole (7-10 stands).
- Erratic pump pressure.
- Poor weight transfer to bit.
- Difficulty orienting toolface.
- Absence of returns at shakers.
- Presence of re-ground cuttings

Tectonically Stressed Formations

- Pack-offs and bridges may occur.
- Cavings at the shakers (splintery).
- Increase torque and drag.
- If stuck, circulation is likely to be impaired or non-existent.
- Increase in volume of returns at the shakers relative to the hole volume drilled.

Appendix B

Well	Cavings Reported	Photos	DDR	GR	RT	RHOB	NPHI	DTCO	DTS	Caliper
AM-1	no	no	yes	89-5970	89-5970	1942-3120	841-3120 4714-5970	841-3120 4714-5970	841-3120 4714-5970	89-5970
AM-11	yes	yes	yes	59-5791	59-5791	854-5804	854-5804	854-5804	854-5804	59-4625
AM-5(1)	yes	no	yes	56-5521	56-5521	n/a	n/a	n/a	n/a	56-4500
AM-8	yes	yes	yes	107-5802	107-5802	n/a	n/a	n/a	n/a	n/a

Figure B. 1. Checklist logs: AM-1, AM-11, AM-5 and AM-8

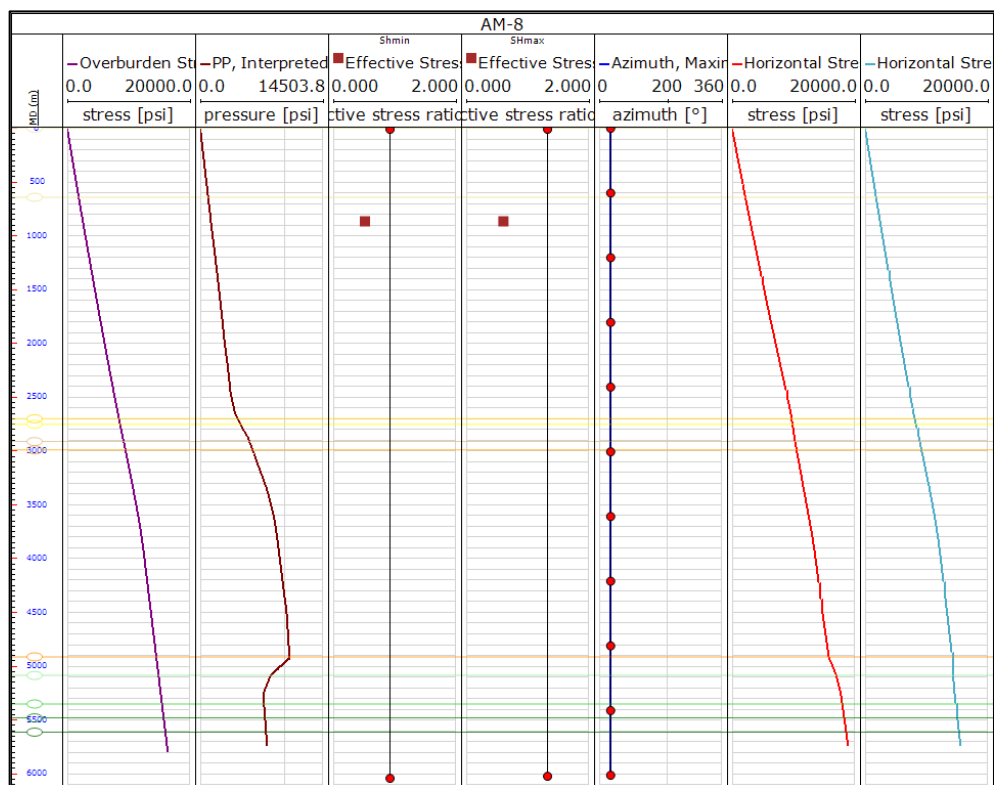


Figure B. 2. Horizontal stresses, AM-8. Geomechanical analysis using same parameters as in AM-1 and AM-11.

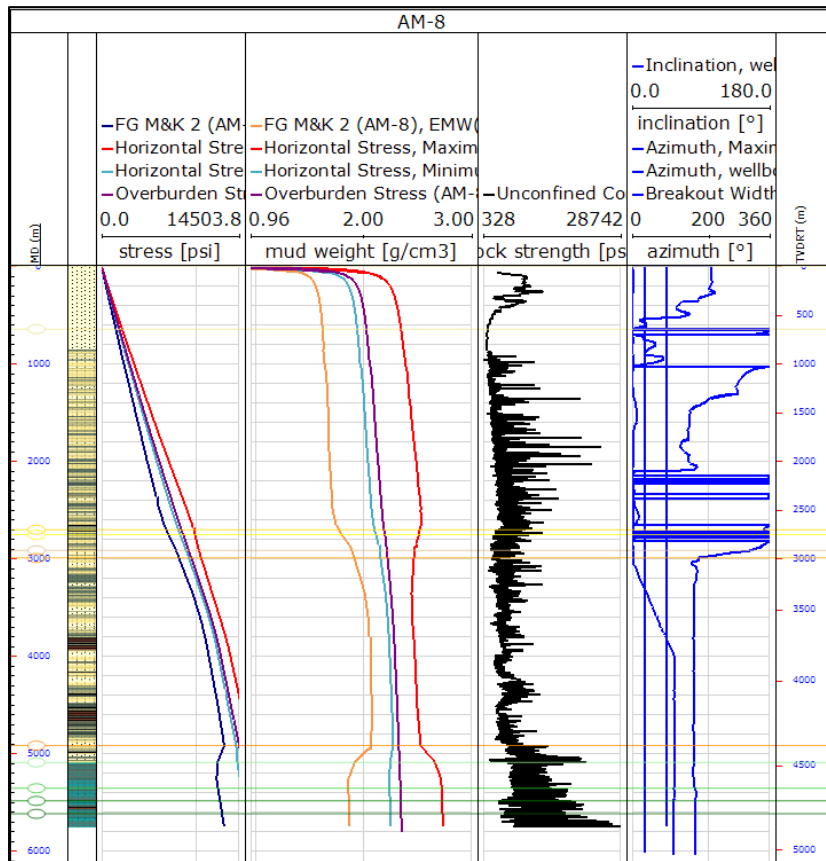


Figure B. 3. PP, FG, S_{Hmax} , S_{Hmin} , UCS, AM-8. Geomechanical analysis using same parameters as in AM-1 and AM-11.

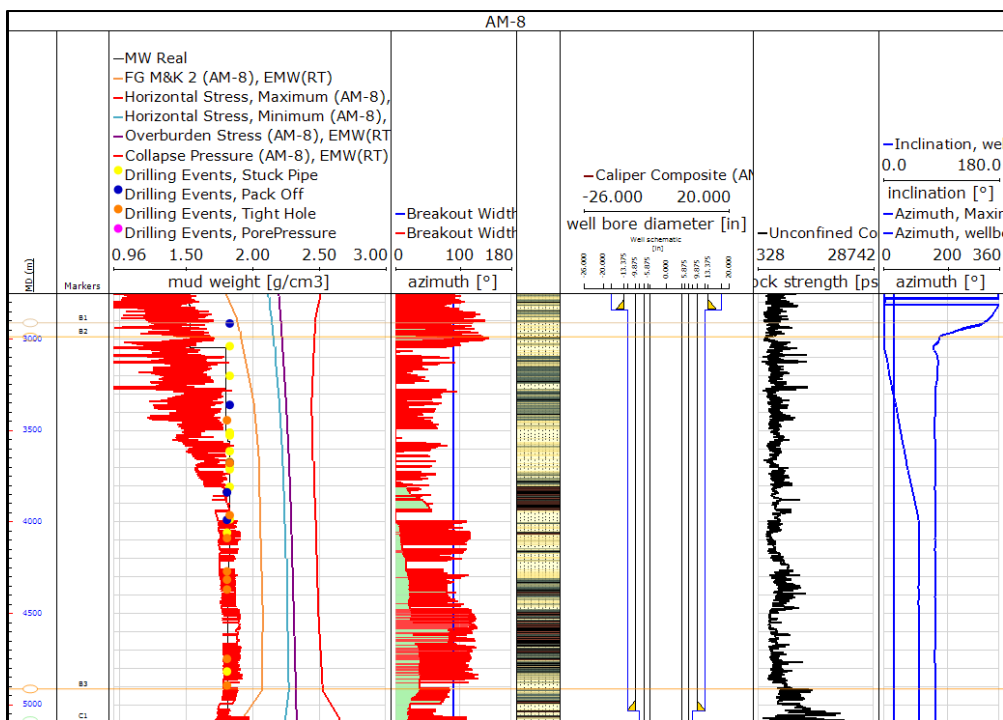


Figure B. 4. Collapse pressure, AM-8, geomechanical analysis using same parameters as in AM-1 and AM-11.

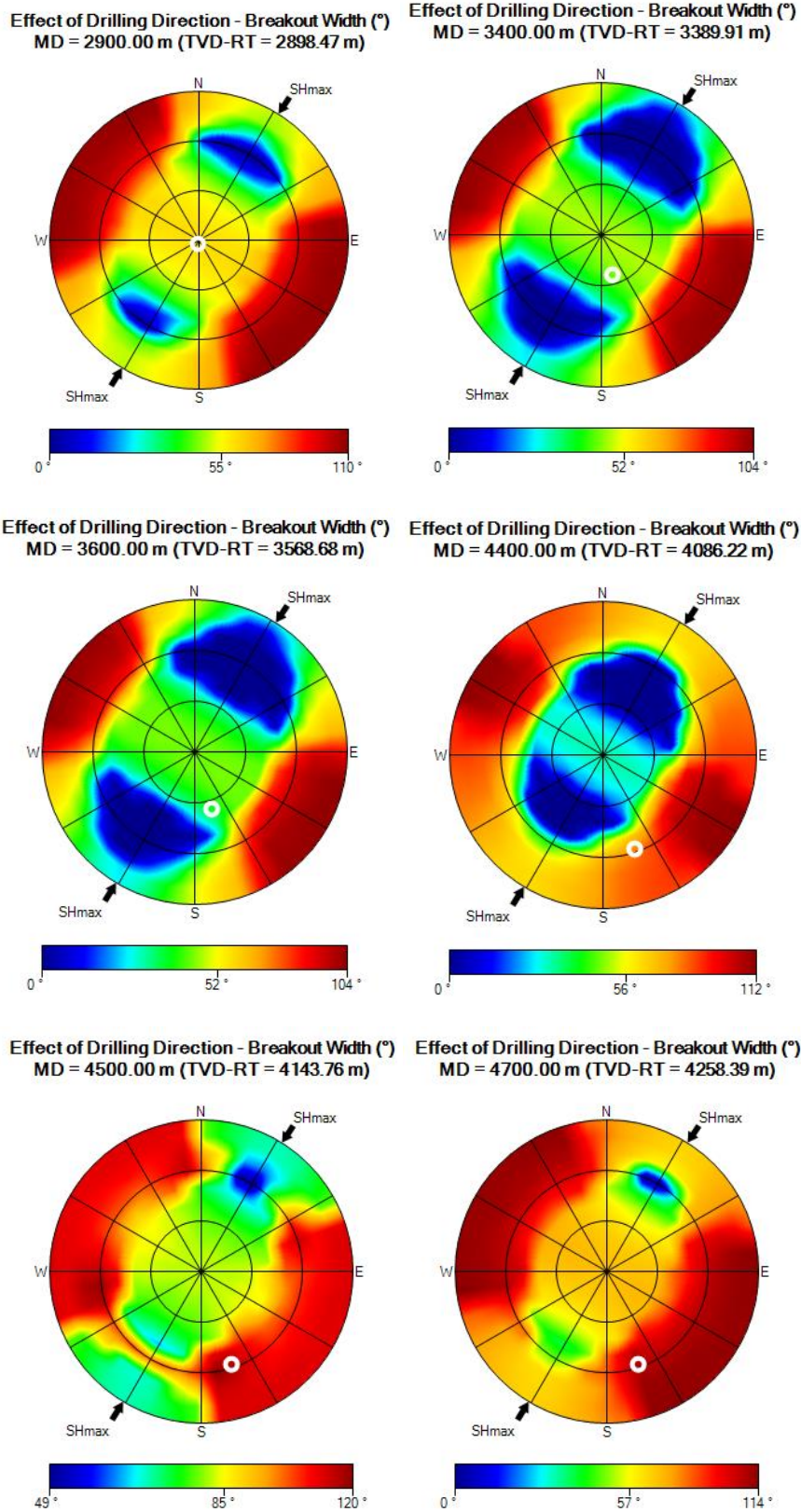


Figure B. 5. Model verification, AM-8. Geomechanical analysis using same parameters as in AM-1 and AM-11.

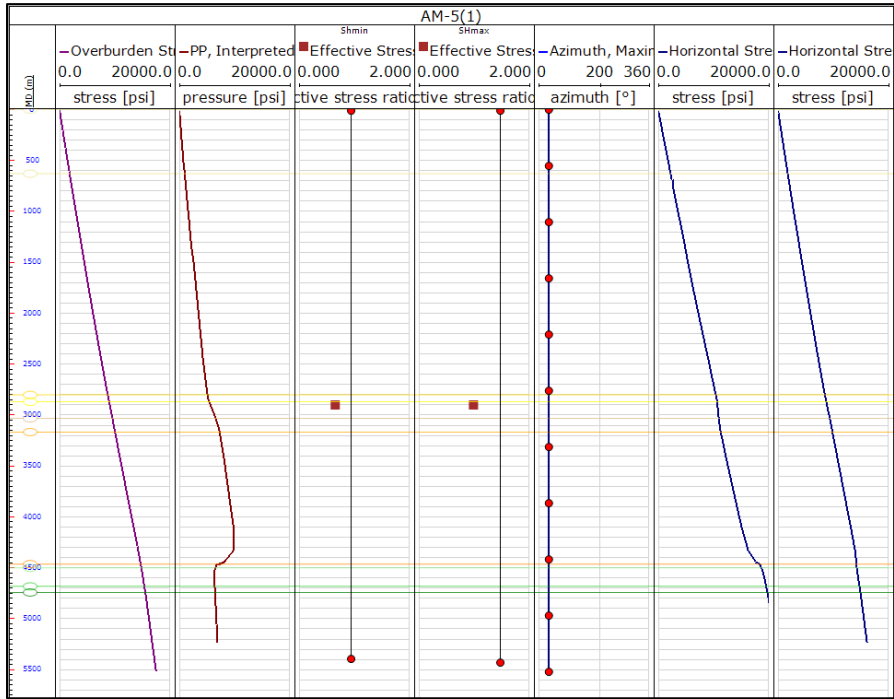


Figure B. 6. Horizontal stresses, AM-5. Geomechanical analysis using same parameters as in AM-1 and AM-11.

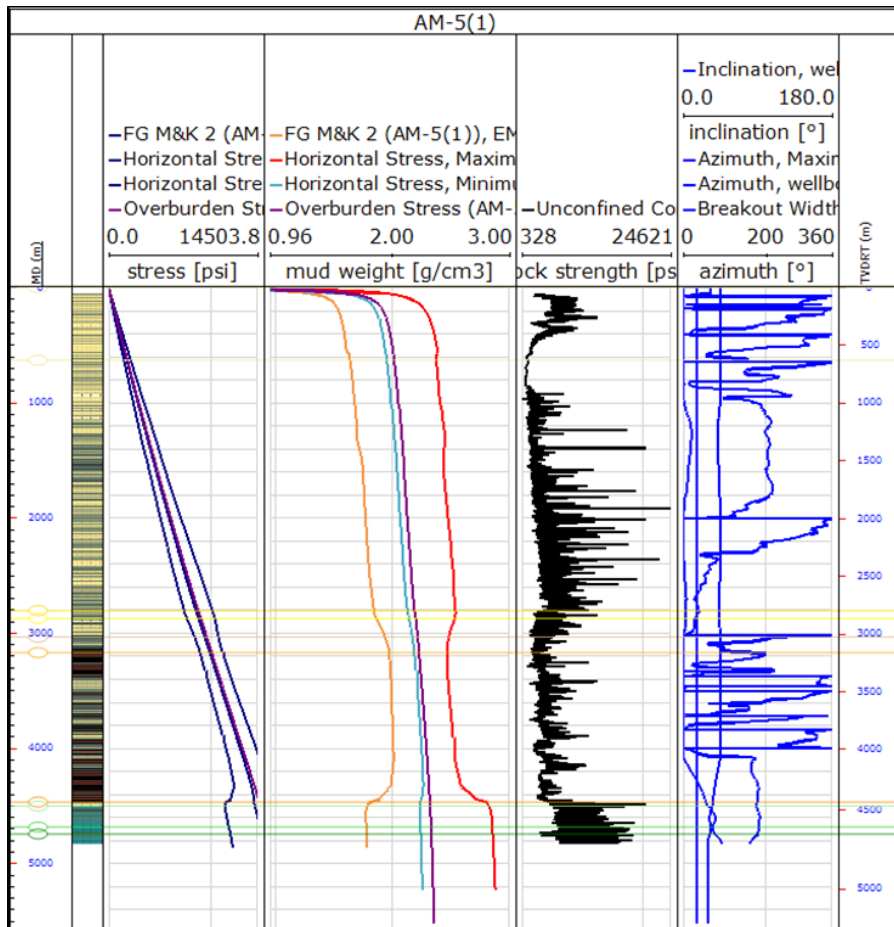


Figure B. 7. PP, FG, SHmax, Shmin, UCS, AM-5. Geomechanical analysis using same parameters as in AM-1 and AM-11.

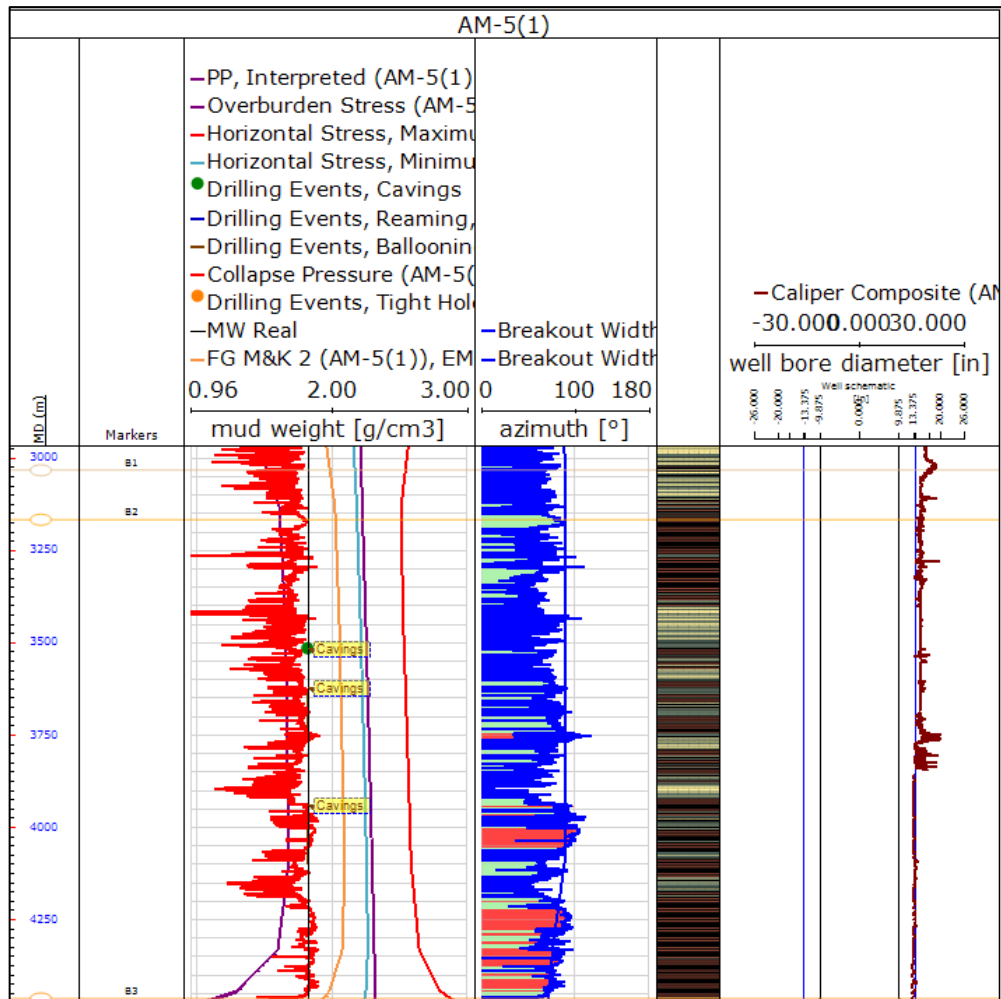
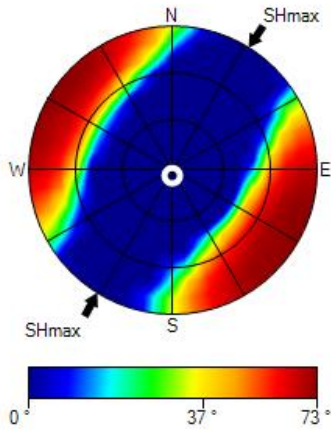
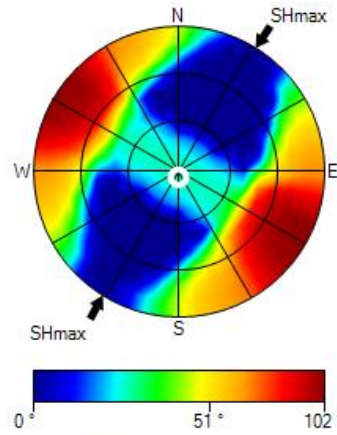


Figure B. 8. Collapse pressure, AM-5. Geomechanical analysis using same parameters as in AM-1 and AM-11.

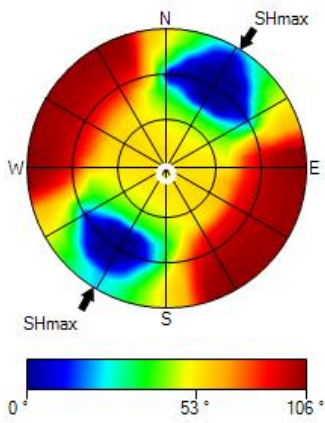
Effect of Drilling Direction - Breakout Width (°)
MD = 3200.00 m (TVD-RT = 3192.76 m)



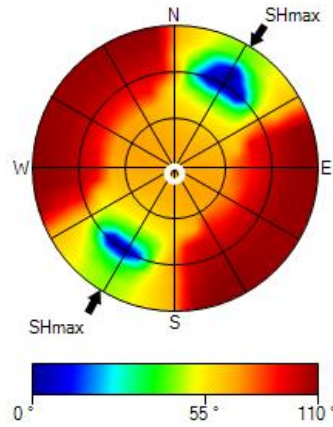
Effect of Drilling Direction - Breakout Width (°)
MD = 3400.00 m (TVD-RT = 3392.76 m)



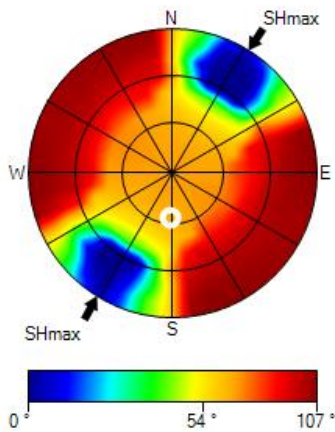
Effect of Drilling Direction - Breakout Width (°)
MD = 3600.00 m (TVD-RT = 3592.75 m)



Effect of Drilling Direction - Breakout Width (°)
MD = 4000.00 m (TVD-RT = 3992.75 m)



Effect of Drilling Direction - Breakout Width (°)
MD = 4400.00 m (TVD-RT = 4382.72 m)



Effect of Drilling Direction - Breakout Width (°)
MD = 4800.00 m (TVD-RT = 4711.39 m)

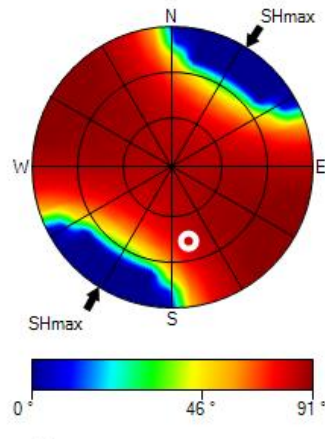


Figure B. 9. Model verification, AM-5. geomechanical analysis using same parameters as in AM-1 and AM-11.

Bibliography

- 3D ProScan. 2016. "Industrial CT Scanning Terms - What Are 'Voxels' And Why Do They Matter?" 3D ProScan. January 8, 2016. <https://3dproscan.com/industrial-ct-scanning-terms-what-are-voxels-and-why-do-they-matter/>.
- A. Eaton, Ben. 1969. "Fracture Gradient Prediction and Its Application in Oilfield Operations." *Journal of Petroleum Technology - J PETROL TECHNOL* 21 (October): 1353–60. <https://doi.org/10.2118/2163-PA>.
- Alisha Fernandes. 2015. "How Might I Avoid Escape of Solvent for Efficient Soxhlet Extraction of Lipids?" Research Gate. 2015. https://www.researchgate.net/post/How_might_I_avoid_escape_of_solvent_for_efficient_Soxhlet_extraction_of_lipids.
- Anderson, E. M. 1905. "The Dynamics of Faulting." *Transactions of the Edinburgh Geological Society* 8 (3): 387–402. <https://doi.org/10.1144/transed.8.3.387>.
- Barton, Colleen, Mark Zoback, and Kerry L. Burns. 1988. "In-Situ Stress Orientation and Magnitude at the Fenton Geothermal Site, New Mexico, Determined from Wellbore Breakouts." *Geophysical Research Letters - GEOPHYS RES LETT* 15 (May): 467–70. <https://doi.org/10.1029/GL015i005p00467>.
- Biot, M. A. 1962. "Mechanics of Deformation and Acoustic Propagation in Porous Media." *Journal of Applied Physics* 33 (4): 1482–98. <https://doi.org/10.1063/1.1728759>.
- Bjorlykke, Knut. 2010. *Petroleum Geoscience*. Berlin, Heidelberg: Springer Berlin Heidelberg. <https://doi.org/10.1007/978-3-642-02332-3>.
- Bowers, Glenn L. 1995. "Pore Pressure Estimation From Velocity Data: Accounting for Overpressure Mechanisms Besides Undercompaction." *SPE Drilling & Completion* 10 (02): 89–95. <https://doi.org/10.2118/27488-PA>.
- Bowes, Colin, and Ray Procter. 1997. "1997 Guidelines & Drillers Handbook Credits," 71.
- Bradford, I. D. R., W. A. Aldred, J. M. Cook, E. F. M. Elewaut, J. A. Fuller, T. G. Kristiansen, and T. R. Walsgrove. 2000. "When Rock Mechanics Met Drilling: Effective Implementation of Real-Time Wellbore Stability Control." In . Society of Petroleum Engineers. <https://doi.org/10.2118/59121-MS>.
- Core Laboratories. 2019. "Core Laboratories: The Reservoir Optimization Company." 2019. <https://www.corelab.com/>.
- Demaison, Gerard, and Bradley J. Huizinga. 1994. "Genetic Classification of Petroleum Systems Using Three Factors: Charge, Migration, and Entrapment." In *The Petroleum System—From Source to Trap*, edited by Leslie B. Magoon and Wallace G. Dow, 60:0. American Association of Petroleum Geologists. <https://doi.org/10.1306/M60585C4>.
- Detournay, Emmanuel M., and A. H. D. Cheng. 1988. "Poroelastic Response of a Borehole in a Non-Hydrostatic Stress Field." *International Journal of Rock Mechanics and Mining Sciences And* 25 (3): 171–82. [https://doi.org/10.1016/0148-9062\(88\)92299-1](https://doi.org/10.1016/0148-9062(88)92299-1).

Bibliography

- Dobroskok, Anastasia, and Ruqaya AL Zadjali. 2016. "Estimating Maximum Horizontal Stress from Multi-Arm Caliper Data in Vertical Wells in Oman." In . Society of Petroleum Engineers. <https://doi.org/10.2118/183204-MS>.
- Eaton, Ben A. 1972. "The Effect of Overburden Stress on Geopressure Prediction from Well Logs." *Journal of Petroleum Technology* 24 (08): 929–34. <https://doi.org/10.2118/3719-PA>.
- — —. 1975. "The Equation for Geopressure Prediction from Well Logs." In . Society of Petroleum Engineers. <https://doi.org/10.2118/5544-MS>.
- Edwards, S., B. Matsutsuyu, and S. Willson. 2004. "Imaging Unstable Wellbores While Drilling." *SPE Drilling & Completion* 19 (04): 236–43. <https://doi.org/10.2118/79846-PA>.
- ELTRA GmbH. 2019. "ELTRA - Elemental Analyzers for C H N O S Analysis." 2019. <https://www.eltra.com/>.
- Geotechnicalinfo. 2012. "Angle of Internal Friction on the Geotechnical Information Website." 2012. http://www.geotechnicalinfo.com/angle_of_internal_friction.html.
- Grauls, D. 1999. "Overpressures: Causal Mechanisms, Conventional and Hydromechanical Approaches." *Oil & Gas Science and Technology* 54 (6): 667–78. <https://doi.org/10.2516/ogst:1999056>.
- Grzegorz Leśniak. 2015. "Estimation of the Width of Microfractures in Shale Rocks." *Nafta-Gaz* 71 (11): 840–46. <https://doi.org/10.18668/NG2015.11.05>.
- Gupta, Ishank, Chandra Rai, Ali Tinni, and Carl Sondergeld. 2017. "Impact of Different Cleaning Methods on Petrophysical Measurements." In . Society of Petrophysicists and Well-Log Analysts. <https://www.onepetro.org/conference-paper/SPWLA-2017-M>.
- Gutierrez, Mario, Neil R. Braunsdor, and Brent Couzens-Schultz. 2006. "Calibration and Ranking of Pore-Pressure Prediction Models." *Geophysics* 25 (December). <https://doi.org/10.1190/1.2405337>.
- Haimson, Bezalel, and Charles Fairhurst. 1967. "Initiation and Extension of Hydraulic Fractures in Rocks." *Society of Petroleum Engineers Journal* 7 (03): 310–18. <https://doi.org/10.2118/1710-PA>.
- Hobart M. King. 2018. "Shale: Sedimentary Rock - Pictures, Definition & More." 2018. <https://geology.com/rocks/shale.shtml>.
- Hubbert, M. King, and David G. Willis. 1957. "Mechanics Of Hydraulic Fracturing," January. <https://www.onepetro.org/general/SPE-686-G>.
- Labcompare. 2019. "Labcompare | The Buyer's Guide for Laboratory Equipment -" 2019. <https://www.labcompare.com/>.
- Life Technologies. 2019. "Life Technologies - AT." 2019. <https://www.thermofisher.com/uk/en/home.html>.
- Lopez, Jorge, Penne M. Rappold, Gustavo A. Ugueto, James B. Wieseneck, and Cung K. Vu. 2004. "Integrated Shared Earth Model: 3D Pore-Pressure Prediction and Uncertainty Analysis." *Geophysics* 23 (January). <https://doi.org/10.1190/1.1645455>.
- M. Kageson-Loe, Nils, Mark W. Sanders, Frederick Growcock, Knut Taugbol, Per Horsrud, Arne V. Singelstad, and Tor Omland. 2009. "Particulate Loss-Prevention Material?The Secrets of Fracture Sealing Revealed!" *SPE Drilling & Completion* 24 (December). <https://doi.org/10.2118/112595-MS>.

- Micro Photonics. 2018. "What Is Micro-CT? An Introduction." *Micro Photonics* (blog). 2018. <https://www.microphotonics.com/what-is-micro-ct-an-introduction/>.
- Osisanya. 2011. "Osisanya: Practical Approach to Solving Wellbore... - Google Scholar." 2011. https://scholar.google.com/scholar_lookup?title=Practical%20approach%20to%20solving%20wellbore%20instability%20problems&author=S.O.%20Osisanya&publication_year=2011.
- Peter Mulroy. 2019. "How Do We Identify Sedimentary Rocks?" Mr. Mulroy's Earth Science. 2019. <http://peter-mulroy.squarespace.com/how-do-we-identify-sedimentary-rocks>.
- Polish Geological Institute. 2014a. "Mechanical Properties of Shale Rocks | Info Shale : Shale Gas & Oil from Shale, Issued by Polish Geological Institute." 2014. <https://infolupki.pgi.gov.pl/en/gas/mechanical-properties-shale-rocks>.
- — —. 2014b. "Mineralogy of Shale Rocks | Info Shale : Shale Gas & Oil from Shale, Issued by Polish Geological Institute." 2014. <https://infolupki.pgi.gov.pl/en/gas/mineralogy-shale-rocks>.
- — —. 2014c. "Petrophysical Properties of Shale Rocks." 2014. <https://infolupki.pgi.gov.pl/en/gas/petrophysical-properties-shale-rocks>.
- ProCon X-ray GmbH. 2014. "CT-ALPHA | ProCon X-Ray GmbH." 2014. <https://www.procon-x-ray.com/ct-alpha/>.
- R. Daines, Stephen. 1982. "Prediction of Fracture Pressures for Wildcat Wells." *Journal of Petroleum Technology - J PETROL TECHNOL* 34 (April): 863–72. <https://doi.org/10.2118/9254-PA>.
- Schlumberger. 1998. "SLB Cavings Morphology Poster | Borehole | Oil Well." Scribd. 1998. <https://www.scribd.com/doc/227988493/SLB-Cavings-Morphology-Poster>.
- "Schlumberger Oilfield Glossary." 2019. 2019. <https://www.glossary.oilfield.slb.com/>.
- Terzaghi, Karl. 1943. *Theoretical Soil Mechanics*. Hoboken, NJ, USA: John Wiley & Sons, Inc. <https://doi.org/10.1002/9780470172766>.
- Tomlin, Marsha. 2017. "HT4700 HPHT Filter Press Instruction Manual," 58.
- Vantico Ltd. 2000. "Araldite DBF956-TD." 2000. <http://polymerteknik.com/doc/Araldite-DBF956-TD.pdf>.
- Vinci Technologies. 2019. "Vinci Technologies | Laboratory and Field Instruments for Petroleum Industry." 2019. <https://www.vinci-technologies.com/>.
- White, Adrian J., Martin O. Traugott, and Richard E. Swarbrick. 2002. "The Use of Leak-off Tests as Means of Predicting Minimum in-Situ Stress." *Petroleum Geoscience* 8 (2): 189–93. <https://doi.org/10.1144/petgeo.8.2.189>.
- Whitfill, Don. 2008. "Lost Circulation Material Selection, Particle Size Distribution and Fracture Modeling with Fracture Simulation Software." In . Society of Petroleum Engineers. <https://doi.org/10.2118/115039-MS>.
- World Stress Map: Data. 2016. "World Stress Map: Data." 2016. <http://www.world-stress-map.org/data/>.
- Zamirian, Mehrdad, Kashy Aminian, and Samuel Ameri. 2015. "Measurement of Key Shale Petrophysical Properties." In . Society of Petroleum Engineers. <https://doi.org/10.2118/174968-MS>.
- Zamirian, Mehrdad, Kashy Kashy Aminian, Samuel Ameri, and Ebrahim Fathi. 2014. "New Steady-State Technique for Measuring Shale Core Plug Permeability." In . Society of Petroleum Engineers. <https://doi.org/10.2118/171613-MS>.

Bibliography

- Zhang, Jincai, and Shang-Xian Yin. 2017. "Fracture Gradient Prediction: An Overview and an Improved Method." *Petroleum Science* 14 (4): 720–30. <https://doi.org/10.1007/s12182-017-0182-1>.
- Zhang, Jon. 2011. "Pore Pressure Prediction from Well Logs: Methods, Modifications, and New Approaches." *Earth-Science Reviews - EARTH-SCI REV* 108 (December): 50–63. <https://doi.org/10.1016/j.earscirev.2011.06.001>.
- . 2013. "Effective Stress, Porosity, Velocity and Abnormal Pore Pressure Prediction Accounting for Compaction Disequilibrium and Unloading." *Marine and Petroleum Geology* 45 (August). <https://doi.org/10.1016/j.marpetgeo.2013.04.007>.
- Zoback, Mark D. 2010. *Reservoir Geomechanics*. Cambridge University Press.

Acronyms

<i>BO</i>	Breakout
<i>DDR</i>	Daily Drilling Report
<i>ES</i>	Effective Stress
<i>ESR</i>	Effective Stress Ratio
<i>FBP</i>	Formation Breakdown Pressure
<i>FCP</i>	Fracture Closure Pressure
<i>FIT</i>	Formation Integrity Test
<i>FPP</i>	Fracture Propagation Pressure
<i>HPHT</i>	High Pressure High Temperature
<i>ISIP</i>	Instantaneous Shut-In Pressure
<i>KOP</i>	Kick-off Point
<i>LCM</i>	Lost Circulation Material
<i>LOP</i>	Leak-Off Pressure
<i>LOT</i>	Leak-Off Test
<i>LWD</i>	Logging While Drilling
<i>MD</i>	Measured Depth
<i>MW</i>	Mud Weight
<i>MWD</i>	Measurement While Drilling
<i>NF</i>	Normal Faulting
<i>NPT</i>	Non-Productive Time
<i>NCT</i>	Normal Compaction Trend
<i>PPT</i>	Pore plugging Test
<i>RF</i>	Reverse Faulting
<i>SRA</i>	Source Rock Analysis
<i>SS</i>	Strike-Slip
<i>TD</i>	True Depth
<i>TOC</i>	Total Organic Carbon
<i>TVD</i>	True Vertical Depth
<i>UCS</i>	Unconfined Compressive Strength
<i>XLOT</i>	Extended Leak-Off Test

Symbols

E	Young's Modulus	[MPa]
$E_{dynamic}$	Dynamic Young's Modulus	[MPa]
E_{static}	Static Young's Modulus	[MPa]
μ_i	Coefficient of Internal Friction	
P_p	Pore Pressure	[psi], [SG]
ρ	Density	[g/cm ³], [SG]
S_{Hmax}	Maximum Horizontal Stress	[psi], [SG]
S_{Hmin}	Minimum Horizontal Stress	[psi], [SG]
S_v	Vertical Stress	[psi], [SG]
ν	Poisson's Ratio	
$\nu_{dynamic}$	Dynamic Poisson's Ratio	
ν_{static}	Static Poisson's Ratio	

List of Figures

Figure 2. 1. The scheme used for sedimentary rock identification (Mulroy, 2019).....	5
Figure 2. 2. Permeability diagram of conventional and unconventional reservoirs (based on: Faraj, 2012; Hughes, 2013; Jarvie, 2012).....	7
Figure 2. 3. Eltra CS-580A analyzer used to measure TC, S and TOC on shale samples placed at the Chair of Petroleum Geology.....	9
Figure 2. 4. a) Rock-Eval 6 apparatus from the Chair of Petroleum Geology at Montanuniversität. b) Samples carrousel with prepared samples.....	10
Figure 2. 5. Soxhlet extractor at DPE – Chair of Reservoir Engineering.....	11
Figure 2. 6. Thermo Scientific™ Dionex™ ASETM at the Chair of Petroleum Geology.....	11
Figure 2. 7. a) Micro and b) Medical CT scanners at the Chair of Reservoir Engineering.....	12
Figure 2. 8. Illustration of the different stress regimes (World Stress Map, 2019).	13
Figure 2. 9. Diagram of the main overpressure causal mechanisms (Grauls, 1999).	15
Figure 2. 10. The use of leak-off tests as means of predicting minimum in-situ stress (White et al., 2002)	16
Figure 2. 11. Illustration of the concept of the Young’s Modulus. Ratio of the stress to strain considering a uniaxial stress applied, F.	17
Figure 2. 12. Illustration of the concept of the Poisson’s ratio. The ratio of the increase of the lateral deformation to the length contraction of a material.....	18
Figure 2. 13. Key characteristics of cavings bounded by preexisting planes of weakness (Schlumberger, 1998).....	19
Figure 2. 14. HPHT Filter Press, 500ml. Model used at the Chair of Drilling and Completion Engineering.....	20
Figure 2. 15. Illustration of the fracture sealing: Function of Loss Prevention Material (Kageson- Loe et al., 2009).....	22
Figure 3. 1. Workflow followed in this study.	25
Figure 3. 2. Contour map of the reservoir of the field AM1, the circle area shows the area analyzed in this study. Company courtesy.	26
Figure 3. 3. Seismic in depth of field AM1. The seismic line is shown in depth domain with NW- SE orientation where the trajectories and targets of the analyzed wells are shown, two discontinuities are marked as red dash lines. Company courtesy	27
Figure 3. 4. Seismic in depth of field AM1 with RMS attribute. Company courtesy.....	28
Figure 3. 5. a) 3D and b) 2D views from JewelSuite™ showing all the wells drilled from drill site AM-1.	31
Figure 3. 6. a) 3D and b) 2D view of the selected wells for this analysis.....	32
Figure 3. 7. Overview of the drilling parameters using the proNova software by TDE, well AM- 8.....	34
Figure 3. 8. Example of a stuck pipe event corrected by the real-time monitoring data, AM-8... 35	
Figure 3. 9. Comparison of the drilling events obtained just from the DDR and real-time monitoring, well AM-8.	35
Figure 3. 10. Example, plot of drilling events, mud weight, casings and top formations in terms of time and depth, AM-8.	36
Figure 3. 11. Overview of the drilling events, actual mud weight, schematics and caliper logs of wells AM-1 and AM-11.	38
Figure 3. 12. Overview of the drilling events, actual mud weight, schematics and caliper logs of wells AM-5 and AM-8. The caliper log of the last one was not available even though it was requested.	39
Figure 3. 13. Cavings from wells AM-21 and AM-11. Company courtesy.	41

List of Figures

Figure 3. 14. Cavings from wells AM-25 and AM-4. Company courtesy.....	42
Figure 3. 15. Cavings from well AM-8. Company courtesy.	43
Figure 3. 16. Reservoir pressure of field AM1. Company courtesy.....	43
Figure 3. 17. Drilling summary, AM-11.	44
Figure 3. 18. Drilling summary, AM-5. Just the main is being analyzed.....	45
Figure 3. 19. Drilling summary, AM-8.	45
Figure 3. 20. Resistivity logs of wells AM-1, AM-11, AM-21, AM-5 and AM-8. AT10 in black and AT90 in red.	46
Figure 3. 21. Gamma Ray logs of wells AM-1, AM-11, AM-21, AM-5 and AM-8.	47
Figure 3. 22. Density logs of wells AM-1, AM-11, AM-21, AM-5 and AM-8.	47
Figure 3. 23. Porosity logs of wells AM-1, AM-11, AM-21, AM-5 and AM-8.	48
Figure 3. 24. Sonic Compressional logs (DTCO) of wells AM-1, AM-11, AM-21, AM-5 and AM-8.	48
Figure 3. 25 Sonic Shear logs (DTSM) of wells AM-1, AM-11, AM-21, AM-5 and AM-8.....	49
Figure 3. 26. Density, direction and dip of the fractures in the reservoir according to the information from image logs of wells 11, 4, 21 and 114. Company courtesy.	50
Figure 3. 27. Azimuth of the S_{Hmax} around the area of interest obtained from the World Stress Map. (World Stress Map: Data 2016)	50
Figure 3. 28. Azimuth of the S_{Hmax} in wells near the area of interest (yellow square) obtained from the World Stress Map. (World Stress Map: Data 2016).....	51
Figure 3. 29. AM-1, actual and depth-stretched logs.....	52
Figure 3. 30. AM-1, final logs used for the geomechanical analysis.....	52
Figure 3. 31. Heading of the master log ran in the exploratory well AM-1.	53
Figure 3. 32. Zonation and lithology models calculated in AM-1.	54
Figure 3. 33. Calculation of the overburden gradient in well AM-1	55
Figure 3. 34. Pore pressure calculation of well AM-1. a) Pore pressure using two different slopes b) Pore pressure using just one trend line.....	56
Figure 3. 35. Fracture gradient calculated with six different equations and calibrated with LOTs available, AM 1.	57
Figure 3. 36. Rock properties curves calculated from logs, AM-1.....	59
Figure 3. 37. Horizontal stress definition using the effective stress method, AM-1.	61
Figure 3. 38. Collapse pressure calculated and calibrated with drilling events and caliper log, AM-1.....	62
Figure 3. 39. Logs used for geomechanical analysis, AM-11.....	63
Figure 3. 40. AM-11, pore pressure calculated using the same trend line as in AM-1 (one trend line).....	64
Figure 3. 41. AM-11, pore pressure calculated using the same trend lines as in AM-1 (two different slopes).	64
Figure 3. 42. Fracture gradient calculation, AM-11.	65
Figure 3. 43. AM-11 calculated breakout width using same methods as in well AM-1.	66
Figure 3. 44. Seismic line in depth across well AM-11. Company courtesy.....	67
Figure 3. 45. Depth based CMW at 2800m, 3200m, 3400m and 3500m displaying the predicted failure, AM-1.	68
Figure 3. 46. Depth based CMW at 3700m, 3900m, 4300m and 4600m, displaying the predicted failure, AM-1.	69
Figure 3. 47. Depth based CMW at 2900m, 3200m, 3600m, 4000m, 4200m and 4400m displaying the predicted failure, AM-11.....	70
Figure 3. 48. Samples measured in Dionex. a) Left to right: complete small caving, crashed to little pieces, milled to powder, well S-6081, 2700m depth. b) Powdered sample, well S- 6081, 2700m depth.	72

Figure 3. 49. Left to right: a) Soxhlet extractor set up, b) refrigerated circulator and c) whole system in the fume hood. DPE Laboratories.	73
Figure 3. 50. Cavings in the extractor chamber.....	73
Figure 3. 51. Samples ready to be analyzed by the ELTRA Elemental Analyzer.....	74
Figure 3. 52. Example of the results obtained from the Rock Eval analyzer.....	75
Figure 3. 53. Sample preparation for the micro-CT scanner. Showing a) the height of sample (30mm), b) the diameter of the sample (10mm) and c) the complete sample.	76
Figure 3. 54. Overview of the gamma ray and resistivity logs (deep and shallow curves) together with the drilling events, well schematics and caliper logs, wells AM-1, AM-11, AM-5 and AM-8.....	76
Figure 3. 55. Closer view of the resistivity logs (deep and shallow curves), drilling events, well schematics and caliper logs, wells AM-1, AM-11, AM-5 and AM-8.	77
Figure 3. 56. Gamma Ray and Resistivity logs compared to the mud weight and drilling events, probable invaded formations shown in red.	78
Figure 4. 1. Cavings collected at the drilling site, well S-6081. a) Showing one sample just taken from the shale shaker, b) All samples collected from the shale shaker.....	81
Figure 4. 2. Cavings cleaned with a fabric and sorted by size, well S-6081.	81
Figure 4. 3. Conventional ceramic disk used in the HP/HT filter press.	82
Figure 4. 4. Building procedure of the shale and epoxy disk to be tested.....	85
Figure 4. 5. HPHT Filter press test using disks made of epoxy and shale rock, and oil-base mud sample.	87
Figure 5. 1. Results of the wellbore instability analysis of well AM-11.....	90
Figure 5. 2. Rock Eval results of the contaminated shale sample with oil-based mud (no cleaning process).	92
Figure 5. 3. Rock Eval results comparison of samples 1 and 2 cleaned with two methods, Soxhlet and Dionex. a) Shale sample from 2700m cleaned with Soxhlet method, b) shale sample from 2700m cleaned with Dionex method. Values shown in Table 5. 2.	92
Figure 5. 4. Rock Eval results comparison of samples 1 and 2 cleaned with two methods, Soxhlet and Dionex. a) Shale sample from 3400m cleaned with Soxhlet method, b) shale sample from 3400m cleaned with Dionex method. Values shown in Table 5. 2.	93
Figure 5. 5. Rock Eval results comparison of samples 4, 5 and 6 cleaned with the Dionex method. a) Complete caving from 3400m, b) sample crushed to small pieces from 3400m and c) sample milled to powder from 3400m. Values shown in Table 5. 2.	93
Figure 5. 6. Histogram of the fracture width measured in the images from the micro-CT scanner from all the micro-fractures found.....	95
Figure 5. 7. Images 166 (top right) and 173 (bottom right) from micro-CT scanner displaying the micro-fracture. Measured width: 207 μ m, 237 μ m, 352 μ m, 223 μ m, 132 μ m.	95
Figure 5. 8. Images 184 (top right) and 208 (bottom right) from micro-CT scanner displaying two micro-fractures with different color and direction. Measured width white: 185 μ m, 117 μ m, 167 μ m, 120 μ m, 92 μ m.....	96
Figure 5. 9. Images 232 (top right), 283 (bottom right) and 287 (left), from micro-CT scanner displaying a white micro-fracture. Measured width: 50 μ m, 55 μ m, 57 μ m, 62 μ m.....	96
Figure 5. 10. Image 320 from micro-CT scanner displaying three micro-fractures, two white (both with the same direction) and one black with different direction. Measured width white: 126 μ m, 111 μ m, 103 μ m.....	97
Figure 5. 11. Images 407 (top right), 396 (bottom right) and 404 (left), from micro-CT scanner displaying a white micro-fracture. Measured width: 103 μ m, 74 μ m.....	97
Figure 5. 12. Images 558 (top right), 564 (bottom right) and 560 (left) from micro-CT scanner displaying a white micro-fracture. Measured width: 62 μ m, 103 μ m, 74 μ m, 92 μ m, 52 μ m..	98

List of Figures

Figure 5. 13 Images 593 (top right), 630 (bottom right) and 595 (left) from micro-CT scanner displaying a possible black micro-fracture or fossil. Measured width: 439 μ m, 323 μ m, 185 μ m, 281 μ m, 269 μ m.	98
Figure 5. 14. Disk 1, shale from 2700md. a) disk placed in the HPHT filter press, b) filter cake after the test, c) shale after removing the filter cake and, d) bottom face of the disk.....	99
Figure 5. 15. Disk 2, shale from 2700md. a) shale disk, b) disk placed in the HPHT filter press, c) shale after test and, d) disk broken to be evaluated.....	100
Figure 5. 16. Disk 3, shale from 3400md. a) disk placed in the HPHT filter press, b) filter cake after the test, c) bottom face of the disk after test and, d) bottom face scratched.	100
Figure 5. 17. Disk 4, shale from 3400md. a) disk placed in the HPHT filter press, b) a drop of filtrate, c) filter cake after the test and, d) bottom face showing sandy texture.	101
Figure 5. 18. Filtrate obtained from the three disks, left to right: disk 1, disk 3 and disk 4.	101
Figure 5. 19. Area of the cavings measured with a commercial application. a) Area, disk 1: 10.93cm ² , b) area, disk 3: 5.27cm ² , c) Area, disk 4: 6.74cm ²	101
Figure B. 1. Checklist logs: AM-1, AM-11, AM-5 and AM-8.....	107
Figure B. 2. Horizontal stresses, AM-8. Geomechanical analysis using same parameters as in AM-1 and AM-11.....	107
Figure B. 3. PP, FG, S _{Hmax} , S _{Hmin} , UCS, AM-8. Geomechanical analysis using same parameters as in AM-1 and AM-11.	108
Figure B. 4. Collapse pressure, AM-8, geomechanical analysis using same parameters as in AM-1 and AM-11.	108
Figure B. 5. Model verification, AM-8. Geomechanical analysis using same parameters as in AM-1 and AM-11.....	109
Figure B. 6. Horizontal stresses, AM-5. Geomechanical analysis using same parameters as in AM-1 and AM-11.....	110
Figure B. 7. PP, FG, SHmax, Shmin, UCS, AM-5. Geomechanical analysis using same parameters as in AM-1 and AM-11.....	110
Figure B. 8. Collapse pressure, AM-5. Geomechanical analysis using same parameters as in AM-1 and AM-11.....	111
Figure B. 9. Model verification, AM-5. geomechanical analysis using same parameters as in AM-1 and AM-11.....	112

List of Tables

Table 2. 1. a) Results of calculation of the microfracture width (for 1 microfracture in a sample). b) Result of permeability measurements, the microfracture width calculated for various confining pressures (Leśniak, 2015).	21
Table 3. 1. Geological column and description of the formations of the wells drilled in the AM1 field. Company courtesy.	29
Table 3. 2. Mud weight used during drilling the problematic area and inclination and azimuth from the top to the bottom of section 12 ¼" bit size.	40
Table 3. 3. Data of the LOTs taken in well AM-1.....	57
Table 3. 4. Rock properties data provided by the company. The UCS was calculated with histogram in each formation, using two methods for comparison. * Company courtesy...	58
Table 3. 5. Methods used to calculate the rock properties, AM-1.	58
Table 3. 6. LOTs taken in the well AM-11 during drilling operations.....	65
Table 3. 7. Bedding planes and rock properties used in the Advance Mode of JewelSuite™, AM- 11.....	67
Table 4. 1. Properties of the fluid used in the PPT. Company courtesy.	86
Table 5. 1. Samples used for the analysis of the shale evaluation at different depth in the formations where the cavings and instability problems were present.	91
Table 5. 2. Calculations of the TIC, calcite equivalent, SPI, HI and PI.....	94
Table 5. 3. Filtrate results based on the ratio epoxy/shale for all samples.	102